

OXIDATION KINETICS OF GRAPHITE AND COAL USING THERMOGRAVIMETRIC
ANALYSIS

A Thesis

Presented in Partial Fulfillment of the Requirements for the

Degree of Master of Science

with a

Major in Mechanical Engineering

in the

College of Graduate Studies

University of Idaho

by

Samuel T. Stuhlman

Major Professor: Kamal Kumar, Ph.D.

Committee Members: Dan Cordon, Ph.D., Steven Beyerlein, Ph.D.

Department Administrator: Steven Beyerlein, Ph.D.

December 2019

Authorization to Submit Thesis

This thesis of Samuel T. Stuhlman, submitted for the degree of Master of Science with a Major in Mechanical Engineering and titled "Oxidation Kinetics of Graphite and Coal Using Thermogravimetric Analysis," has been reviewed in final form. Permission, as indicated by the signatures and dates below, is now granted to submit final copies to the College of Graduate Studies for approval.

Major Professor: _____ Date: _____

Kamal Kumar, Ph.D.

Committee Members: _____ Date: _____

Dan Cordon, Ph.D.

_____ Date: _____

Steven Beyerlein, Ph.D.

Department

Administrator: _____ Date: _____

Steven Beyerlein, Ph.D.

Abstract

This thesis examines the combustion of carbon-containing solid fuels using thermogravimetry, evolved gas analysis, and Energy Dispersive X-ray spectroscopy on solid products. The first set of experiments involves oxidation of graphite nanoparticles with copper oxide as the oxygen carrier. This simple system results only in the production of carbon monoxide and carbon dioxide. The oxidation process was followed using evolved gas analysis using an NDIR analyzer. Results show early production of CO leading to the subsequent rapid production of CO₂. The evolution of gaseous products is related to the weight lost from solid samples. A total of three peaks occur in both carbon monoxide and carbon dioxide evolution. Modulated TGA experiments were also conducted to obtain the activation energy during the reaction. The progress of the reactions during various stages of heating was followed by Energy Dispersive X-ray spectroscopy (EDS) on solid products. The EDS results indicate that the reduction of CuO to Cu during heating follows a sigmoidal trend. The second part of this work focusses on the oxidation of a real solid fuel, coal, with air as the oxidizer. Coal specimens drawn from the Argonne premium coal sample program were studied using thermogravimetric analysis. The combustion behavior for various ranks of coal was studied using both the TGA weight loss as well as evolved gas analysis using a Fourier transform infrared spectroscopy. The weight loss profile for all samples except for the lignite and sub-bituminous coal shows that there is a slight mass gain in the temperature range of 200 to 320°C. A strong absorption feature for what appears to be aromatic nitro compounds was detected for the high volatile bituminous coals. Additionally, modulated TGA experiments were also conducted to obtain the activation energy trends for each of the test fuels.

Acknowledgments

The Energy Dispersive X-ray Spectroscopy (EDS) was carried out at the Electron Microscopy Center at the University of Idaho. I gratefully acknowledge the assistance of Dr. T.J. Williams with the EDS experiments.

I also acknowledge the assistantship support from the department of mechanical engineering at the University of Idaho. I was aided in my transfer to the University by Prof. Steven Beyerlein and Becky Colpaert. While studying at the University of Idaho, I had regular support from staff members Debbie Edwards, Ankit Gupta, Bill Magnie, and (especially) Molly Steiner.

Special thanks are dedicated to Dan Cordon, Ph.D., who served on my committee and instructed me in thermodynamics. It was his lectures and lessons which sparked my interest and taught me useful tools for the analysis of energy systems.

The assistance from my lab-members Rick Leathers, Salman Alharbi, and Samuel Van Horn in the Energy Systems Lab is also acknowledged. Special thanks to Elyasa Al-Gharibeh for sharing an office, hotel rooms at conferences, travel accommodations, and friendship with me.

Finally, I would like to acknowledge with gratitude Prof. Kamal Kumar. He taught me how to design laboratory experiments that convey meaning through analysis. He spent long hours to ensure that I understood the experiments performed and taught me to communicate in a manner that peers in our field could find insightful. I owe any success I have concerning education and my vocational future to the extra effort he provided for me.

Dedication

I dedicate this thesis to my mother and father.

Table of Contents

Authorization to Submit Thesis	ii
Abstract	iii
Acknowledgments.....	iv
Dedication	v
Table of Contents	vi
List of Tables.....	viii
List of Figures	ix
1 Introduction – Progression of Thermogravimetry.....	1
1.1 Weight Measure	1
1.1.1 Temperature Measurement and Control.....	2
1.1.2 The Thermobalance.....	3
1.2 Thermogravimetry Techniques and Applications.....	5
1.2.1 TGA Requirements	6
1.2.2 TA Instruments Q500.....	7
1.2.3 Modulated TGA Methods	7
1.3 Combustion and Pyrolysis	8
1.4 Solid Fuels.....	9
1.5 Evolved Gas Analysis	13
1.5.1 NDIR Gas Analysis.....	14
1.5.2 Fourier Transform Infrared Spectroscopy for Gas Analysis.....	15
1.6 Intentions of this Study	20
1.6.1 Solid Oxygen Carriers.....	21
1.6.2 The Premium Argonne Sample Program	23
2 Combustion of Graphite Nanoparticles with Copper (II) Oxide in a Thermogravimetric Analyzer with Evolved Gas Analysis	26
2.1 Introduction.....	26
2.2 Experimental Apparatus and Procedure.....	26
2.3 Results.....	27
2.3.1 Sample Weight Loss during Heating	28

2.3.2	Effect of Heating Rate on Conversion	29
2.3.3	Evolved Gas Analysis	31
2.3.4	Determination of Activation Energy	34
2.3.5	Energy Dispersive X-ray Spectroscopy Analysis	38
2.4	Conclusion	41
3	Modulated Thermogravimetric Experiments on Argonne Premium Coal Samples with Combustion Gas Analysis.....	43
3.1	Introduction.....	43
3.2	Experimental Apparatus and Methods.....	43
3.3	Results.....	45
3.3.1	TGA Weight Loss	45
3.3.2	Evolved Gas Analysis: Quantitative Results	48
3.3.3	High Volatile Bituminous Coal.....	49
3.3.4	Low Volatile and Medium Bituminous Coals	52
3.3.5	Sub-Bituminous Coal and Lignite.....	53
3.3.6	Qualitative Comparison of Species Evolution Trends.....	55
3.3.7	Modulated TGA Experiments and Activation Energy Results.....	58
3.4	Conclusion	62
4	Discussion, Conclusion, and Future Work.....	63
4.1	Thermal Analysis on Argonne Premium Coal Samples	64
4.2	Thermal Analysis on Argonne Premium Coal Samples	72
4.3	Future Work	79
5	References Cited	81

List of Tables

Table 3.1: Test conditions.....	44
Table 3.2: Argonne Premium Coal Samples and characteristics %C, H, O, on moisture and ash-free basis. Sulfur and Ash on dry basis [25].	45
Table 4.1: Temperature and activation energies corresponding to approximated transitions in subregions of TG curves.	66

List of Figures

Figure 1.1: Honda's original thermobalance. [7].....	4
Figure 1.2: Carbon combustion and reactions.....	12
Figure 1.3: Principle diagram for NDIR type analyzers	15
Figure 1.4: Top is an example IR spectrum of CO_2 from NIST, bottom is FTIR spectrum results of experiments on coal samples from chapter 3.....	17
Figure 1.5: Principle diagram for Michelson Interferometer.....	19
Figure 2.1: Weight loss vs. temperature with for various heating rates.....	28
Figure 2.2: Derivative weight with respect to temperature for $10^\circ C/min$ heat rate.....	29
Figure 2.3: Fractional conversion at various heating rates.	30
Figure 2.4: Fractional conversion as a function of reduced time.....	30
Figure 2.5: Evolution of CO and CO_2 with respect to temperature.....	32
Figure 2.6: CO and CO_2 trajectory during the combustion of graphite with copper oxide.....	33
Figure 2.7: Modulated temperature, weight loss, and modulated derivative weight as a function of time.	35
Figure 2.8: Weight loss and derivative of modulated weight as a function of temperature. ...	36
Figure 2.9: Activation energy and weight loss profiles as a function of temperature.	37
Figure 2.10: Activation energy peak values compared with derivative weight.....	38
Figure 2.11: SEM images showing the state of the sample during various stages of reaction.....	39
Figure 2.12: Energy dispersive spectroscopy analysis for unreacted mixture showing characteristics of copper and oxygen peaks.....	40
Figure 2.13: Average element weight percent of Copper and Oxygen at various reaction temperatures obtained from Energy-Dispersive X-ray Analysis.....	41
Figure 3.1: Weight loss characteristics for high volatile bituminous coals.....	46
Figure 3.2: Medium and low volatile coal weight characteristics.....	46
Figure 3.3: Weight characteristics for sub-bituminous and lignite coals.....	47
Figure 3.4: Pre-Combustion weight gain.....	47

Figure 3.5: Infrared spectra for a high volatile bituminous coal.....	48
Figure 3.6: CO and CO ₂ evolution for high volatile bituminous coal from the Illinois #6 seam.	49
Figure 3.7: CO and CO ₂ evolution for high volatile bituminous coal from the Pittsburgh #8 seam.....	50
Figure 3.8: CO and CO ₂ evolution for high volatile bituminous coal from the Blind Canyon seam.....	50
Figure 3.9: CO and CO ₂ evolution for high volatile bituminous coal from the Lewiston- Stockton seam.	51
Figure 3.10: CO and CO ₂ evolution for medium volatile bituminous coal from the Upper Freeport seam.	52
Figure 3.11: CO and CO ₂ evolution for high volatile bituminous coal from the Pocahontas #3 seam.....	53
Figure 3.12: CO and CO ₂ evolution for subbituminous coal from the Wyodak-Anderson seam.	54
Figure 3.13: CO and CO ₂ evolution for lignite coal from the Beulah-Zap seam.	54
Figure 3.14: Qualitative species evolution trends for high volatile bituminous coal from the Pittsburgh #8 seam.....	55
Figure 3.15: Qualitative species evolution trends for medium volatile bituminous coal from the Upper Freeport seam.	56
Figure 3.16: Qualitative species evolution trends for low volatile bituminous coal from the Pocahontas #3 seam.	56
Figure 3.17: Qualitative species evolution trends for sub-bituminous coal from the Wyodak- Anderson seam.	57
Figure 3.18: Modulated temperature, weight loss, and a derivative of modulated weight as a function of time.	59
Figure 3.19: Activation energies vs. temperature for high volatile bituminous coals.	60
Figure 3.20: Activation energies vs. temperature for medium and low volatile bituminous coals.	60
Figure 3.21: Activation energies vs. temperature for sub-bituminous and lignite coals.....	61
Figure 4.1: Activation energy and derivative weight as a function of temperature.	65

Figure 4.2: Activation energy and derivative weight as a function of temperature.	67
Figure 4.3: Derivative weight percent with respect to temperature at heating ramps from CuO/C experiments in chapter 2.	68
Figure 4.4: CO and CO ₂ evolution with weigh and derivative weight profiles with respect to temperature.	69
Figure 4.5: Image at left is unreacted carbon-copper oxide mixture before milling, image right is mixture post thermogravimetry.	71
Figure 4.6: TG curves for high volatile coals from the Premium Argonne Sample Program. 73	
Figure 4.7: TG, DTG, and major gas evolution for high volatile bituminous coal from Illinois #6 seam.	74
Figure 4.8: Qualitative species evolution for medium volatile bituminous coal from the Upper Freeport seam.	75
Figure 4.9: TG and DTG for 701 high volatile bituminous and 202 sub-bituminous coals. ...	76

1 Introduction – Progression of Thermogravimetry

1.1 Weight Measure

By definition Thermal Analysis (TA) is the term applied to a group of methods and techniques in which a physical property of a substance is measured as a function of temperature [1]. One method in this group is thermogravimetry, a technique whereby the weight of a substance is recorded as a function of time or temperature while it remains in a heated environment [2]. Measuring weight change to understand chemical reactions is an old concept, and there are instances of the weight of reaction being recorded as early as the Ptolemaic period for the purpose of removing mercury from gold. More relative examples of early thermogravimetric concepts can be attributed to Antoine Lavoisier, also known as the “father of modern chemistry”. Lavoisier noticed that metals gained weight as they began to rust then lost weight as the rust turned to powder, he assumed the weight change was due to the absorbance and the release of air into the metal. He tested this assumption by burning organic material while carefully collecting all gaseous, liquid, and solid products and showed that the weight of the products was equal to that of reactants. These tests led Lavoisier to the naming of oxygen, and he showed that it was consumed from the atmosphere during combustion [3].

Lavoisier and his peers, like Joseph Black and Dr. Bryan Higgins, owe some of their scientific success to their pursuit of precision regarding the instrumentation used to measure weight change. These eighteenth-century researchers were limited in their efforts due to having only beam and spring balances available at the time. The advancement in precision for mechanical balances increased over the next century and led to the invention of the microbalance by Warburg and Ihmori in 1886. This first microbalance was a beam balance, in a vacuum, pivoted on a razor blade [4]. There was much excitement in the scientific community concerning the

potential to analyze microscale weight change, and from 1890 to 1910, several important advancements were achieved by numerous researchers. For example, in 1901, Salvioni measured deflection with a microscope, and later that year, Nernst added a quartz rod balance. With these advancements, balances had become precise, durable, and convenient enough to be used in thermobalances, but advanced thermal control and measure were also required for their design. The progression of devices used to measure and control the temperature for the thermobalance is described in the next section.

1.1.1 Temperature Measurement and Control

As old as the concept of measuring weight change is the concept of measuring temperature. There are many instances of people describing temperature in relative terms, and some credit is attributed to Plato. However, concerning the development of instrumentation for the measure and control of temperature, it is appropriate to recall the work of Galileo Galilei. Galileo noticed that matter contracts and expands with the removal or addition of heat; this observation was then used by himself and other instrument makers to create thermometers [2]. These original thermometers used alcohol as a working fluid until Daniel Fahrenheit invented the in-glass mercury thermometer, which lead to the Fahrenheit scale.

Further advancements in thermometry came from Andreus Celsius and Lord Kelvin, who introduced the Celsius and Kelvin scales, respectively. However, the range in which thermometers are useful is limited by the boiling and freezing temperatures associated with their working fluids. The thermometer's limited range is below temperatures commonly reached in experimental furnaces, so further advancements were needed to achieve a working thermobalance. The first major advancement came from potter Josiah Wedgwood in the form of the pyrometer, where Wedgwood would use the shrinkage of precisely cut pieces of clay to

measure high temperatures in kilns. Modern pyrometers sense infrared radiation from objects. Thomas Seebeck provided the next advancement in thermometry. He noticed that when two wires of different conductive metals are joined at their ends, and there is a temperature difference between the tail of the wires and their junction, a magnetic field is induced [5]. Seebeck's discovery led others to create a new temperature measuring device named the thermocouple. For some time, it was difficult to produce thermocouples that had accurate and repeatable results because it was difficult to produce metals with high purities. In 1885 Henry Le Chatelier solved the problem using rhodium-platinum alloys coupled with pure platinum, he also suggested calibrating the instruments using known boiling and fusion point temperatures rather than thermometers [6]. Le Chatelier's discovery gave the scientific community a tool to measure very high and low temperatures, and with thermocouples and microbalances being available to researchers by the early twentieth century, it would be possible to combine the two inventions into modern thermobalances.

1.1.2 The Thermobalance

Early contributors to the invention of the thermobalance used techniques such as weighing before and after combustion and weighing at several different temperatures across experiments. In 1912 Georges Urbain made a thermobalance which was housed in a gas-tight compartment. Because of this compartment experiments could be performed in vacuum and product analysis was possible, Urbain also incorporated Ångström's principle of null point electromagnetic compensation, where deviation from the beams null point is detected and compensated for. However, the early model, unfortunately, was not accurate or precise with regards to weight measurement and temperature control [2].

In 1915 a professor from Japan published a paper titled 'On a Thermobalance.' With this paper

by Professor Kôtarô Honda, the term ‘thermobalance’ was published for the first time. The paper followed Honda’s development of the first instrument capable of continuously following mass change at high temperatures. A schematic of the thermobalance is shown below.

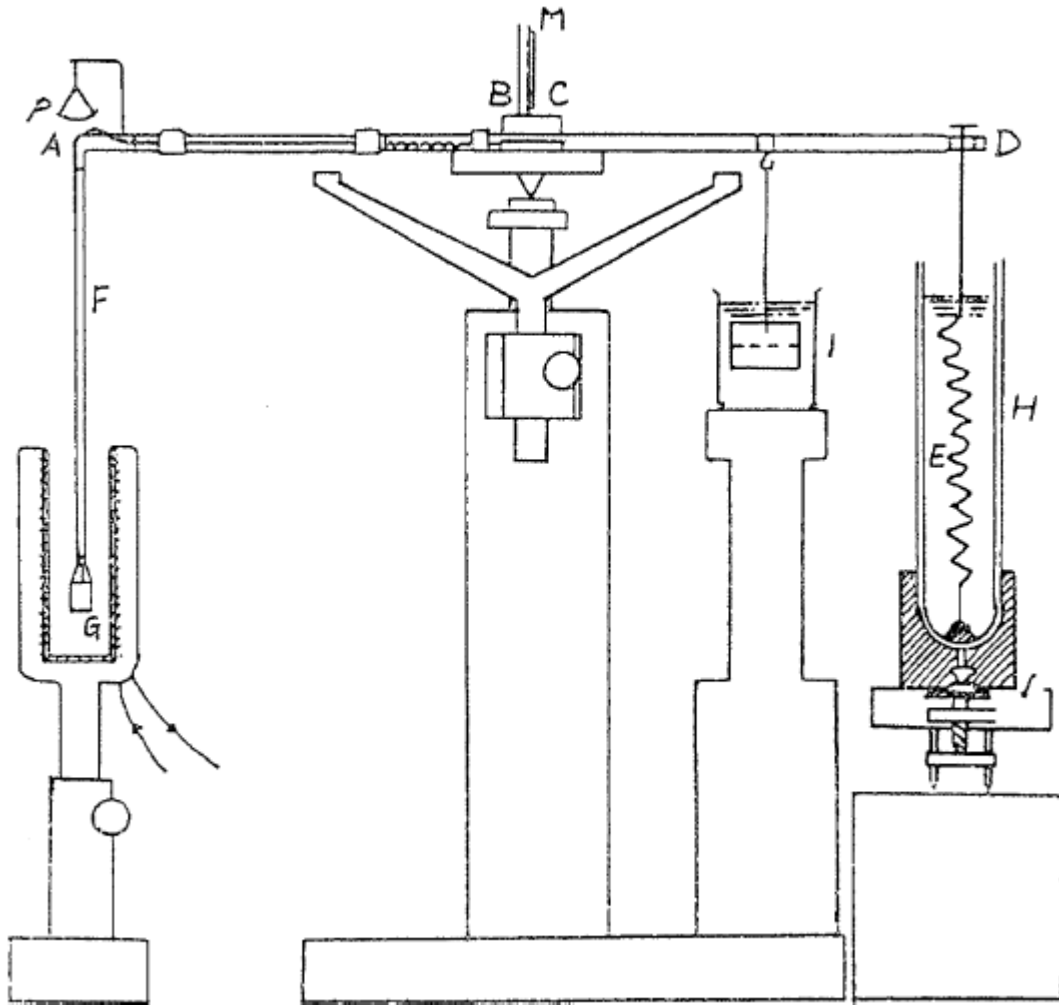


Figure 1.1: Honda's original thermobalance. [7]

Honda's thermobalance was impressively designed, its arms (AB and CD) are made of quartz which has a low coefficient of thermal expansion and is balanced on knife-edge, there is a mirror (M) which reflects the image of the vertical scale into a telescope (not shown), and there

is a vibration damper (I). Attached to the (A) side of the balance is a thin porcelain tube, hanging from it is the platinum sample pan (G) and the junction end of the thermocouple. The cold end of the thermocouple is connected at (B). On the (D) side of the balance is a Dewar vessel (H), which has a spring (E) connecting it to the arm. The Dewar vessel dampens rapid temperature change in the spring, and the system is designed to be adjusted up or down until the beam is level, then the zero-point measurement is read with the mirror and telescope. Honda's first experiment was on manganese (II) sulfate tetrahydrate ($MnSO_4H_2O$), where the sample was heated and held until the change in mass became zero. Data from this experiment were plotted in mass vs. temperature manner; thus, the first thermal decomposition (TG) curve was created [7]. There were many advancements to Honda's design and many significant advancements in thermal analysis until research was interrupted by World War II. In 1945 the first commercial thermogravimeter was produced, and since then, improvements have been vast. Because of the early pioneers mentioned in this section, thermogravimeters today are precise, accurate, and easy to operate.

1.2 Thermogravimetry Techniques and Applications

Although today's thermogravimetric analyzers (TGAs) are easy to operate, there are guidelines associated with their operation and the analysis of the data they provide. Knowing how to operate experiments properly ensures a safe lab environment and ensures that the results can be reported in a manner which meets the standards of the scientific community. This section describes those standards, first for conducting experiments, and second for reporting the results.

1.2.1 TGA Requirements

During the development of TGAs, it was required that the instrument have a precision balance, a furnace capable of linear heating rates, and the ability to measure time and temperature. Now those features are standard on commercial models, and the standard requirements are more stringent. The list below is summarized from 'An Introduction to Thermogravimetry' by Keatch and Dollimore, and the same specifications are found in most books regarding the subject.

1. The furnace should reach 100-200°C above the maximum experimental temperature.
2. The hot zone of the furnace is to remain within 5°C of the desired temperature.
3. The crucible must stay in the hot zone.
4. Conducting and magnetic samples must not interact with the furnace windings.
5. The heat rate should be reproducible over the complete temperature range.
6. The sensitivity of the balance should be appropriate for the sample size.
7. Radiation and convection from the furnace must not affect the balance.
8. The recorded temperature should be the sample temperature.
9. The apparatus must not be affected by volatile chemicals from the experiment.
10. The TGA should continuously record weight with respect to temperature and time.
11. The instrument should be able to:
 - a. vary the heating rate,
 - b. maintain desired temperatures,
 - c. allow experimentation in a variety of gas atmospheres, and
 - d. allow attachments for complementary techniques like evolved gas analysis.

Keatch and Dollimore continue by describing the accuracy, sensitivity, reproducibility, and

capacity required of the TGA's balance; however, modern TGAs easily exceed these demands due to the advancement of electronics. Experiments described in chapters 2 and 3 of this report were conducted using a Q500 TGA from TA instruments, and its abilities and specifications are described in the next section.

1.2.2 TA Instruments Q500

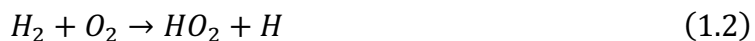
The Q500 TGA from TA Instruments is a popular research-grade thermogravimetric analyzer, its easy to use design and reliable results have made it a good option for experimentation, and it can be found in laboratories around the world. The Q500 furnace uses resistance heating to reach a maximum temperature of 1000°C, when held at isothermal temperatures has an accuracy of $\pm 1^\circ\text{C}$ and 0.1°C precision. The unit includes a temperature compensated thermobalance that can measure the weight of samples up to one gram with 0.01% precision and 0.1 μg sensitivity. Several additions are available to the TGA that add complexity to the analysis, such as evolved gas analysis and modulated TGA. Both methods were used for experimentation described herein. [8]

1.2.3 Modulated TGA Methods

Modulated Thermogravimetry was used to quantify activation energy for the experiments discussed in chapters 2 and 3 of this work. For modulated testing, the Q500 TGA can modulate furnace temperature about a linear ramp to obtain kinetic information. The modulated methods and results are summarized herein, and more thoroughly explained in the works of Blaine and Hahn [9, 10].

1.3 Combustion and Pyrolysis

Combustion is a chemical reaction between fuel and oxidant, and pyrolysis is the thermal decomposition of fuel in the absence of an oxidant. Chemical reactions in both cases rearrange atoms from colliding molecules. Reaction kinetics is the measurement of the rates at which these reactions and collisions occur. Using spectroscopy to analyze the products of these reactions allows researchers to understand global and elementary reactions. Only initial reactants and final products are considered in global reactions. Elementary reactions take account of all the intermediate species formed and consumed during the global reaction. Reactions 1.1 through 1.5 are examples of global and elementary reactions.



Where M represents molecules with which the reacting species may collide. The first of these reactions from Turns is the overall global conversion of hydrogen and oxygen to water, and reactions 1.2 through 1.5 are some of the elementary reactions that occur to complete the global reaction. During elementary reactions radicals, molecules or atoms with unpaired electrons, like O , OH , H , and HO_2 , are formed. Which intermediate species are formed during reaction depends on the lowest energy required, so in the second reaction H_2 and O_2 form HO_2 rather than OH because it requires single bonds to be broken and formed rather than double bonds. The number of elementary steps to describe a global reaction can be in the hundreds, and

collectively they are known as a reaction mechanism [11].

Reactions analyzed in chapters 2 and 3 of this study are bimolecular, where two reactant molecules form two product molecules, as are reactions 1.2-4 shown above. Each reaction has temperature-dependent activation energy and a rate at which it proceeds, all of which are determined by the Arrhenius equation:

$$k(T) = Ae^{-E_A/R_u T} \quad (1.6)$$

Where $k(T)$ is the bimolecular rate coefficient, A is the pre-exponential factor, E_A is the activation energy, R_u is the universal gas constant, and T is temperature. The Arrhenius equation can be represented in terms of collision theory between molecules and the partial pressure or concentration of gasses involved in the reaction. The equation is necessary to properly model chemical reactions using software and quite useful in predicting reactions where reactants and products are gaseous; however, a substantial amount of complexity is added when some or all of the reactants and products are solids.

1.4 Solid Fuels

Solid fuels are solids that are combusted with oxygen to produce energy. Humans have been burning solids for heat and light since before recorded history. There is a wide variety of these fuels, including coal, animal dung, wood, and many forms of biomass. Coal combustion for energy production far exceeds the use of other solid fuels, and it is the fuel used for experimentation later explained in this document. According to the U.S. Department of energy, coal is the second most used energy source to generate electricity after natural gas and consists of 33.8 percent U.S. electricity generated [12]. It is comprised of carbon, moisture, ash, and a variety of hydrocarbons. During combustion, the hydrocarbons provide a large amount of

energy; however, they are much more volatile than the solids in coal and are consumed more rapidly. Because of the rapid combustion of the volatiles, it is necessary to understand the combustion of pure graphite carbon, which almost solely remains after these volatiles are consumed and therefore controls the burning rate of coal. [13]

Reactions that occur during surface oxidation are different from those that occur in gaseous combustion in that they are heterogeneous. The simplest of these reactions involve gas-phase molecules in contact with solid molecules, but in complex situations, several different phases (liquid, oxidized, etc.) can be included, and the two-dimensional surfaces between phases also need considered. The process has been summarized by Gardiner [14] in five steps:

1. Transport of the reactant molecule to the surface by convection or diffusion.
2. Adsorption of the reactant molecule on the surface.
3. Elementary reaction steps involving various combinations of adsorbed molecules, the surface itself, and gas-phase molecules.
4. Desorption of product molecules from the surface.
5. Transport of the product molecules away from the surface by convection and diffusion.

The first and fifth steps describe mass transfer either to or away from the surface, which is governed by Fick's Law shown for one-dimensional binary diffusion on a mass basis in equation 1.7:

$$m''_A = Y_A(m''_A + m''_B) - \rho \mathcal{D}_{AB} \frac{dY_A}{dx} \quad (1.7)$$

Where subscripts A and B represent different molecules, m'' is the mass flux, Y is the mass fraction, ρ is the density of the fluid, and \mathcal{D}_{AB} is the binary diffusivity. Fick's Law written in this manner states that the flux of species A, m''_A , is equal to the sum of flux from bulk fluid

flow, $Y_A(m''_A + m''_B)$, and the diffusional flux, $-\rho \mathcal{D}_{AB} \frac{dY_A}{dx}$. The last term of Equation 1.7 shows that species A moves from a region of higher concentration to a region of lower concentration, where the negative sign causes flux to be positive about the x-direction [11].

The second and fourth steps from Gardiner's summarization are especially important to heterogeneous reactions. The second step accounts for adsorption, the act of the solid surface holding a gas-phase molecule, and the fourth step accounts for desorption of molecules that were formed at the surface and later released. These steps can be clarified by studying the adsorption/desorption rates independently of molecular conversion rates. Irving Langmuir, a chemical physicist, and Nobel Laureate, found relationships between adsorption and the partial pressure of the adsorbed gas [14], and equation 1.8 shows the Langmuir adsorption theorem:

$$\theta = \frac{bp}{1 + bp} \quad (1.8)$$

Where θ is the fraction of total adsorbed sites, b is the associated equilibrium constant, and p is the partial pressure of the adsorbed gas. Derivation of equation 1.8 can be found in chapter 7 of Gardiner's work.

Figure 1.2 gives a general visualization for carbon combustion with heterogeneous and homogeneous reactions. The four global mechanisms shown in the lower-left corner of Figure 1.2 are reactions in the boundary layer. The left wall is of pure carbon, and it can react with any of the gas-phase species as they diffuse inward. The species can then be adsorbed at the surface, react, and then desorb back into the gas phase. The most common of the desorbed species is carbon monoxide; however, it most often reacts with the inward diffusing species as well, most commonly forming carbon dioxide.

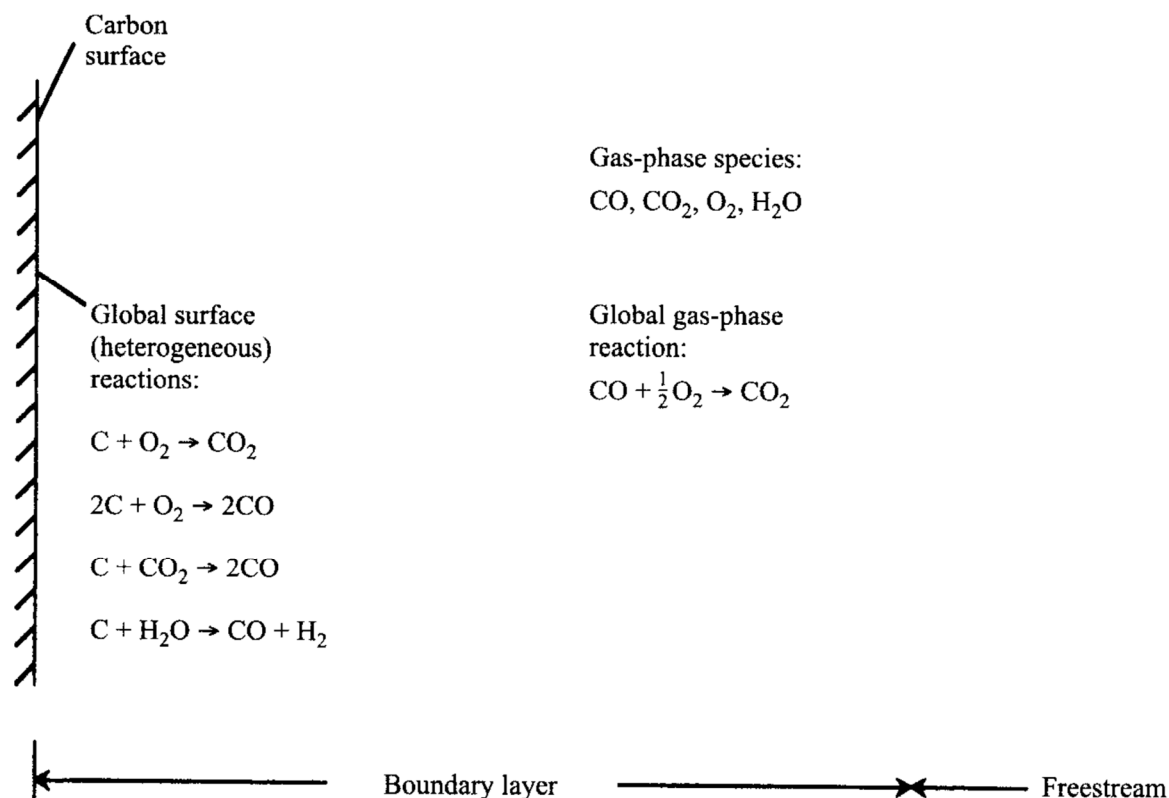


Figure 1.2: Carbon combustion and reactions.

It is important to note that all the reactions illustrated in Figure 1.2 are global reactions. There are several hundred elementary reactions simultaneously occurring, which is described by the third step in Gardiner's summarization. These elementary reactions are of particular importance because their chemical-kinetic parameters control the burning rate during combustion. However, the reaction mechanism is unknown due to the large number of conditions that add complexity to their analysis. The work of Caram and Amundson provides a simplified model for diffusion and reaction in the boundary layer surrounding a burning carbon particle, but their study ignores factors like intraparticle diffusion, convection, and requires guessing of the surface temperature. Their paper summarizes and validates 12 models predating 1977, and compares many methods used to investigate carbon combustion [15].

1.5 Evolved Gas Analysis

Evolved gas analysis (EGA) is the measure of volatile products from a substance during temperature-controlled tests. It differs from evolved gas detection in that it quantifies the products rather than only identifying them. Most commonly, EGA is used in conjunction with thermal analysis techniques like TGA. It is these simultaneous methods that have led to the determination of widely accepted rate expressions associated with solid combustion. There are various types of evolved gas analyzers, some quantify products intermittently while others record results continuously, and there are different methods of analysis like gas chromatography or mass spectrometry. EGA performed for chapters 2 and 3 of this report were done using a non-dispersive infrared (NDIR) analyzer and a Fourier-transform infrared spectrometer (FTIR), respectively, and these instruments will be the focus of discussion herein.

The following is a list of issues one should consider while performing EGA and is summarized from Thermal Analysis – Techniques and Applications by Warrington [16].

1. The product/purge gas mixture should not travel far from the source of the products to the detector.
2. The products should be transported to the detector as quickly as possible. This lowers the chance of diffusion broadening and helps ensure simultaneous recording between the EGA and TGA.
3. The transfer line should be inert.
4. The response time of the detector should be considered.
5. Products and purge gasses need consideration when choosing the material and size of the interface.
6. Optimum flow rates of the TGA and EGA may differ, and collection methods may need

adjusting accordingly.

7. The performance of the TGA and the conditions of the experiment should not be compromised.

These guidelines were considered before starting the experimentation described in chapters 2 and 3, as well as reconsidered while analyzing results.

1.5.1 NDIR Gas Analysis

For testing described in chapter 2, the exhaust from the Q500 TGA evolved gas furnace was coupled to a Fuji model ZRE NDIR gas analyzer. The analyzer simultaneously measures the concentration of SO_2 , NO , CO_2 , CO , and CH_4 by using the Lambert-Beer law to measure the absorption spectrum of molecules in a waveband of infrared rays [17]. The Lambert-Beer law is given in equation 1.9.

$$A = \epsilon lc \quad (1.9)$$

Where A is a substance's capacity to absorb light known as absorbance, ϵ is the absorptivity constant, l is the length of the analyzer's optic cell, and c is the concentration of the substance being analyzed. Since optic cell length can be measured and the absorptivity constant is known for many gasses, only the absorbance is needed to measure the concentration of species. The absorptivity is found by measuring the intensity of the infrared spectra before and after it passes through the sample and then using equation 1.10 to solve for A .

$$A = -\log \left(\frac{I}{I_0} \right) \quad (1.10)$$

Where the ratio of infrared intensity before and after the sample, $\left(\frac{I}{I_0} \right)$, is called transmittance and is a common vertical axis for infrared spectrum plots. A principle diagram for the analyzer

is shown in Figure 1.3. In the diagram, infrared radiation moves from the source across a spinning wheel, the chopper, and is split into each of the two gas cells. The chopper corrects for offset and gain of the instrument, and some choppers have IR filters to allow the concentration of several gasses to be measured in the same cells. Absorption of IR energy by gas molecules in the sample cell cause a pressure imbalance between reference and sample cells; the imbalance is detected and converted to an electrical signal [16].

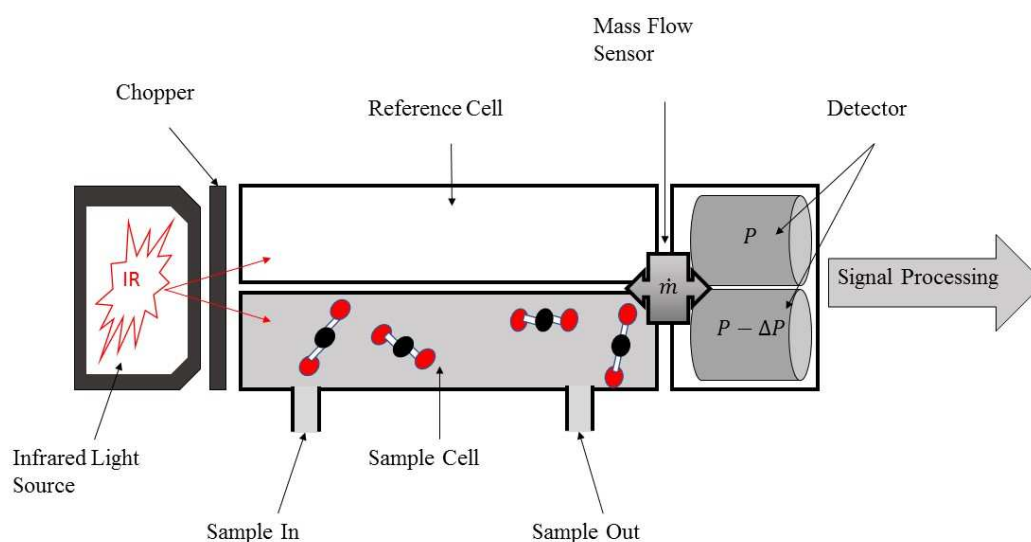


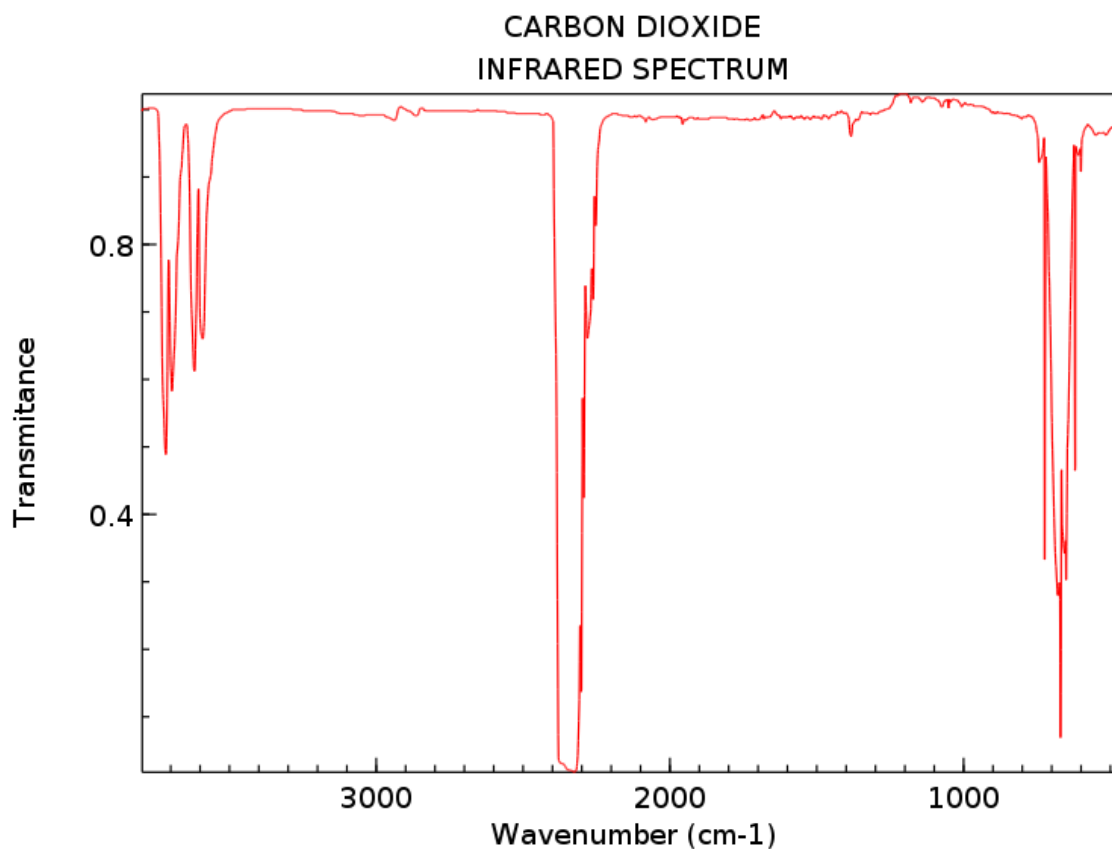
Figure 1.3: Principle diagram for NDIR type analyzers

Results from NDIR analysis are described in chapter 2.3.3 and shown in Figures 2.3 and 2.4. The figures are good examples of how NDIR type analyzers can be used in series with TGAs to create data for product gas evolution.

1.5.2 Fourier Transform Infrared Spectroscopy for Gas Analysis

Fourier Transform infrared analysis shares many similarities with NDIR gas spectroscopy, but it also has many advantages. The working principle for the two types of analyzers is similar in

that infrared energy is passed through a sample, and the energy absorbed by the molecules in the sample is detected and converted to data. However, the manner in which FTIR analyzers source infrared radiation allows them to identify and quantify unknown materials more completely and quickly. After data collection, FTIR analyzers yield plots called IR spectrums, the data of which is unique to all mixtures. A report by instrument manufacturer Thermo Nicolet summarized the nature of IR spectrums well, “An infrared spectrum represents a fingerprint of a sample with absorption peaks which correspond to frequencies of vibrations between the bonds of the atoms making up the material. Because each different material is a unique combination of atoms, no two compounds produce the same infrared spectrum. Therefore, infrared spectroscopy can result in a positive identification (qualitative analysis) of every different kind of material. Also, the size of the peaks in the spectrum is a direct indication of the amount of material present.” [18]. An example spectrum for carbon dioxide from the National Institute of Standards and Technology (NIST) is shown at the top of Figure 1.4. The horizontal axis of the figure represents the wavelength of infrared energy absorbed by molecules in the sample, and the vertical axis is of transmittance, which is described in the previous section following equation 1.10. Below the example is a spectrum measured with an FTIR analyzer from the exhaust gas of bituminous coal, which was heated in a TGA for experimentation described in chapter 3. The horizontal axis of the plot from chapter 3 is wavenumber in cm^{-1} like that of the carbon dioxide spectrum, but the vertical axis is of absorbance. The vertical axes of both plots differ; however, the relationship between the two qualities ensure that they have data in the same range of wavenumber so that the troughs of



NIST Chemistry WebBook (<https://webbook.nist.gov/chemistry>)

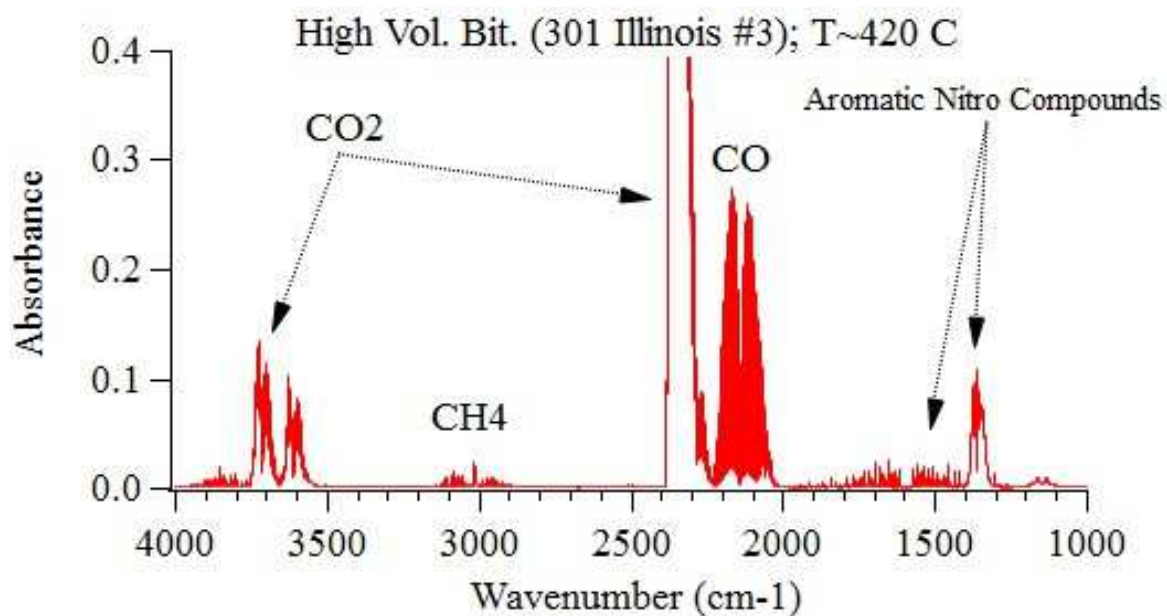


Figure 1.4: Top is an example IR spectrum of CO₂ from NIST, bottom is FTIR spectrum results of experiments on coal samples from chapter 3.

transmittance has the same wavenumbers as the peaks of absorbance. The two plots share data at wavenumbers between 2200-2400 cm^{-1} and again between 3500-3800 cm^{-1} , these shared frequencies show that there is carbon dioxide present in the sample of coal from chapter 3 experiments. Computers use the same logic to find and identify the substances present during FTIR spectrometry. An additional trough in the plot for carbon dioxide under 1000 cm^{-1} is in what is known as the fingerprint region. Many molecular groups have vibrational resonance in the fingerprint region (800-1800 cm^{-1}), but the spectrum can be crowded with many peaks that make it difficult to identify chemical structures [19].

Early IR spectrometers were dispersive; they used an instrument called a grating to separate (disperse) the IR spectrum into individual frequencies in the same manner that a prism separates visible light into colors. These instruments require that energy be measured at each frequency of IR light and the intensity of that energy be recorded, but the method is slow and operates in narrow frequency ranges. FTIR analyzer's most significant advantage over dispersive IR detectors is their ability to measure all frequencies rapidly; this advantage is a result of a device called an interferometer. The first and most common version of these is named the Michelson Interferometer; it operates by producing an IR signal, which is a function of a change in pathlength between two IR beams. The working principle for a Michelson Interferometer is shown in Figure 1.5. The figure shows IR light leaving the broadband source, meaning the source emits a larger spectrum of wavelengths than is to be measured by the detector. The light is separated by a beam splitter which transmits half of the light, ideally, to the fixed mirror opposite the source and reflects the rest of the light to the moving mirror. The separated beams of light reflect off the mirrors, recombine at the beam splitter, and are directed through the sample and into the detector. One mirror is in a fixed position, and the other mirror moves

toward and away from the beam splitter. Some mirrors in interferometers rotate toward and away from the perpendicular path of the beam instead of moving in and out, but in either case, the motion causes the signal at the detector to vary sinusoidally with frequency $\omega = V_m/\lambda$ where V_m is the velocity of the moving mirror, and λ is the wavelength of IR light. The intensity of the light and position of the mirror are recorded and compared, the result of which is called an interferogram. Computers then use a fast Fourier transform to convert the detected signal as a function of the difference in path length (retardation) to a function of wavelength. The signal is also converted to transmittance or absorbance and plotted against wavenumber, as shown in

Figure

1.4

[20].

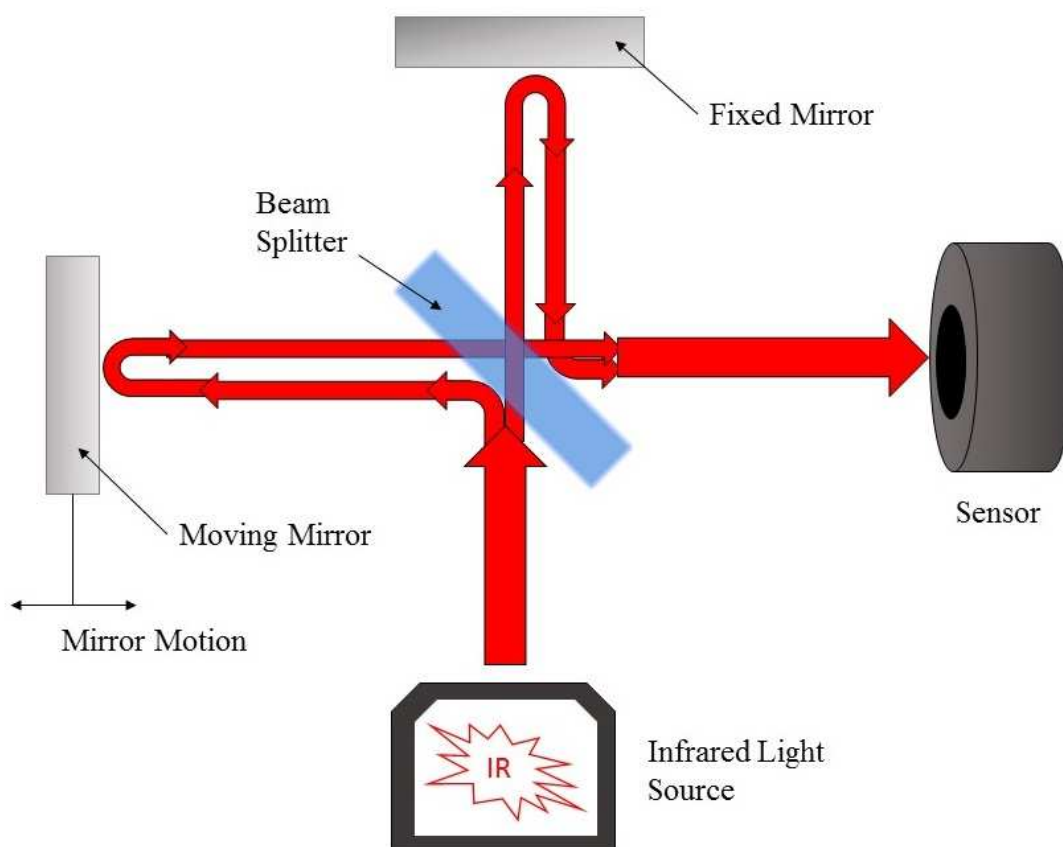


Figure 1.5: Principle diagram for Michelson Interferometer.

A general understanding of the Michelson interferometer provides a general understanding of Fourier transform infrared spectrometers. However, there is more information available regarding the FTIR spectrometry than can be addressed by this introduction. For example, the first experiment dedicated to the Michelson interferometer was performed by its inventor, Albert Michelson, and a chemist, Edward Morley. The experiment used the interferometer to find the speed of light with great accuracy, which leads to Einstein's theory of relativity and can be studied with greater detail in The Gale Encyclopedia of Science [21]. There are also many advantages FTIR spectrometers have over other analyzers, like higher signal-to-noise ratios and higher frequency accuracy. Methods of how to optimize these advantages are discussed in detail in the work of Ferraro [20]. The mathematics developed by Joseph Fourier, the fast Fourier transform algorithm, and the Cooley-Tukey algorithm used to convert signals for FTIR spectrometers are interesting and in-depth studies also and are explained well in the work of Kauppinen and Partanen [22]. There are countless books, articles, and papers on FTIR spectroscopy; in fact, the development of the instrument and understanding of material information the spectrometers provide remain to be researched by scientists and students in the future.

1.6 Intentions of this Study

This thesis on oxidation of coal and graphite consists of four chapters. This section concludes chapter 1 and has provided a basic description of principles and equipment used for experimentation explained in chapters 2 and 3. Both chapters are of previously submitted and accepted conference papers whose results were presented for the Combustion Institute. The details of the conferences and papers are listed below.

- Chapter 2: S. Stuhlman and K. Kumar "*Combustion of Graphite Nanoparticles with*

Copper (II) Oxide in a Thermogravimetric Analyzer with Evolved Gas Analysis," Paper 38IE-0021, Fall Technical Meeting of the Western States Section of the Combustion Institute, Oregon State University, Cascades, March 25-27, 2018.

- Chapter 3: S. Stuhlman and K. Kumar "*Modulated Thermogravimetric Experiments on Argonne Premium Coal Samples with Combustion Gas Analysis,"* Paper 71CB-0260, 11th U. S. National Combustion Meeting, Pasadena, California, March 24-27, 2019.

Chapter 2 is the description of procedures and results obtained by TG analysis on a stoichiometric mixture of graphitic carbon and copper oxide heated beyond combustion. The results include TG curves, activation energy, CO and CO₂ product gas datum, and elemental composition of solid reactants.

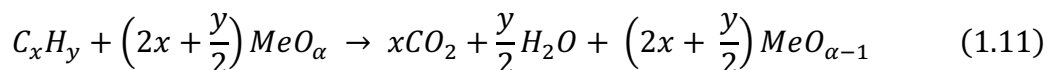
Chapter 3 describes TG-FTIR analysis conducted on the set of Argonne Premium Coals, which were selected by the U.S. Department of Energy to provide the scientific community consistent samples of American Coal. The TGA and evolved gas analysis results for various ranks of coals are provided as well as discussion on the relative experimental activation energy trends for the coals.

The thesis is concluded in chapter 4. Additionally, the chapter discusses CLOU techniques related to chapter 2 results and provides specific data values concerning chapter 3. The sections are followed by suggestions for additional experiments to progress the work performed for this study. Before chapters 2 and 3 brief explanations of the principles concerning the chapters are provided in sections 1.6.1 and 1.6.2.

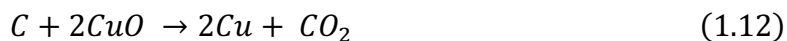
1.6.1 Solid Oxygen Carriers

Studies on solid oxygen carriers (OCs) typically are related to chemical looping combustion (CLC). While chemical looping is not fully performed in chapter 2 experiments, a basic

description of its process is useful in understanding the nature of solid OC research. CLC is a process where fuel is combusted for energy in the absence of air. A metal oxide is added to the process to supply oxygen for combustion. After combustion, the oxygen has bonded to carbon in the fuel to form CO_2 and the solid product is pure metal. The metal is then moved from the reduction reactor, where combustion occurs, to the oxidation reactor, where it re-oxidizes to again form metal oxide, which is returned to the reduction reactor to again act as oxygen carrier. The absence of air and control of temperature during combustion help ensure that the gaseous product of reaction is pure CO_2 , this product can be captured and used instead of released into the atmosphere as a pollutant. Equation 1.11 shows the ideal global equation for the reduction process:



Where Me represents the metal contained in the metal oxide, and α the amount of oxidizer. Experimentation in chapter 2 used pure graphitic carbon mixed stoichiometrically with copper oxide; therefore, the equation can be simplified to:



In both equations, the carbon dioxide is separated from the rest of the products, and more importantly, it is the only gaseous product. It is this separation of states that allows the CO_2 to so easily be separated from the rest of the products and stored rather than released into the atmosphere.

The most significant distinction between chemical looping combustion and the study described in chapter 2 is that oxidization was not performed in the experiments, and therefore, the experiments lack any cyclic nature. Rather the carbon/copper oxide mixture was analyzed at

several heating rates in the TGA and N_2 was used to purge gaseous products from the evolved gas furnace to the NDIR analyzer.

1.6.2 The Premium Argonne Sample Program

For discussion in chapter 3, the weight loss profiles of the eight Premium Argonne Coal samples were found using a TGA. Additionally, modulated TGA methods were used to obtain activation energies associated with the process, and FTIR evolved gas analysis was performed to observe the evolution trends in CO and CO₂ evolution. The samples provided a good range of results because they were chosen to have different concentrations of composition parameters C, H, O, and S. Each sample type was mined from a different seam, and great effort was taken to provide researchers across the nation with sets of samples which are as chemically and physically identical as possible. The introduction of chapter 3 includes table 3.2, which lists the name of each sample, the location it was mined, and its composition. The table is shown again in this section to accompany the description of how coals are ranked, provide details on the composition of each Argonne Premium Coal, and help visualize the reason each coal was selected for the program.

According to Vorres, the samples were selected by using the Pennsylvania State Coal Sample Database to plot composition data for 200 samples of U.S. coal with carbon and oxygen content on one axis vs. hydrogen and sulfur content on the other. Maceral groups were also considered, and one coal was selected for its coking properties. Coal consists of fossilized remains of buried plant debris which underwent chemical changes from temperature and pressure over time, this process is called coalification, and the type of plant matter which changed defines the maceral type. There are three classifications of macerals; liptinite, inertinite, and vitrinite. The vitrinite group consists of vascular land plant remains, liptinite is made from plant and animal remains

derived from algae and bacteria, and inertinite is comprised mainly of charred remains like burnt peat [23]. Heat and pressure increase the rank of coal over time, with the lowest ranks being lignite and brown coal, then increasing to sub-bituminous, bituminous, and anthracites. However, anthracites were not used because they have low reactivity and are relatively scarce. As the rank increases, so does the concentration of carbon, because of this the moisture content decreases. Coals with strong caking properties soften and form a solid product called coke as they are heated then cooled. The properties caking coals possess are useful in the production of liquid metals in blasting furnaces, but not as useful for energy production through combustion [24].

Table 3.2: Table from chapter 3 shows Argonne Premium Coal Samples and Characteristics.

	<i>Seam</i>	<i>State</i>	<i>Rank</i>	<i>C</i>	<i>H</i>	<i>O</i>	<i>S</i>	<i>Ash</i>
1	Upper Freeport	PA	Med. Vol. Bit.	86	4.7	8	2.3	13
2	Wyodak-Anderson	WY	Subbituminous	75	5.4	18	0.6	9
3	Illinois No. 6	IL	High. Vol. Bit.	78	5.0	14	4.8	15
4	Pittsburgh (No. 8)	PA	High. Vol. Bit.	83	5.3	9	2.2	9
5	Pocahontas No. 3	VA	Low. Vol. Bit.	91	4.4	2	0.7	5
6	Blind Canyon	UT	High. Vol. Bit.	81	5.8	12	0.6	5
7	Lewiston-Stockton	WV	High. Vol. Bit.	83	5.3	10	0.7	20
8	Beulah-Zap	ND	Lignite	73	4.8	20	0.8	10

Table 3.2 shows the seam and state each coal was mined, the rank, and composition, including ash. Vorres states, “Samples 1, 2, 3, 5, and 8 were selected to give a range of compositional parameters, primarily carbon, hydrogen, oxygen, which vary with the degree of coalification of the sample. In addition, no. 3 provides a sample with relatively high sulfur content. Coal no. 4 was also selected for its known good coking properties, coal no.6 was selected for high liptinite, and coal no. 7 was selected for high sporinite and inertinite contents.” [25]

An understanding of the logic followed to select coal sample types for the Premium Argonne Coal Sample Program is beneficial in understanding the results explained in chapter 3. Those results were obtained through experimentation on kinetic rates, activation energies, and evolved gas products of the coal samples, all of which are affected by elemental composition and moisture content. Chapter 4 of this study discusses areas of results from chapter 3 that align with what one would expect from analysis on a variety of coal ranks, areas that differ from expected results, and possible explanations for both. However, first, it is advised to read chapters 2 and 3 to familiarize one's self with the experimentation which was performed and the results obtained.

2 Combustion of Graphite Nanoparticles with Copper (II) Oxide in a Thermogravimetric Analyzer with Evolved Gas Analysis

2.1 Introduction

The combustion of fossil fuels provides for the bulk of our energy needs and is largely responsible for environmental pollution. Combustion of solid fuel such as coal is expected to remain at current levels over the next three decades [26]. It is, therefore, important to develop technologies that will alleviate problems arising out of fossil fuel combustion while utilizing them in the most efficient manner. The idea of using a solid oxygen carrier to burn coal and natural gas to enable the efficient capture of carbon dioxide has gained much attention in the past decade [27-29]. Much effort has also been dedicated to the development of novel oxygen carriers for chemical-looping combustion [30-34]. A thermogravimetric analyzer (TGA) has been frequently used as a laboratory tool to study combustion and pyrolysis in the solid-state. It is a technique in which the variation in the weight of a reacting substance is monitored as it is subjected to a controlled variation of temperature in a suitable environment [2]. The TGA, when coupled to additional diagnostic tools, can provide valuable information on the kinetics of solid fuel oxidation. The objective of this study is to understand the combustion of carbon in its graphitic form with copper oxide as the oxygen carrier. Conventional TGA analysis is augmented with evolved gas analysis and energy dispersive x-ray spectroscopy to follow the progress of reactions for the graphite-copper oxide system.

2.2 Experimental Apparatus and Procedure

A Q500 thermogravimetric analyzer from T.A. Instruments was used for the current study. The TGA is equipped with an evolved gas analysis furnace. The evolved gases were analyzed using a non-dispersive infrared analyzer capable of detecting carbon monoxide, carbon dioxide, and

methane.

The reactants consisted of graphite and copper oxide nanoparticles obtained from US Research Nanomaterials Inc. The graphite and copper oxide powders had particle sizes in the range 400 nm to 1.2 microns and 40 nm, respectively. The fuel and oxidizer were stoichiometrically mixed by dissolving them in methanol and mixing them at 1000 rpm for ten minutes. The slurry obtained was poured over a Pyrex tray, and the methanol was allowed to evaporate. The solid residue was then scraped, and ball milled for 20 minutes. An IKA Ultra-Turrax tube drive system was used for both homogenization and ball milling. No further particle size characterization for the mixture was done. The powder was then poured into a glass vial, which was heated to a temperature of 40°C for 4 hours.

For experimental testing, approximately 100 mg of the solid premixture was loaded onto 100 µl platinum pans and subjected to heating rates of 5, 10, 15, and 20°C per minute with a nitrogen purge gas flow of 120 ml/min. Both the TGA and the NDIR analyzer acquired data at a rate of 2 Hz in a synchronous manner. The exhaust of the TGA was connected to the NDIR analyzer by 1/8-inch tubing of length 120 cm to minimize dead volume and diffusional spreading of the gas concentration signal. The NDIR provided measurements of carbon dioxide and carbon monoxide. The gas analyzer was spanned and zeroed, and the sample pan for the TGA was tared before each experiment.

2.3 Results

The progress of the reactions was followed through weight loss, gas evolution, and dispersive x-ray spectroscopy. Modulated TGA experiments were also conducted to obtain the activation energy as the sample was heated at a prescribed ramp rate with temperature modulation. The following sub-sections describe the results obtained using each of these techniques.

2.3.1 Sample Weight Loss during Heating

The reduction of sample weight percent as the furnace temperature is increased at various ramp rates is shown in Figure 2.1. The samples were heated at specified heating rates starting at room temperatures and were held at 975°C for twenty minutes. As expected, higher heating rates lead to reduction in time needed to initiate the combustion reactions. An appreciable loss in the weight of the sample begins at approximately 620°C, and subsequently, there is a continuous variation in slope of the weight loss versus temperature curve.

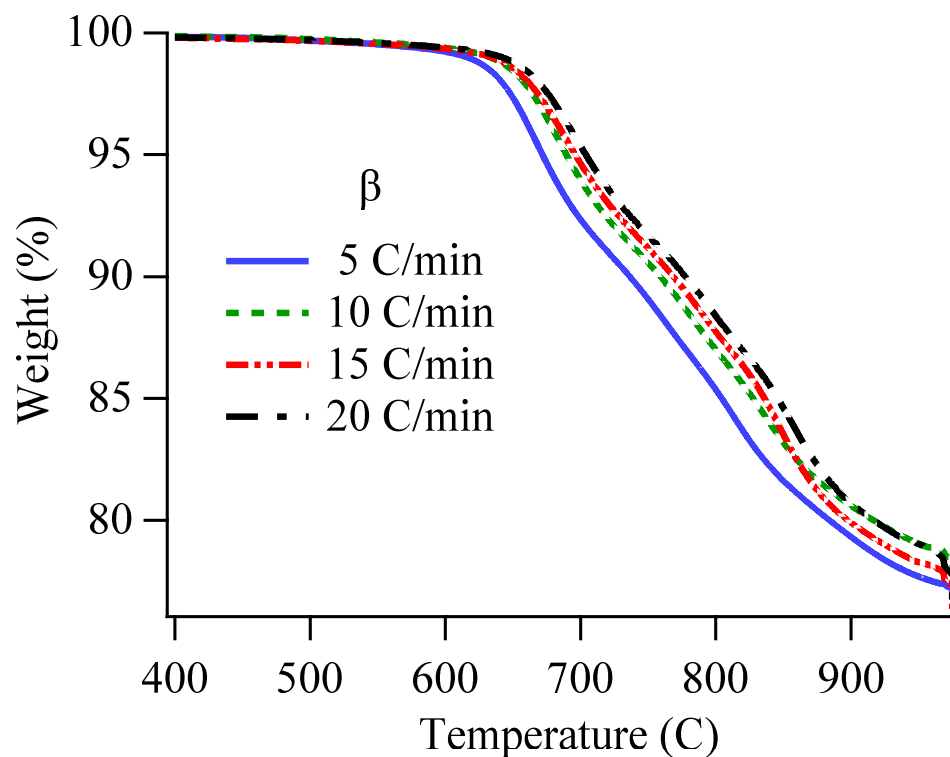


Figure 2.1: Weight loss vs. temperature with for various heating rates.

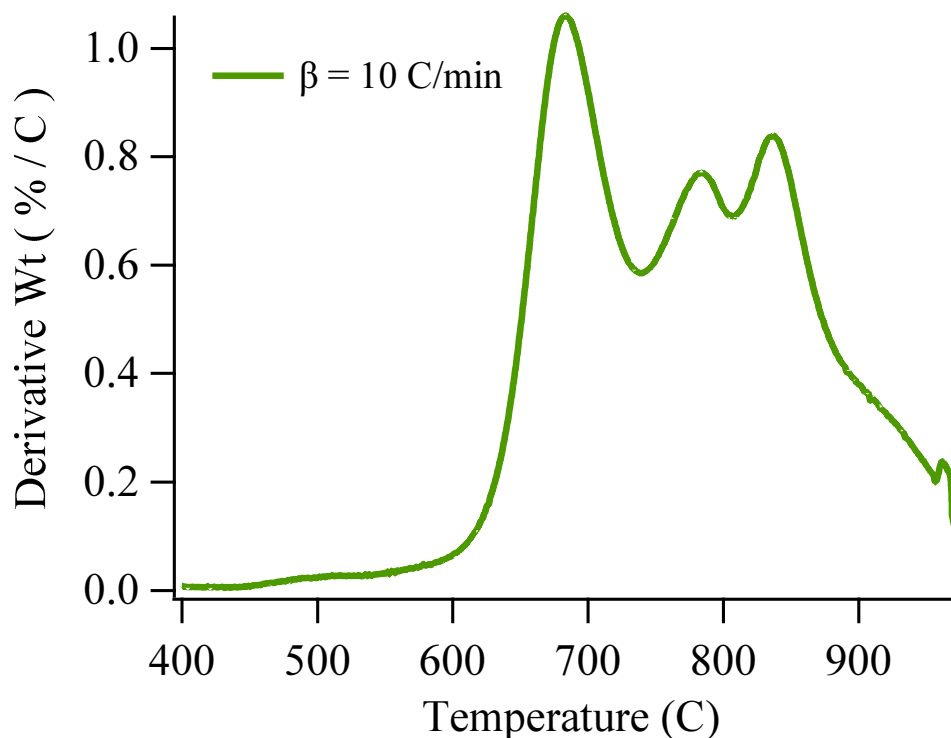


Figure 2.2: Derivative weight with respect to temperature for 10°C/min heat rate.

The maximum rate of weight loss occurs at approximately 690°C, as can be seen in Figure 2.2. This is followed by two additional peaks of a lower magnitude in the vicinity of 780 and 840°C. These values of temperature correspond to a heating rate of 10°C/min, and very similar values can be seen for other heating rates as well.

2.3.2 Effect of Heating Rate on Conversion

The effect of heating rates on the fractional conversion (α) as a function of time are shown in

$$\alpha = \frac{W_i - W(t)}{W_i - W_f} \quad 2.1$$

Where W_i and W_f are the initial and final sample weights, and $W(t)$ is the sample weight at time t during the heating process. Figure 2.3 shows that between the initial and terminal regions, the rising part of the curves are made up of at least three sub-regions with varying slopes.

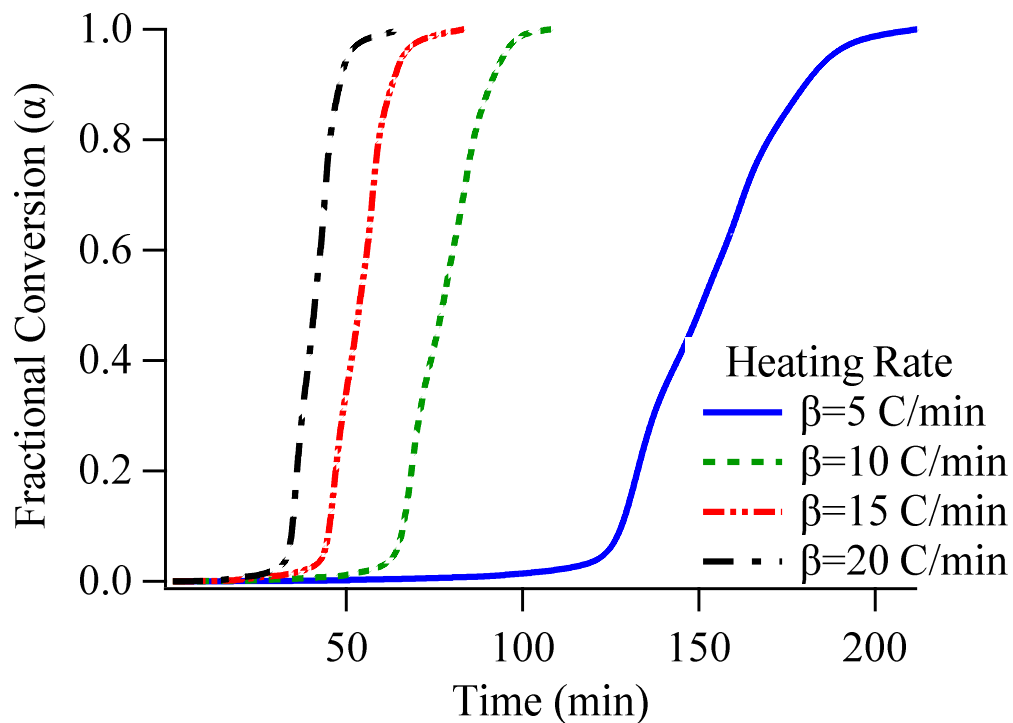


Figure 2.3: Fractional conversion at various heating rates.

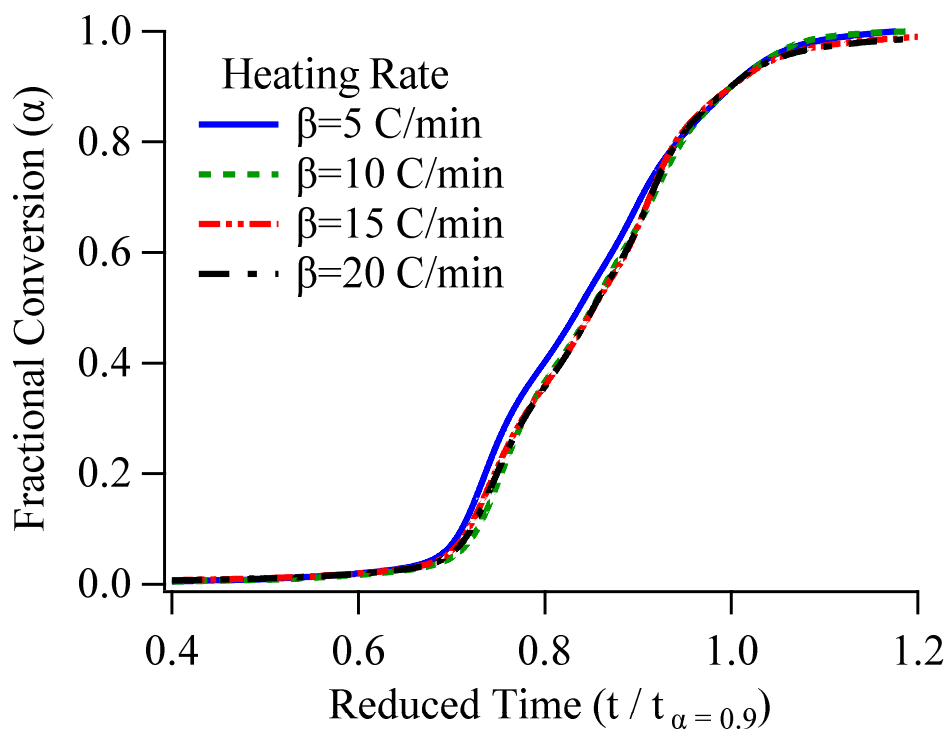
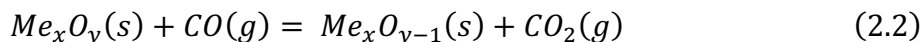


Figure 2.4: Fractional conversion as a function of reduced time.

The existence of sub-regions with different slopes is readily apparent at the low heating rates, but less so at higher heating rates in Figure 2.3. However, if one plots the fractional conversion as a function of reduced time ($t_r = t/t_{\alpha=0.9}$), as shown in Figure 2.4, the regions associated with distinct slopes become apparent at all heating rates. Furthermore, it is interesting to note that the curves for different heating rates collapse together when plotted as a function of reduced time. The existence of various sub-regions with varying slopes precludes the possibility of representing the rate of fractional conversion as a simple function of time i.e. $\frac{d\alpha}{dt} = f(\alpha, T)$. The mechanism of oxidation for carbon has been known to involve gas-solid processes instead of direct solid-solid reactions on account of gaseous intermediaries such as CO and CO₂, which allow for efficient transfer of carbon to the oxygen in the oxide [35]. It has been shown to involve the following reaction steps [36].



2.3.3 Evolved Gas Analysis

The evolution of gaseous products of reaction was tracked using a NDIR analyzer. Figure 2.5 shows evolved gas analysis and thermogravimetric data with respect to temperature from an experiment with a heating rate of 10°C/min. The purge gas flow rate is fixed at 120 ml/min. The plot shows a very early production of carbon monoxide that begins close to 400°C, attains a local peak, and then goes through two additional peaks and valleys. The minima in the first valley of CO production appears to trigger a rapid CO₂ production around 600°C. The production of carbon dioxide is also associated with three overlapping peaks that closely track the weight loss rate curve shown as blue dashed lines. A small, but perceptible, phase shift is evident between the rate of weight loss and the CO₂ production curves, with the CO₂ production

leading the rate of weight loss.

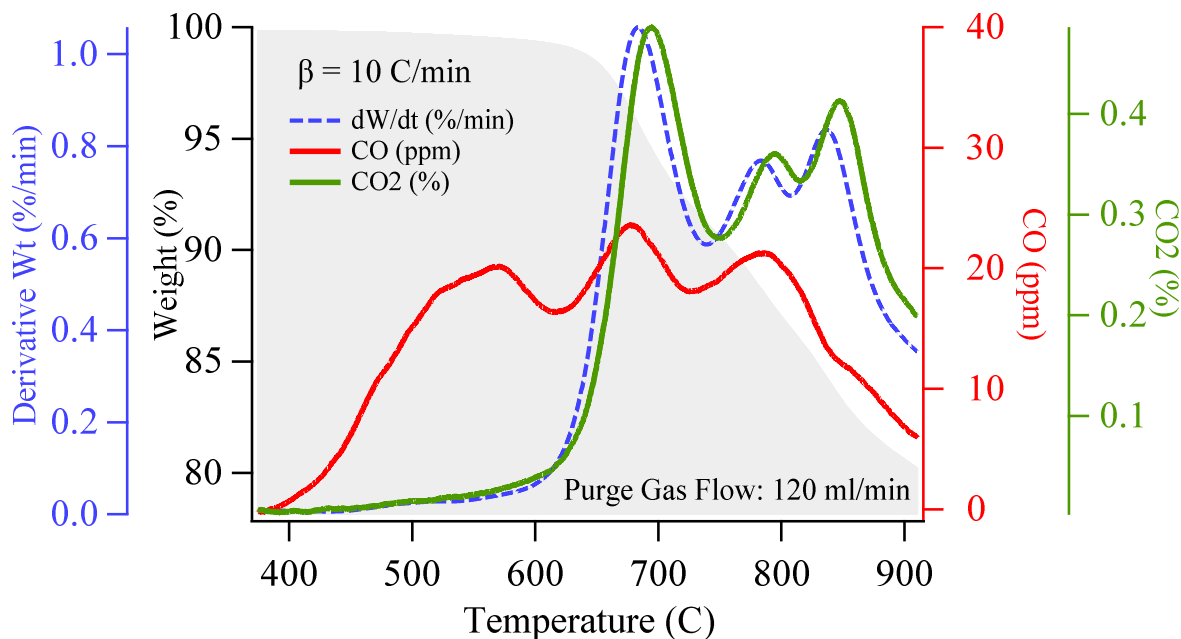


Figure 2.5: Evolution of CO and CO₂ with respect to temperature.

The continuous variation of the sample weight during the heating process is shown as a shaded area in the background. It is somewhat difficult to correlate the CO and CO₂ production over the entire temperature range based on the plots in Figure 2.5. The relationship between CO and CO₂ production can be examined in a much better manner if one looks at the trajectory of the reactions in the CO and CO₂ plane, as shown in Figure 2.6.

The initial cold conditions correspond to the bottom left-most point 0 in Figure 2.6, and the temperature increases as one traverses along the curve to its endpoint located again at the bottom left in the plot. The shading applied to the curve is based on the temperature of the system at the given point. The locus of the CO-CO₂ trajectory indicates that initially, there is a continual increase in the CO production with relatively low CO₂ being produced (0 → 1). At the peninsula corresponding to point 1 shown in Figure 2.6 the path moves towards a reduction

in CO production (1 → 2), and turns around sharply at point 2 in a very small temperature range 570-618°C and subsequently leads to sharp rise in CO₂ production with a minimal increase in CO production (2 → 3). It is almost as if the region (1 → 2), represents an unstable branch, and point 1 at 570°C is the ignition point, for this particular test case. A region of deceleratory production for both CO and CO₂ is seen in the region (3 → 4). This is followed by a slight uptick in both CO and CO₂ production for the region (4 → 5).

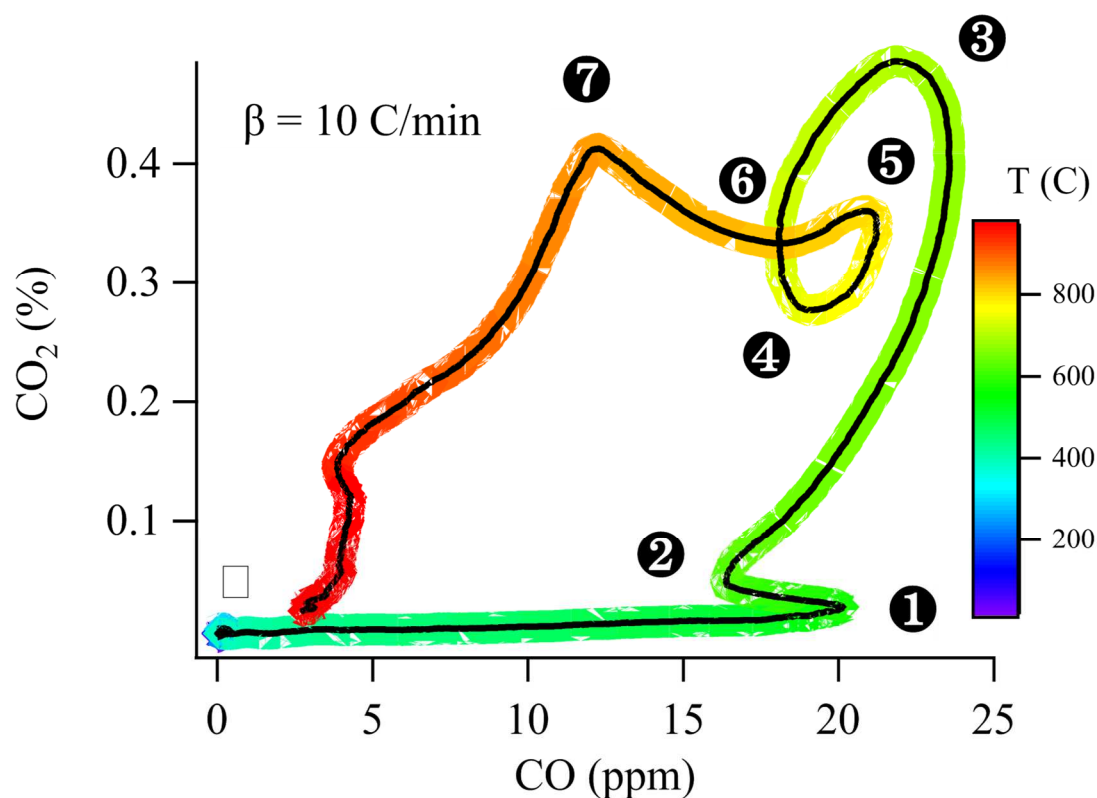


Figure 2.6: CO and CO₂ trajectory during the combustion of graphite with copper oxide.

From the trajectory shown in Figure 2.6, it appears that the system requires a buildup of a critical CO production rate before the combustion process picks up speed at point 1. It is also fair to conclude that the region 2 → 4 possibly represents the reaction step corresponding to $Me_xO_y(s) + CO(g) = Me_xO_{y-1}(s) + CO_2(g)$, as noted in equation 2.2.

2.3.4 Determination of Activation Energy

A modulated TGA experiment was conducted on the sample to obtain the kinetic parameters related to the combustion of stoichiometric graphite/copper oxide mixture. The details of this method are described in the work of Blaine and Hahn [9]. The method superposes a sinusoidal oscillation on the linear temperature ramp. The oscillating temperature is associated with a corresponding oscillatory heat flow. A discrete Fourier transform (DFT) deconvolution of the oscillating temperature and heat flow leads to a separation of the overall heat flow into a reversing (heat capacity component) and a non-reversing (kinetic) component [9]. For thermogravimetry experiments, they state that the rate of mass loss depends only on the kinetic term and the overall expression for the rate is shown to be:

$$\frac{d\alpha}{dt} = Z \times f(\alpha) \times e^{-\frac{E}{RT}} \quad 2.4$$

Here Z is the pre-exponential factor, $f(\alpha)$ the kinetic expression, and E the activation energy. An evaluation of equation 2.4 at adjacent peaks ($d\alpha_p/dt$) and valleys ($d\alpha_v/dt$), followed by taking a ratio of the two derivatives, provides an expression for the activation energy as:

$$E = \frac{RT_p T_v [\ln(d\alpha_p) - \ln(d\alpha_v)]}{T_p - T_v} \quad 2.5$$

The expression assumes that there is a minimal change in the reacted fraction, and consequently $f(\alpha)$, between an adjacent peak and valley. The resultant equation for the activation energy is therefore model-free as the expression for $f(\alpha)$ is not needed. The results for the modulated TGA experiment are shown in Figures 2.7 and 2.8. Figure 2.7 shows the signals for the weight percent, derivative of the modulated weight, and the linear temperature ramp with the superposed temperature oscillations as a function of time. The peaks and valleys

in the derivative of the modulated weight are quite apparent. The experimental case shown in Figures 2.7 and 2.8 was run at a ramp rate of $2^{\circ}\text{C}/\text{min}$ to 975°C , and the temperature modulation amplitude was set to $\pm 4^{\circ}\text{C}$ over a 200-second duration.

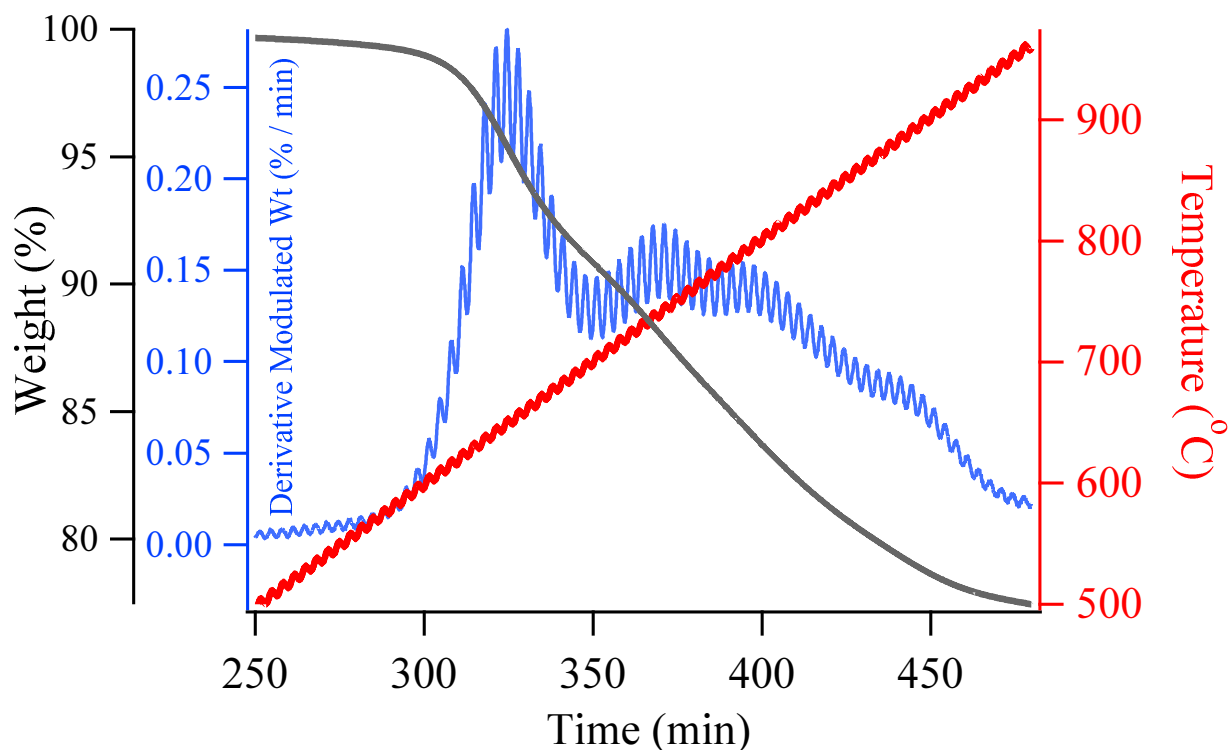


Figure 2.7: Modulated temperature, weight loss, and modulated derivative weight as a function of time.

The modulated TGA experiment enables the determination of the activation energy over entire temperature range of interest. This method is particularly useful when the weight loss is not characterized by a single reaction but may be a result of several competing processes.

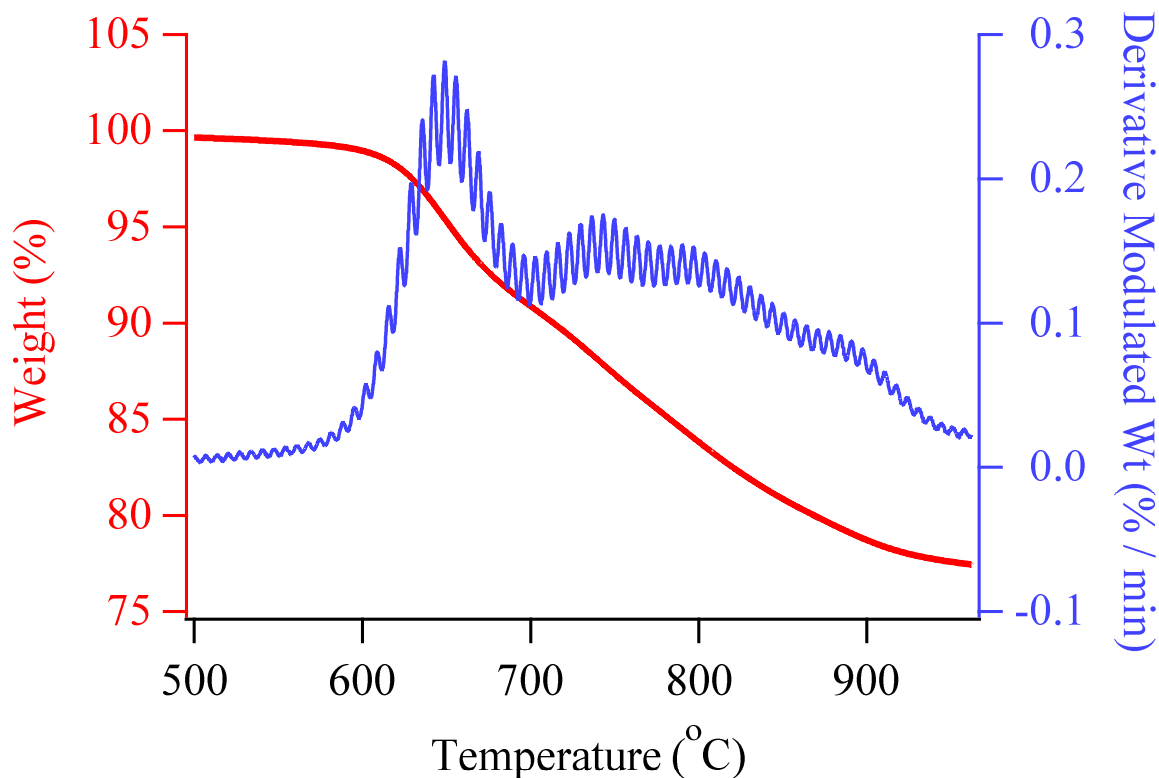


Figure 2.8: Weight loss and derivative of modulated weight as a function of temperature.

As seen in Figure 2.8, we have the evolution of at least two components (CO and CO_2) occurring simultaneously and at varying rates through the entire process of heating. The plots for activation energies are continually plotted as a function of temperature in Figures 2.9 and 2.10. The plot in Figure 2.9 shows the activation energy plotted alongside the weight loss curve, while that of Figure 2.10 represents it alongside the derivative of the weight loss with respect to temperature.

A closer examination of Figure 2.10 shows that there are two peaks that occur in the activation energy plot at 667 and 741°C, corresponding to activation energies of 255 and 279 kJ/mol, respectively. The two points are annotated as E_1 and E_2 in Figure 2.10. The two peaks correspond to the two maxima observed in carbon dioxide evolution during the heating process, as can be seen by referring back to Figure 2.5. It can also be seen that in the region between E_1

and E_2 , there are at least two overlapping peaks. The low heating rates used in the modulated TGA experiments helps separate out the peaks to a much better extent compared to higher ramp rates [10].

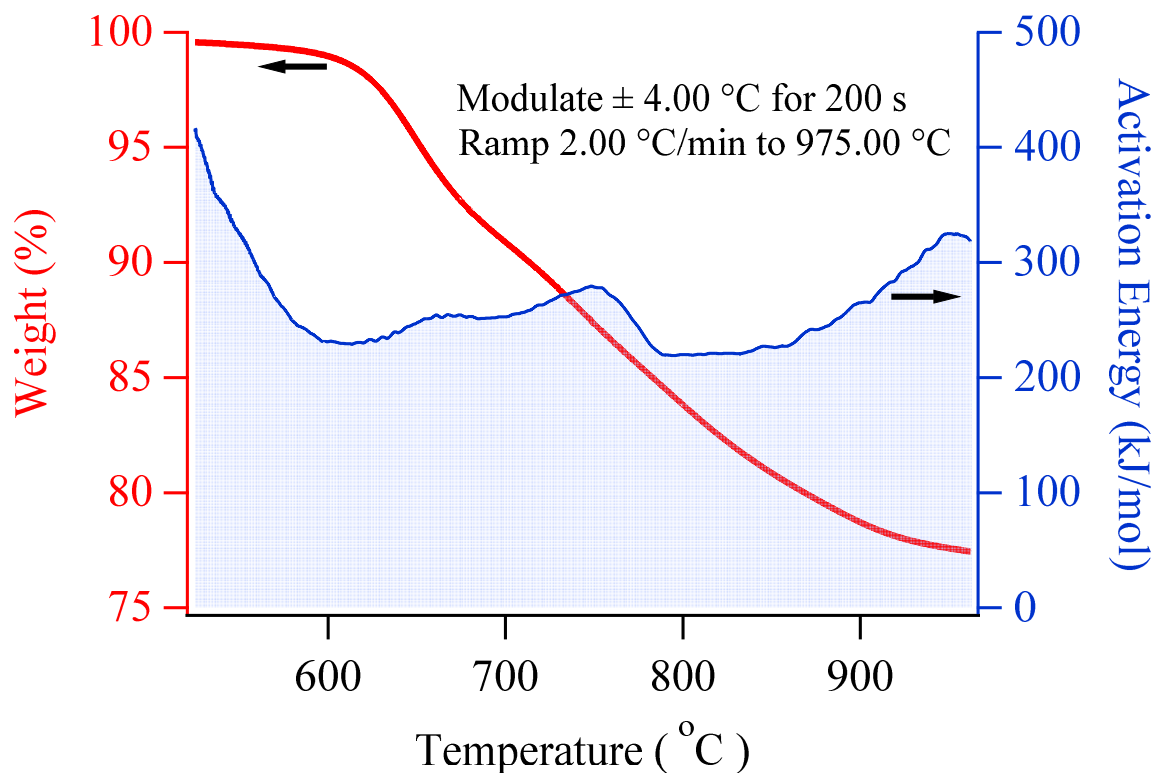


Figure 2.9: Activation energy and weight loss profiles as a function of temperature.

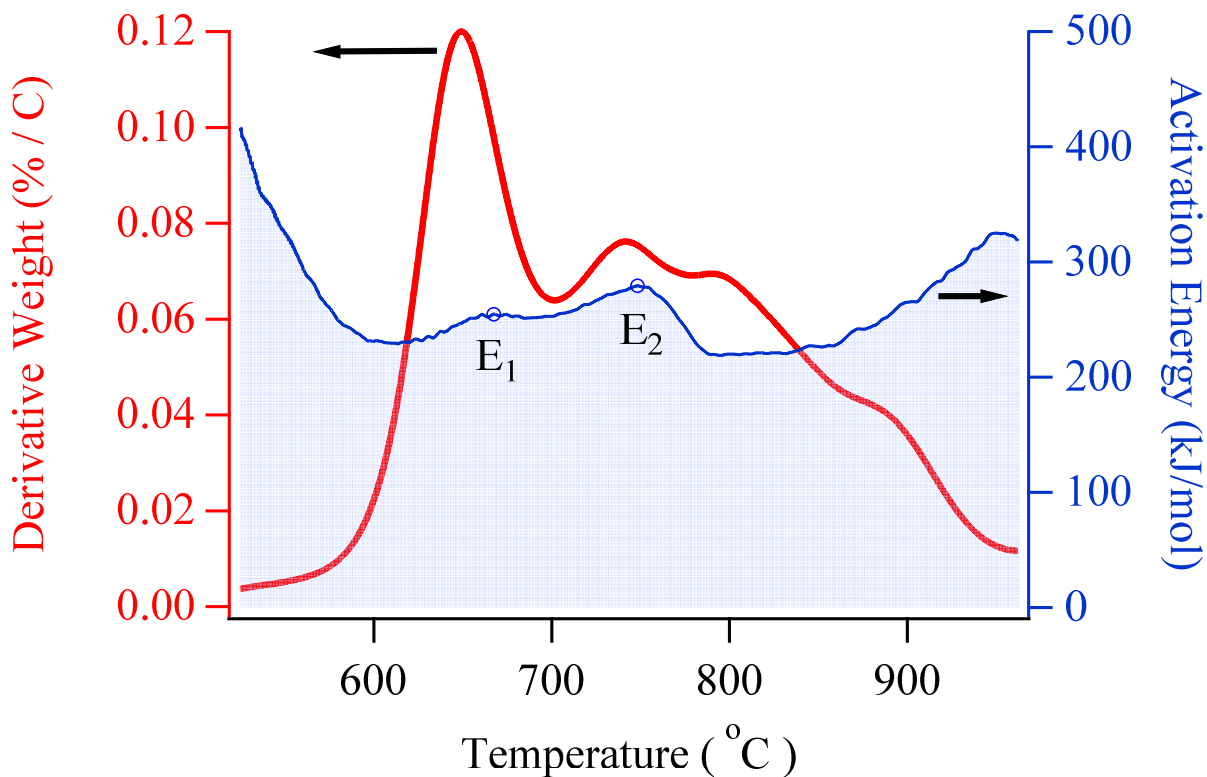


Figure 2.10: Activation energy peak values compared with derivative weight.

2.3.5 Energy Dispersive X-ray Spectroscopy Analysis

The progress of the reactions during various stages of heating was also followed by Energy Dispersive X-ray spectroscopy (EDS). A set of samples was prepared where each was heated to a specific temperature and removed from the TGA furnace to freeze the reaction. The heating rate for each of the samples was set to 10 degrees per minute. SEM images of the product samples during various stages of combustion are shown in Figure 2.11(a)-(d). The first image is of an unreacted sample. The remaining images are of samples heated to 551, 676, and 975°C, respectively. Each image has points labeled 1 through 4 with crosshairs. Each of the four points in a given image correspond to a location for obtaining the EDS spectrum.

A visual examination of the images shows that the unreacted sample consists of particles that are typically smaller than 20 microns. The sample particles tend to agglomerate and increase in

size as the reaction proceeds due to heating. The image shown in Figure 2.11(d) corresponds to the largest extent of conversion (88.79% Cu) and appears to be a contiguous porous structure where it is difficult to discern individual particles.

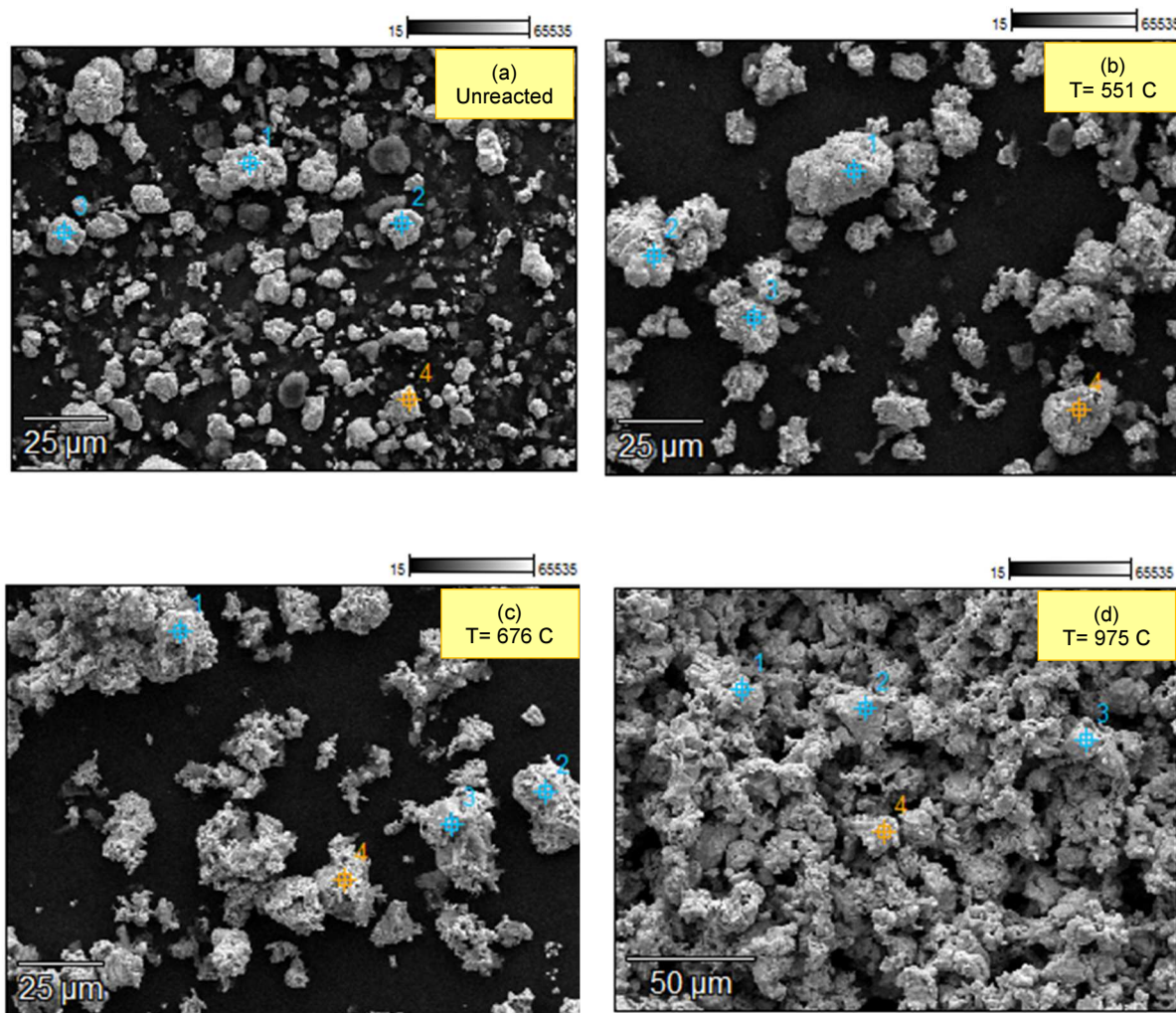


Figure 2.11: SEM images showing the state of the sample during various stages of reaction.

The EDS spectrum corresponding to the average of the four points shown in Figure 2.11(a) is shown below as Figure 2.12. The copper and oxygen weight percentages obtained from the EDS spectrum for the unreacted sample show a composition corresponding to 78.99 % Cu and 9.17% O. As expected, this is very close to the elemental composition of CuO (79.89 % Cu). Note that carbon was excluded in the EDS analysis.

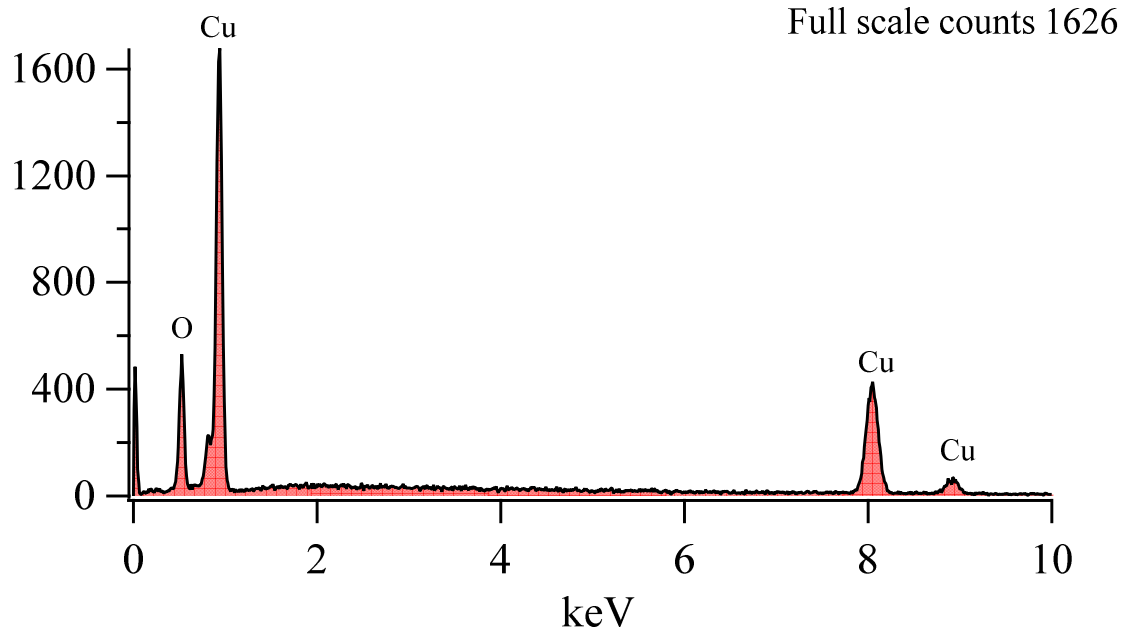


Figure 2.12: Energy dispersive spectroscopy analysis for unreacted mixture showing characteristics of copper and oxygen peaks.

Element weight percent of copper and oxygen were averaged over the four points chosen for each sample shown in Figure 2.11 (a)-(d), the results of which are shown in Figure 2.13, as a function of the respective sample quench temperatures. The conversion of CuO to Cu during the oxidation of graphite is seen to be a sigmoidal function over the temperature range.

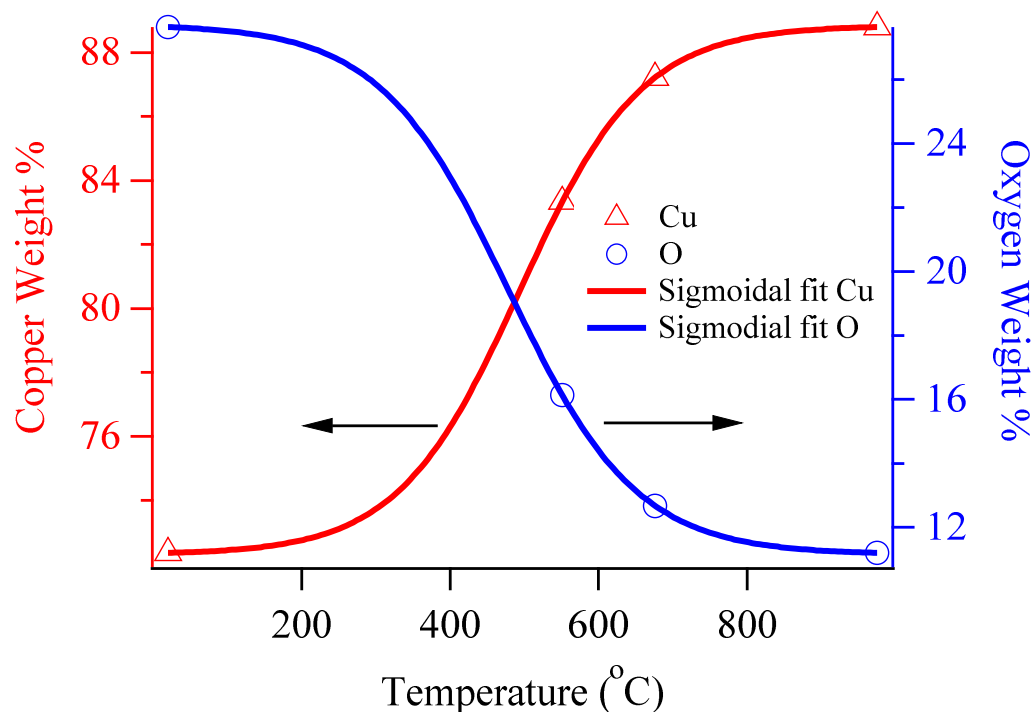


Figure 2.13: Average element weight percent of Copper and Oxygen at various reaction temperatures obtained from Energy-Dispersive X-ray Analysis.

2.4 Conclusion

The combustion reaction of carbon in its graphitic form with copper oxide as the oxidizer was studied in this work. The reaction of stoichiometric proportion of the two components was followed using thermogravimetry, evolved gas analysis, and Energy Dispersive X-ray spectroscopy. The results show that CO formation dominates the early stages up to a temperature of 570°C. A rapid production of CO₂ begins at around 618°C. High rates of CO₂ production correlate to rapid rates of weight loss. Modulated TGA experiments were also carried out to obtain the activation energy over the entire temperature range, and changes in activation energy values correlated well to trends observed in the evolved gas analysis. The EDS results indicate that the reduction of CuO to Cu during the course of heating follows a sigmoidal trend. The results of this work provide insights into the mechanism of oxidation of

carbon with a metal oxide in the solid-state.

3 Modulated Thermogravimetric Experiments on Argonne Premium Coal Samples with Combustion Gas Analysis

3.1 Introduction

Understanding the oxidation and pyrolysis of coal is important for processes that use it for the production of value-added chemicals or in combustion for power production. The production of gaseous fuels from coal via gasification technologies also requires a good understanding of the kinetics of coal oxidation under various temperature conditions. Previous studies on the kinetics of pyrolysis of U.S. coals include studies by Burnham et al. [37], Li et al. [38], and Wang et al. [39]. This work examines the combustion of eight samples of coal from the Argonne premium coal sample program. Specifically, we obtain the weight loss profiles, the CO and CO₂ evolution trend, and infer activation energies using the modulated TGA technique. Additionally, the qualitative combustion characteristics are compared for selected samples by means of infrared absorbance spectra over the wavenumbers of 1000-4000 cm^{-1} .

3.2 Experimental Apparatus and Methods

A Q500 Thermogravimetric Analyzer (TGA) from T.A. Instruments was used for the results presented in this study. The TGA was used to study the oxidation of coal samples with air as the oxidizer. The apparatus is equipped with an Evolved Gas Furnace that interfaces with an infrared spectrometer for analysis of the gases evolved during the combustion process. Purge gas enters a quartz furnace through a sample tube and sweeps the products of combustion for external analysis through an unheated transfer line. A short path length gas cell in the Nicolet® iS5 spectrometer was used for gaseous product analysis. The resolution of the FTIR data collection was 0.8 cm^{-1} . The TGA is also capable of temperature modulation that permits the continuous determination of activation energy over the temperature range of interest. The

estimation of activation energy using the Hahn TGA technique is “model-free” in that no prior knowledge or assumption for the functional form of the kinetic expression is needed [8]. The test conditions used for both the evolved gas analysis and the Modulated TGA tests are presented in Table 3.1.

Table 3.1: Test conditions.

	Evolved Gas Analysis Tests	Modulated Tests
Samples Tested	8 Argonne Coals (100 mesh)	8 Argonne Coals (100 mesh)
Gas Flow rate	25 ml/min	25 ml/min
Gas Type	Bottled Air (20.9 % O ₂)	Bottled Air (20.9 % O ₂)
Initial Sample Weight	40 mg	30 mg
Sample pan	Platinum (100 μ l)	Platinum (100 μ l)
Ramp	5°C/min to 750.00°C	Ramp 2°C/min to 750°C
Modulation	—	Modulate +/- 5°C every 200 seconds

The samples tested in this study are drawn from the Argonne Premium Coal Sample Program. This program was established by the U.S. Department of Energy to provide the scientific community consistent samples of American Coal for basic research. The full set of 8 coals were selected to have a range of C, H, S, and O content [25]. They were selected to highlight the differences among the various types of coals mined in the U.S. Further details on the rationale for selection of these coal samples can be found in the work of Vorres [25]. Following Vorres [25], we summarize the key characteristics of the 8 coal samples in Table 3.2.

The samples span a range of coal ranks from lignite to low-volatile bituminous, which is indicative of the degree of metamorphism of the original organic matter [40].

Table 3.2: Argonne Premium Coal Samples and characteristics %C, H, O, on moisture and ash-free basis. Sulfur and Ash on dry basis [25].

	<i>Seam</i>	<i>State</i>	<i>Rank</i>	<i>C</i>	<i>H</i>	<i>O</i>	<i>S</i>	<i>Ash</i>
101	Upper Freeport	PA	Med. Vol. Bit.	86	4.7	8	2.3	13
202	Wyodak-Anderson	WY	Subbituminous	75	5.4	18	0.6	9
301	Illinois No. 6	IL	High. Vol. Bit.	78	5.0	14	4.8	15
401	Pittsburgh (No. 8)	PA	High. Vol. Bit.	83	5.3	9	2.2	9
501	Pocahontas No. 3	VA	Low. Vol. Bit.	91	4.4	2	0.7	5
601	Blind Canyon	UT	High. Vol. Bit.	81	5.8	12	0.6	5
701	Lewiston-Stockton	WV	High. Vol. Bit.	83	5.3	10	0.7	20
801	Beulah-Zap	ND	Lignite	73	4.8	20	0.8	10

3.3 Results

3.3.1 TGA Weight Loss

The coal samples were subjected to identical linear temperature ramps in the TGA. The resulting weight loss for the samples are shown in Figures 3.1-3. Figure 3.1 shows the weight-loss trends with respect to temperature for the four high volatile bituminous coals, Figure 3.2 plots the results for the medium and low volatile bituminous, and Figure 3.3 shows the results for sub-bituminous coal and lignite. Among the four high volatile bituminous coals shown in Figure 3.1, the Pittsburgh #8 and the Lewiston-Stockton coal samples follow very similar trends for up to 350°C, followed by a slightly larger rate of weight change with temperature for the Pittsburgh #8. The Illinois #6 sample exhibits one of the most rapid weight losses with an abrupt change in slope around 400°C. A comparison of the medium volatile and low volatile bituminous coals is shown in Figure 3.2. The low volatile bituminous coal exhibits lower reactivity in the 300-400°C range as compared to the high volatile bituminous coal. It may be noted that the post-combustion weight percentages near 600°C are very close to the ash content values provided in the original work of Vorres [25].

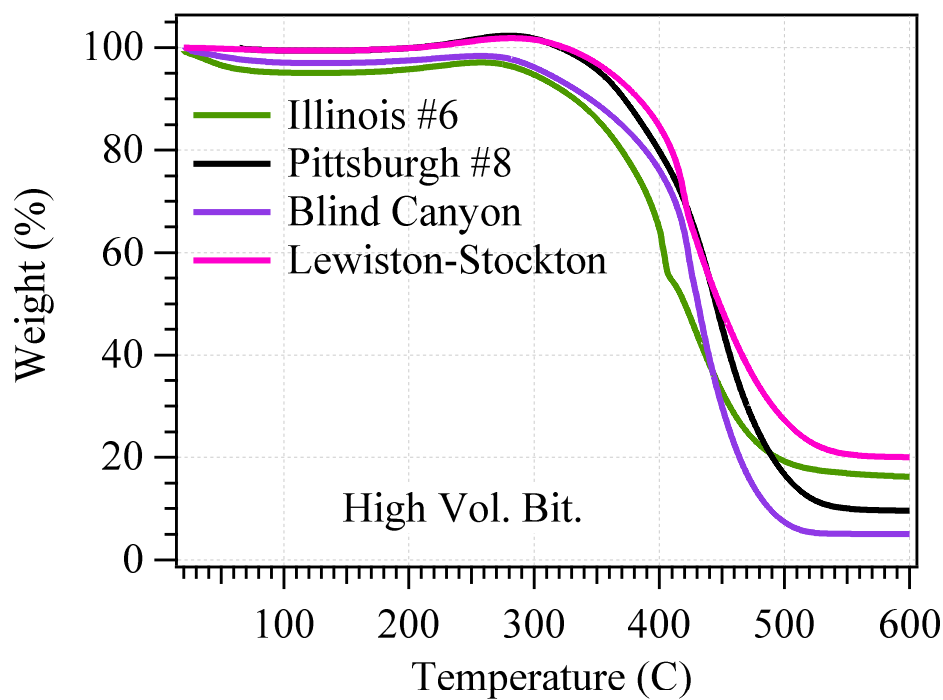


Figure 3.1: Weight loss characteristics for high volatile bituminous coals.

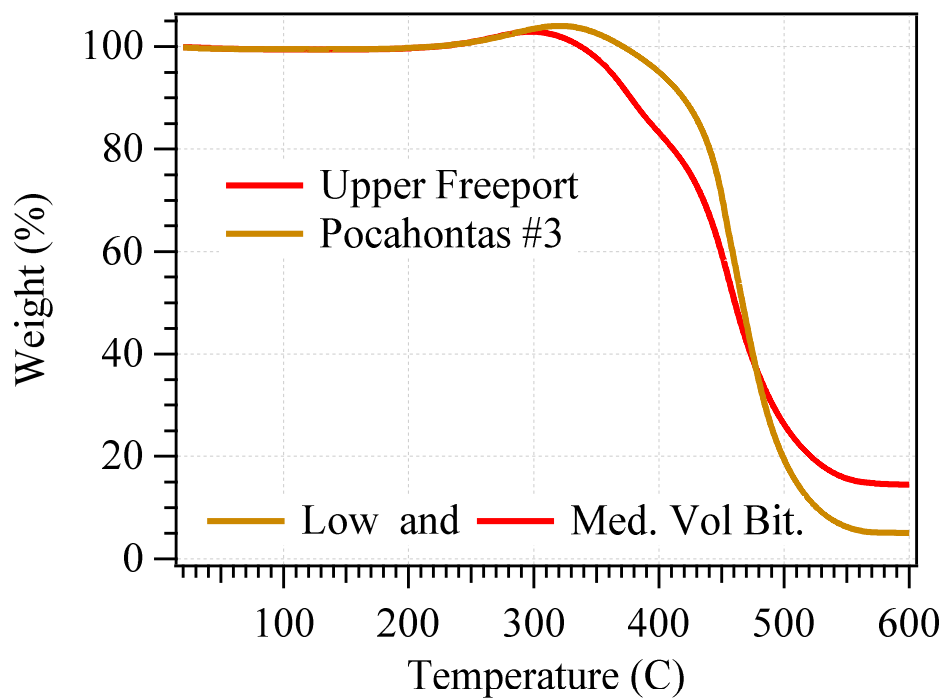


Figure 3.2: Medium and low volatile coal weight characteristics.

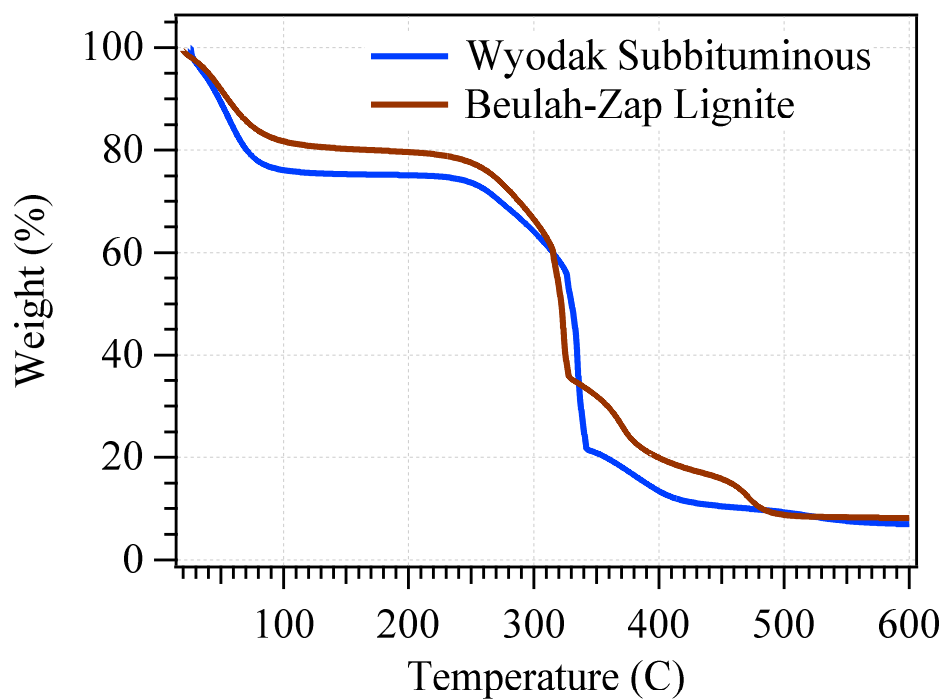


Figure 3.3: Weight characteristics for sub-bituminous and lignite coals.

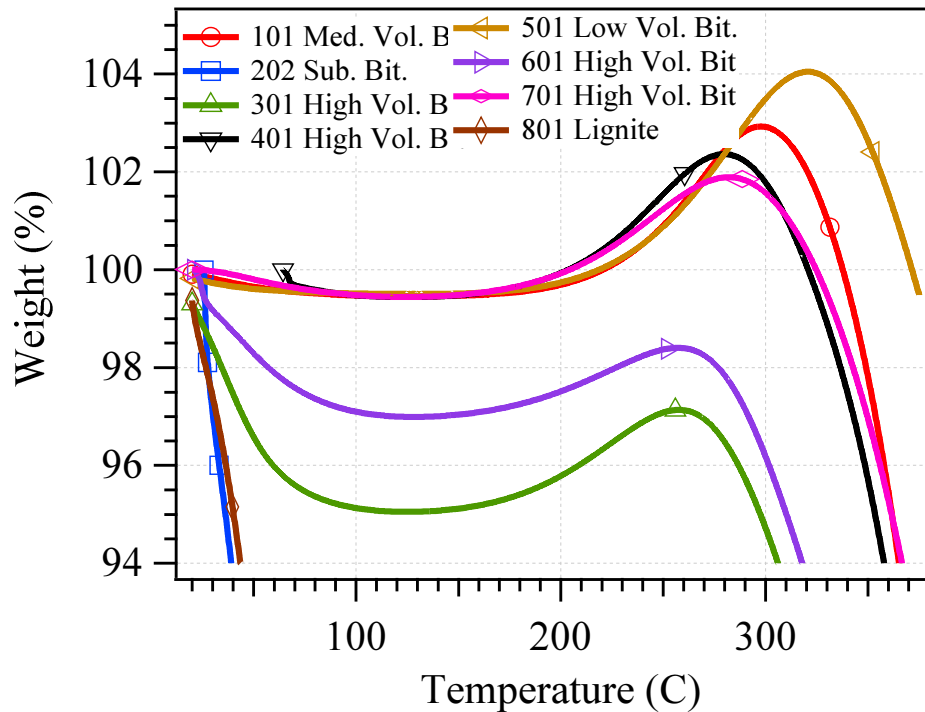


Figure 3.4: Pre-Combustion weight gain.

The low-rank coals in Figure 3.3 are associated with multistep processes that start immediately after the temperature is raised above room temperature. There is a rapid decrease in weight up to around 100°C, followed by a plateau region between 100-230°C. This is followed by a very rapid reaction in a small window from 320-340°C and a relatively slow burnout above that temperature. The low-rank coals have relatively low ash content compared to the medium volatile bituminous and two of the high volatile bituminous coals. The rate of weight loss and the evolution of CO and CO₂ for each sample will be discussed in a subsequent section. Close inspection of the weight loss profile for all samples except for the lignite and sub-bituminous coal shows that there is a weight gain in the temperature range of 200 to 320°C (c.f. Figure 3.4). This pre-combustion mass gain has been attributed to oxygen chemisorption by Slovác and Taraba [41], and Jones et al.[42].

3.3.2 Evolved Gas Analysis: Quantitative Results

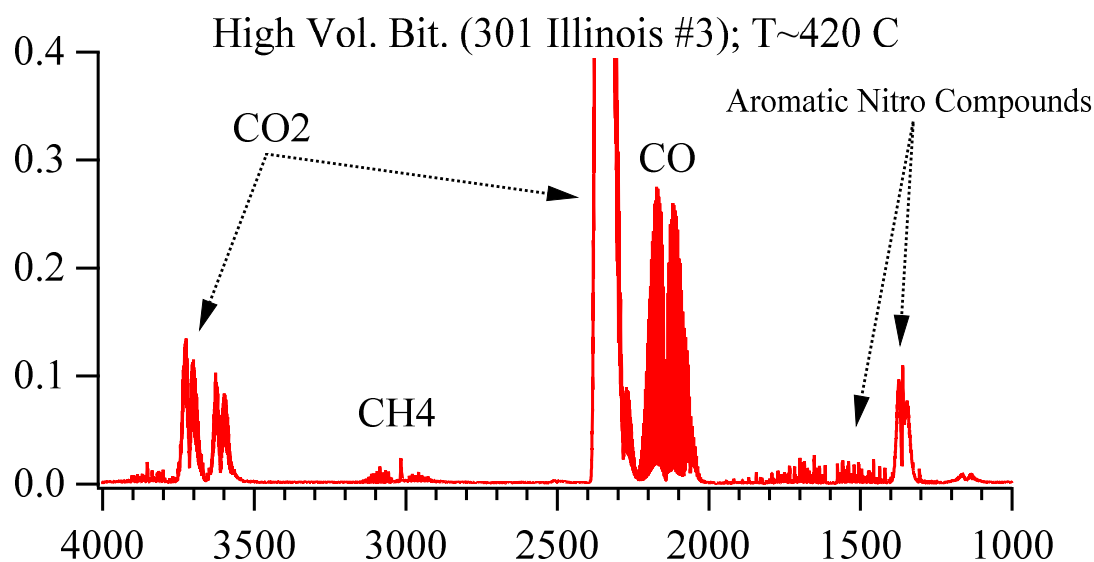


Figure 3.5: Infrared spectra for a high volatile bituminous coal.

Evolved gases were quantified using a FTIR spectrometer. The plot in Figure 3.5 displays an example of the IR spectra obtained at a temperature corresponding to a maximum in the

derivative of the weight loss. The spectra can be used to identify the contributions to the absorbance from CO, CO₂, and what appears to be methane. There also appears absorbance peaks at wavenumbers typically associated with aromatic nitro compounds. Multiple spectra were collected at an interval of 0.56 minutes over the entire combustion process in the TGA, and a least squares-based method was used to quantitate the CO and CO₂ evolved.

3.3.3 High Volatile Bituminous Coal

Figures 3.6-9 show the evolution of major gaseous products of combustion for high volatile bituminous coals.

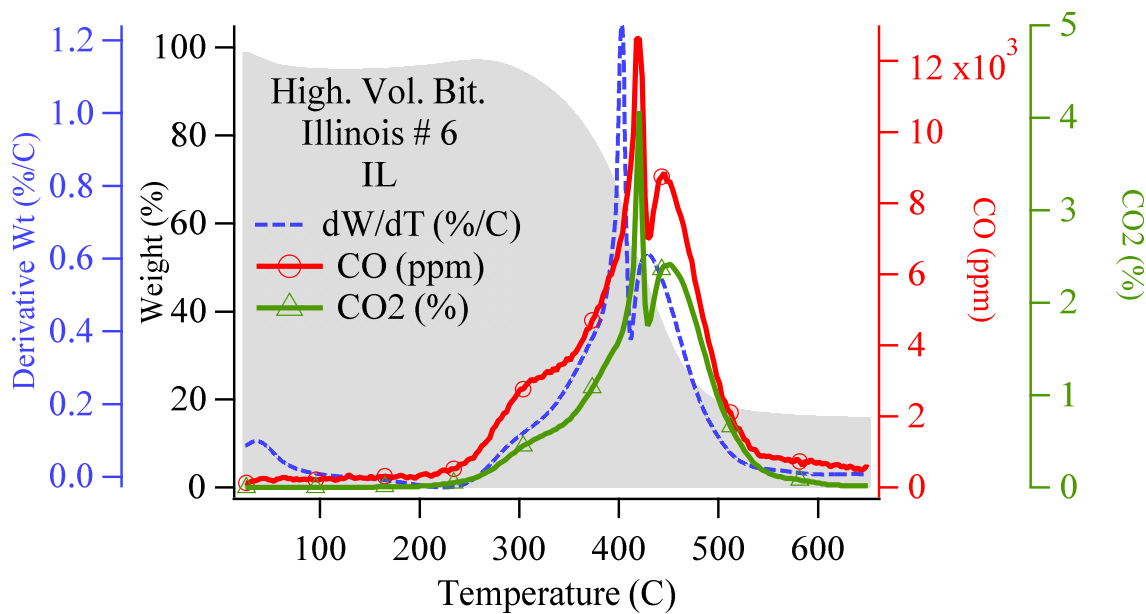


Figure 3.6: CO and CO₂ evolution for high volatile bituminous coal from the Illinois #6 seam.

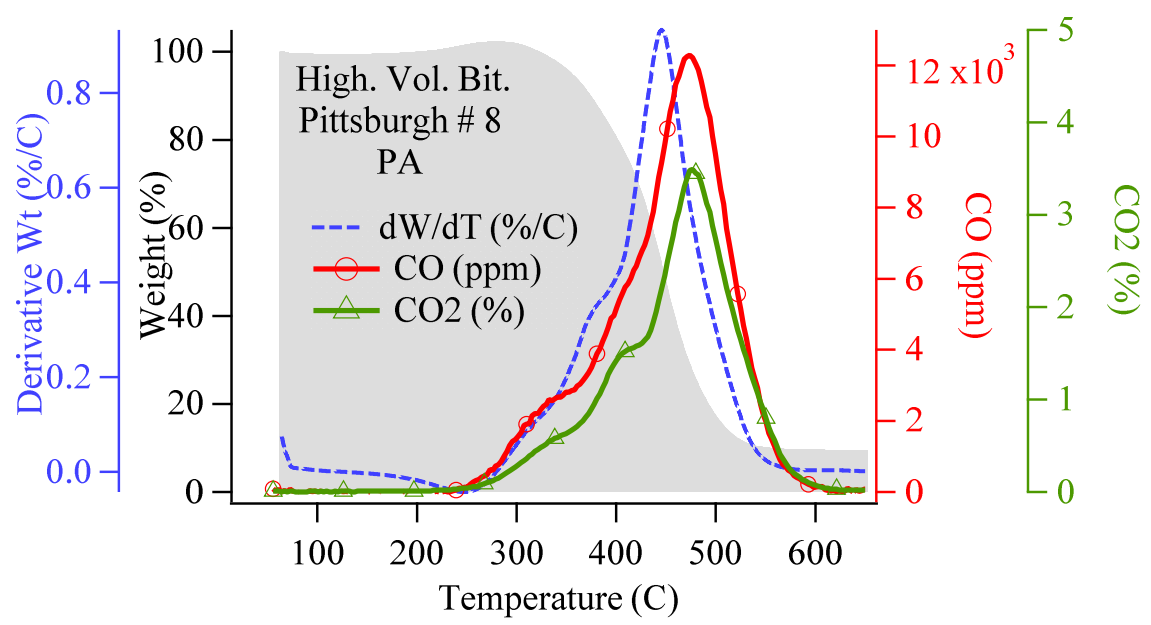


Figure 3.7: CO and CO₂ evolution for high volatile bituminous coal from the Pittsburgh #8 seam.

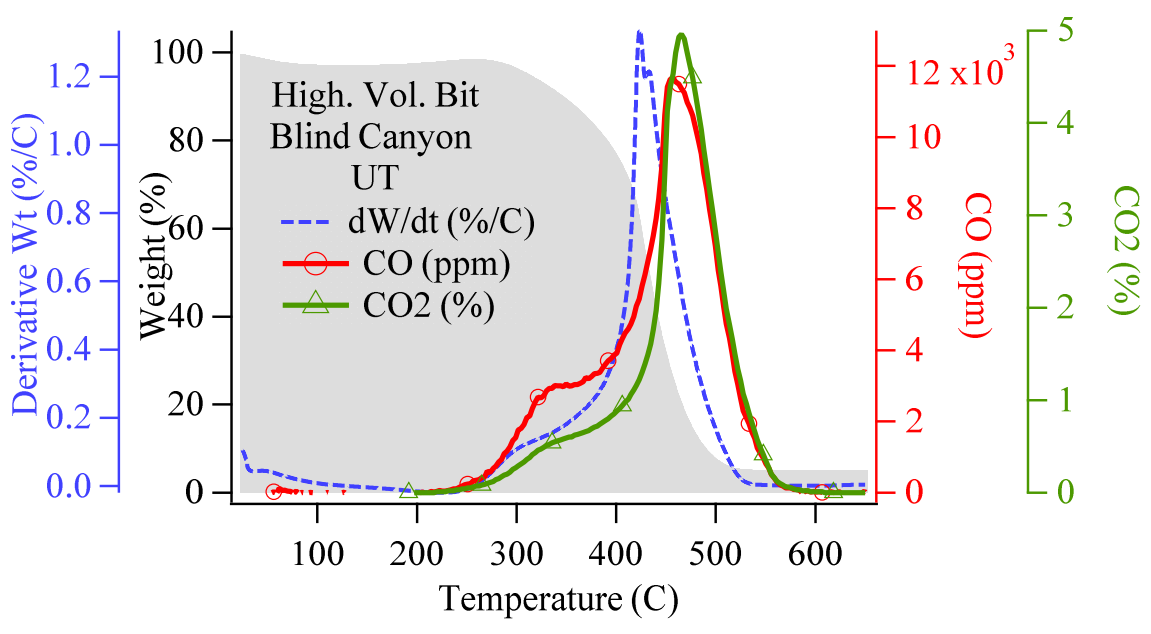


Figure 3.8: CO and CO₂ evolution for high volatile bituminous coal from the Blind Canyon seam.

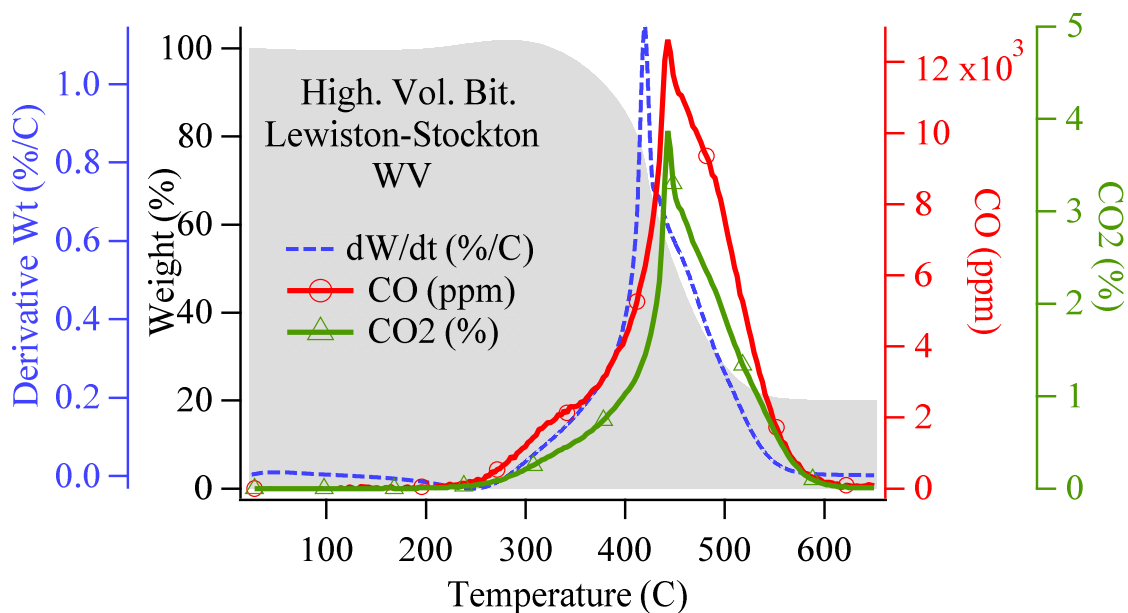


Figure 3.9: CO and CO₂ evolution for high volatile bituminous coal from the Lewiston-Stockton seam.

The shaded area in the background of Figures 3.6-9 represents the weight percent during the experiments; its derivative with respect to temperature is shown in dotted blue. Significant production of carbon monoxide and carbon dioxide starts at approximately 250°C for the high volatile bituminous coal samples. The derivative weight loss has a shape very similar to the gaseous species evolution profile but is shifted slightly toward lower temperatures. The peaks for the CO and CO₂ gas evolutions occur between 420-476°C, with Illinois #6 being the earliest and the Pittsburgh #8 coal seam showing the most delayed evolution for the major products of combustion. The plot for Illinois #6 exhibits two peaks for both CO and CO₂, while the other three have a single peak. A reduction in the rate of both CO and CO₂ evolution with temperature can be seen for all four high volatile bituminous coal samples in the range of 310-340°C. In terms of the peak value of CO₂ production, the coal sample from the Blind Canyon seam exceeds all the other samples. This may be attributable to the relatively low ash content in this coal. The peak CO production is similar for all four samples.

3.3.4 Low Volatile and Medium Bituminous Coals

Figures 3.10 and 11 show evolution of the two major products of combustion for the medium and low volatile bituminous coals. The medium volatile bituminous coal (Figure 3.10) shows dual peaks in the plots for CO and CO₂ evolution, which closely follows the trend for the derivative weight loss. While the peak value for the CO produced during its oxidation is similar to the high volatile samples, the peak CO₂ production is much lesser. The results for the low volatile bituminous coal shown in Figure 3.11 are significantly different from the medium volatile coal. Though its derivative weight loss has two local maxima's, similar to the medium volatile bituminous coal, they are very closely spaced and lie within a 12°C interval. Additionally, the peak CO₂ production is approximately 26% higher compared to the medium volatile bituminous coal.

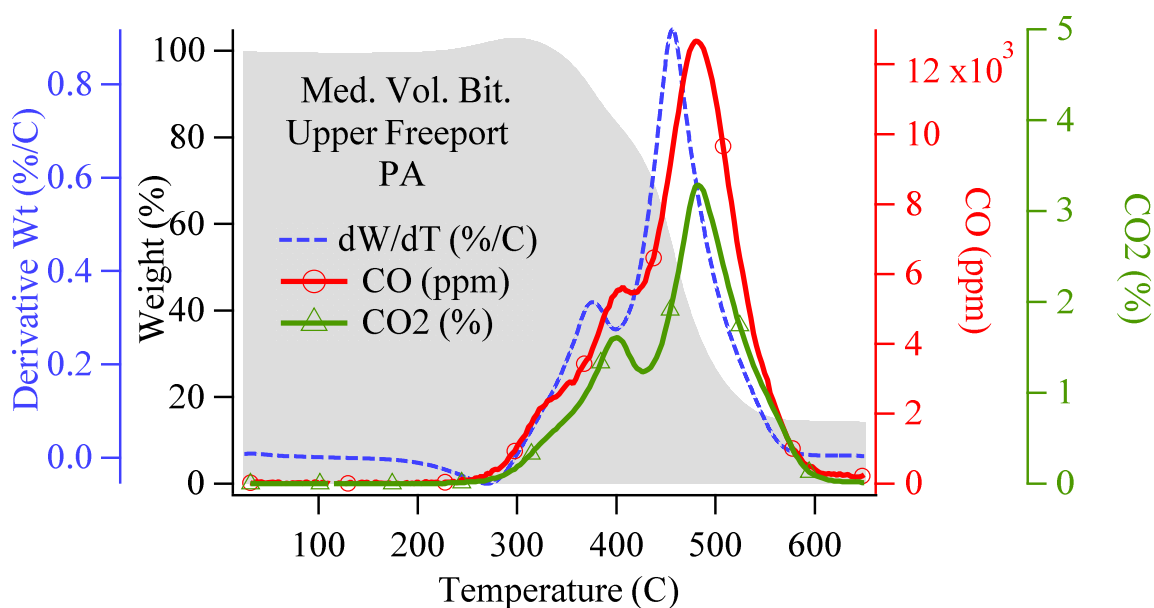


Figure 3.10: CO and CO₂ evolution for medium volatile bituminous coal from the Upper Freeport seam.

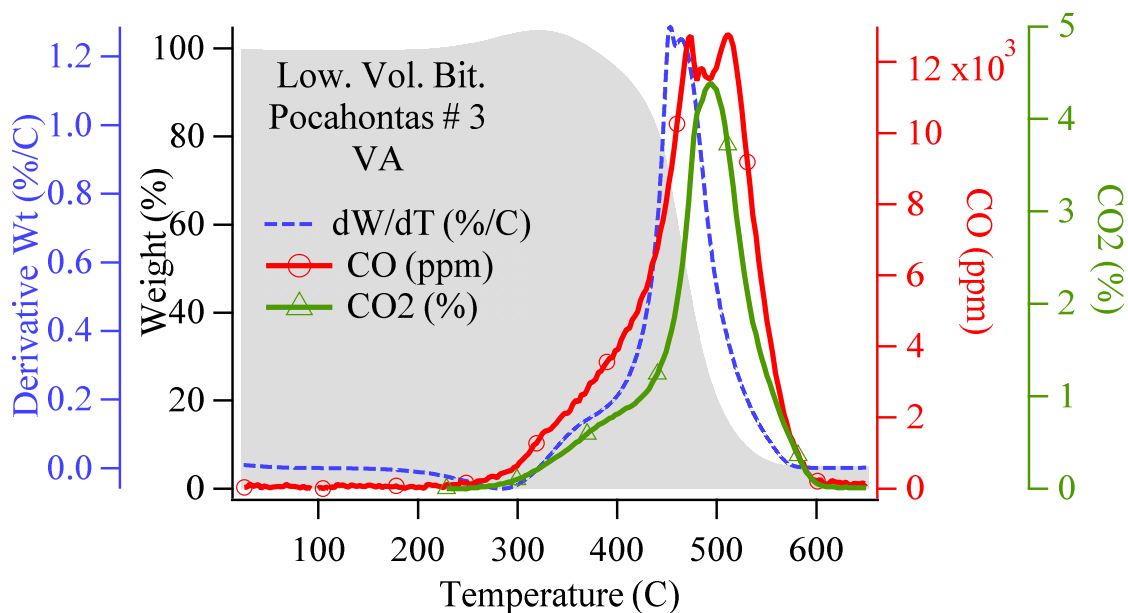


Figure 3.11: CO and CO₂ evolution for high volatile bituminous coal from the Pocahontas #3 seam.

3.3.5 Sub-Bituminous Coal and Lignite

Figures 3.12 and 13 are more plots showing the weight loss, its derivative, and the evolution of CO and CO₂ during the combustion process; however, the data is from lignite and sub-bituminous coals. The lower-ranking Wyodak-Anderson sub-bituminous and Beulah-Zap lignite have less carbon content than the mid and high volatile bituminous coals. In fact, Table 3.1 shows the sub-bituminous and lignite coals to have carbon contents of 75 and 73 percent, respectively, whereas the other coals have higher carbon contents from 78 to 91 percent. As can be seen in Figures 3.12-13, the low carbon coals have a narrow, steep weight loss profile compared to their higher-quality counterparts. The starting temperatures associated with the reactions are like those of the other coals, but there is a faster reaction portion from about 300 to 400°C associated with a higher weight loss rates, and the entire process ends at a lower temperature of approximately 500°C.

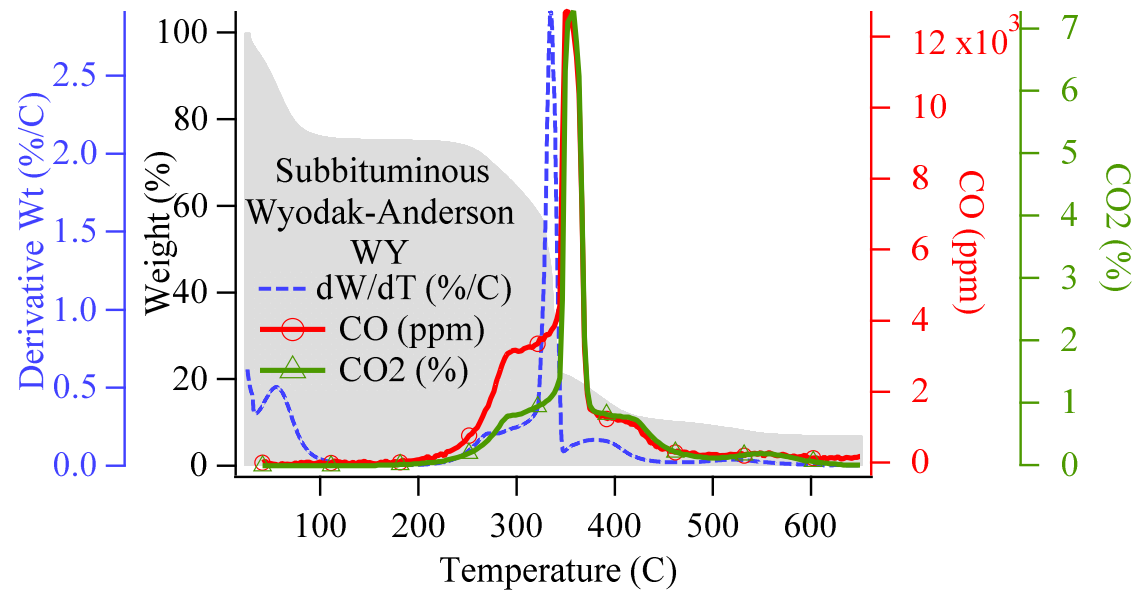


Figure 3.12: CO and CO₂ evolution for subbituminous coal from the Wyodak-Anderson seam.

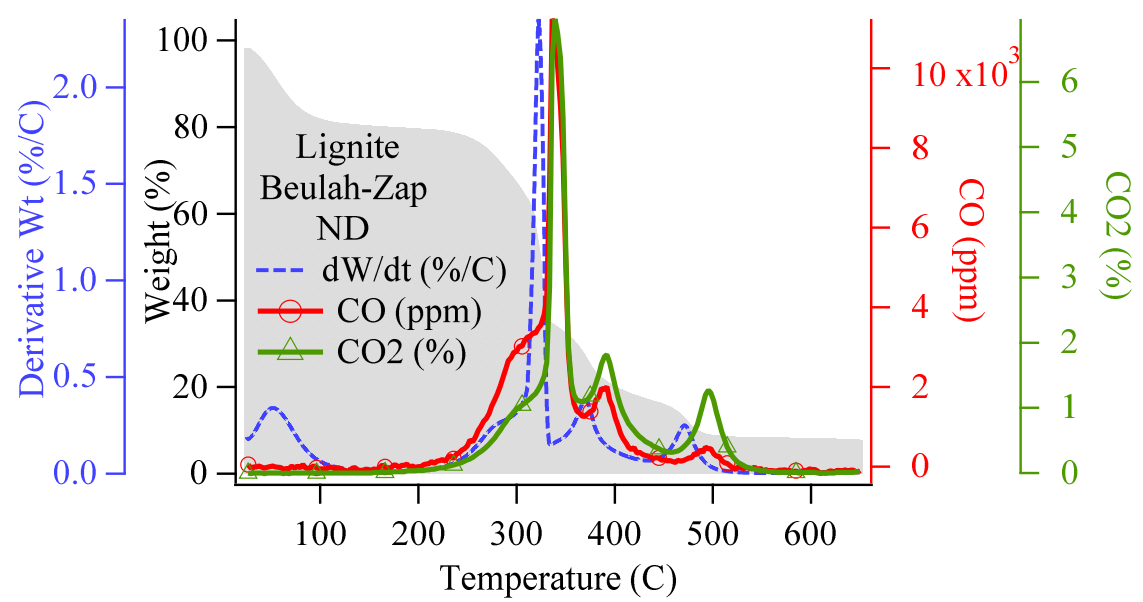


Figure 3.13: CO and CO₂ evolution for lignite coal from the Beulah-Zap seam.

3.3.6 Qualitative Comparison of Species Evolution Trends

A qualitative comparison of the species evolution trend over the entire temperature range for the four types of coal studied in this work is shown in Figures 3.14-17. One representative sample from each rank is chosen for comparison, and the lignite is not included. The bands for CO and CO₂ are the most prominent for the four samples, and the sub-bituminous coal exhibits a very large absorption for these two species over a relatively smaller temperature range. There is also a strong absorption feature for the aromatic nitro compounds 1300-1400 cm⁻¹ range, particularly for the high and medium volatility bituminous coals.

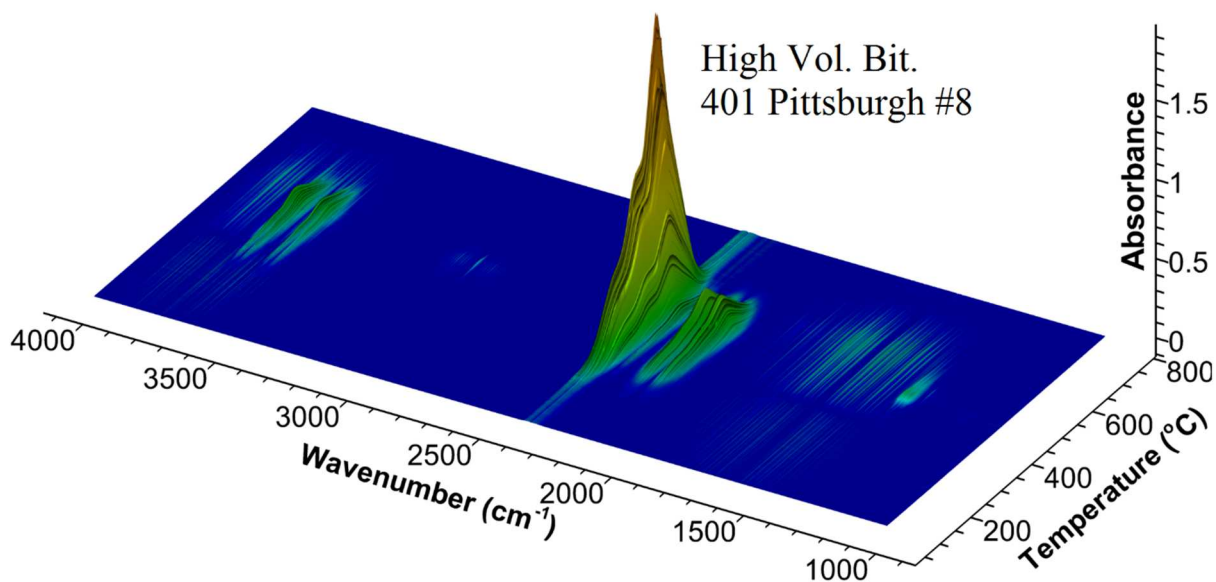


Figure 3.14: Qualitative species evolution trends for high volatile bituminous coal from the Pittsburgh #8 seam

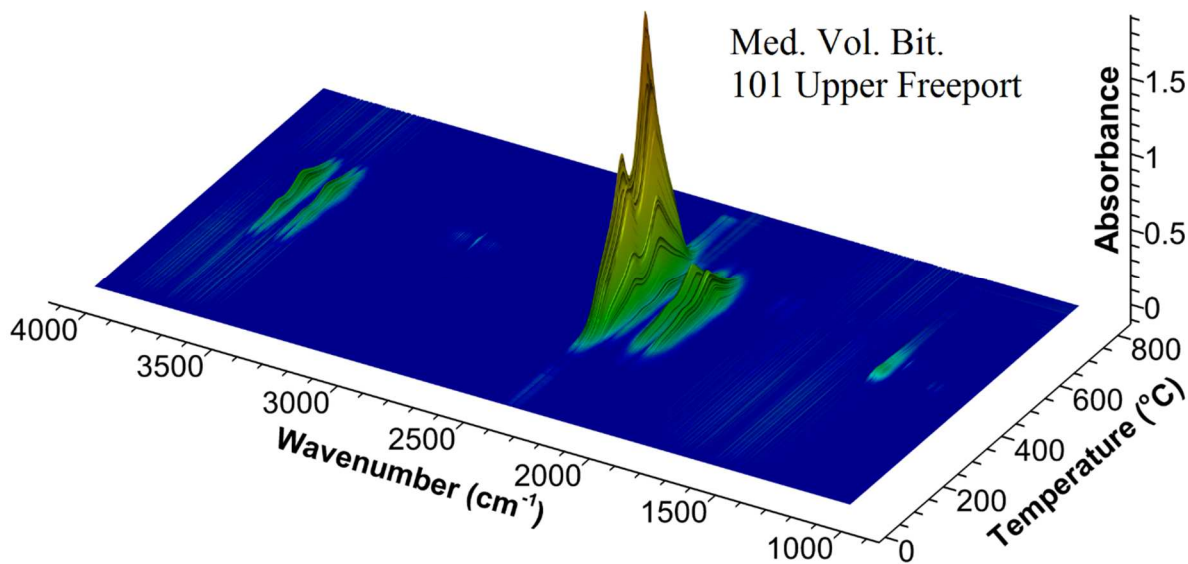


Figure 3.15: Qualitative species evolution trends for medium volatile bituminous coal from the Upper Freeport seam.

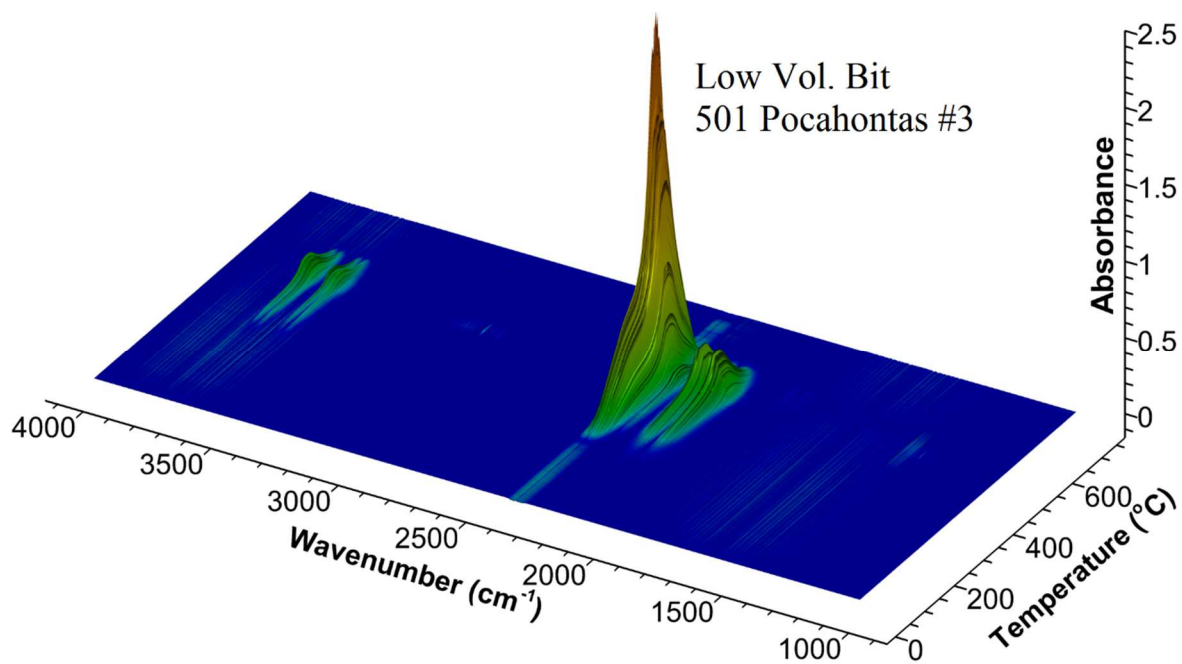


Figure 3.16: Qualitative species evolution trends for low volatile bituminous coal from the Pocahontas #3 seam.

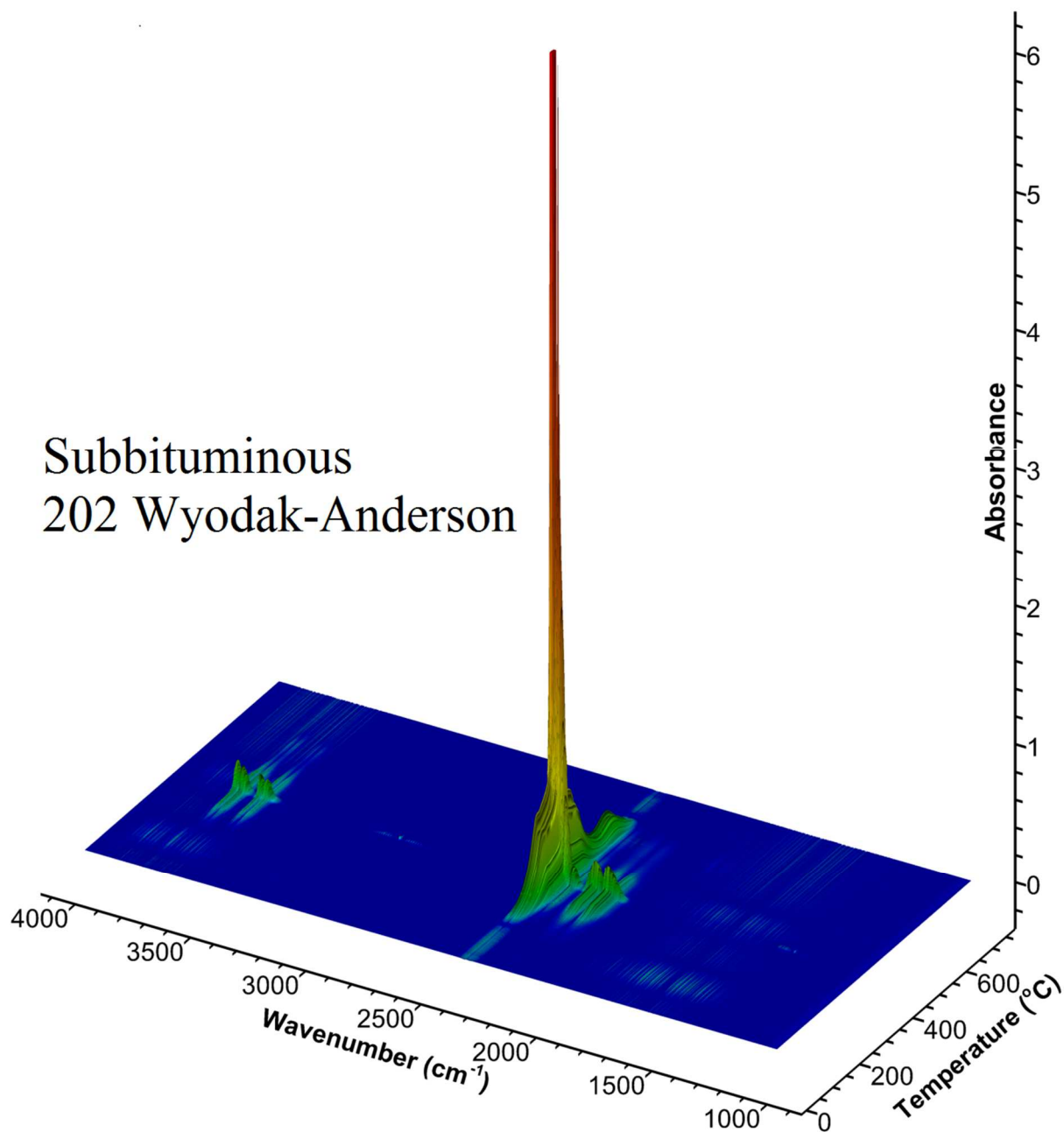


Figure 3.17: Qualitative species evolution trends for sub-bituminous coal from the Wyodak-Anderson seam.

There is also a faint presence of what is most probably methane evolution around 2880-3160 cm^{-1} . Its evolution is restricted to a small temperature window of 15-20°C. The high volatile bituminous coal has several other absorption features between the bands for the aromatic nitro

compounds and carbon monoxide. The low volatile bituminous sample has relatively weaker absorbance features related to the aromatic species. Finally, the sub-bituminous coal has completely different qualitative trend in terms of the absorption features for the various species. In general, the product evolution is confined to a much tighter temperature window resulting in compact and sharper peaks. It is also of interest to note that the evolution of carbon dioxide begins relatively early in the heating process at temperatures well below a 100°C for all the samples shown in Figure 3.14-17.

3.3.7 Modulated TGA Experiments and Activation Energy Results

Modulated TGA experiments use sinusoidal oscillations of temperature about a linear ramp to associate the heat flow with activation energy. The details of this method are discussed in the work of Blaine and Hahn [9]. The heat flow is separated into reversing (heat capacity) and non-reversing (kinetic) components. Then, for TGA experiments, the overall expression for the rate is given by:

$$\frac{d\alpha}{dt} = Z \times f(\alpha) \times e^{-\frac{E}{RT}} \quad 3.1$$

Where Z is the pre-exponential factor, $f(\alpha)$ the kinetic expression, E the activation energy, and α the fractional conversion rate. The fractional conversion rate is defined as:

$$\alpha = \frac{W_i - W(t)}{W_i - W_f} \quad 3.2$$

Where W_i and W_f are the initial and final sample weights, and $W(t)$ is the sample weight at time t during the heating process. Equation 3.1 is then evaluated at its peaks and valleys, and the ratio of the two provides an expression for activation energy which is independent of the kinetic expression in equation 3.3:

$$E = \frac{RT_p T_v [\ln(d\alpha_p) - \ln(d\alpha_v)]}{T_p - T_v} \quad 3.3$$

Here the subscripts p and v represent peak and valley, respectively. This form for the activation energy assumes that there is a minimal change in the reacted fraction between an adjacent peak and valley. Figure 3.18 shows percent weight loss, derivative weight loss, and modulated TGA furnace temperature, all with respect to time for a high volatile bituminous coal sample.

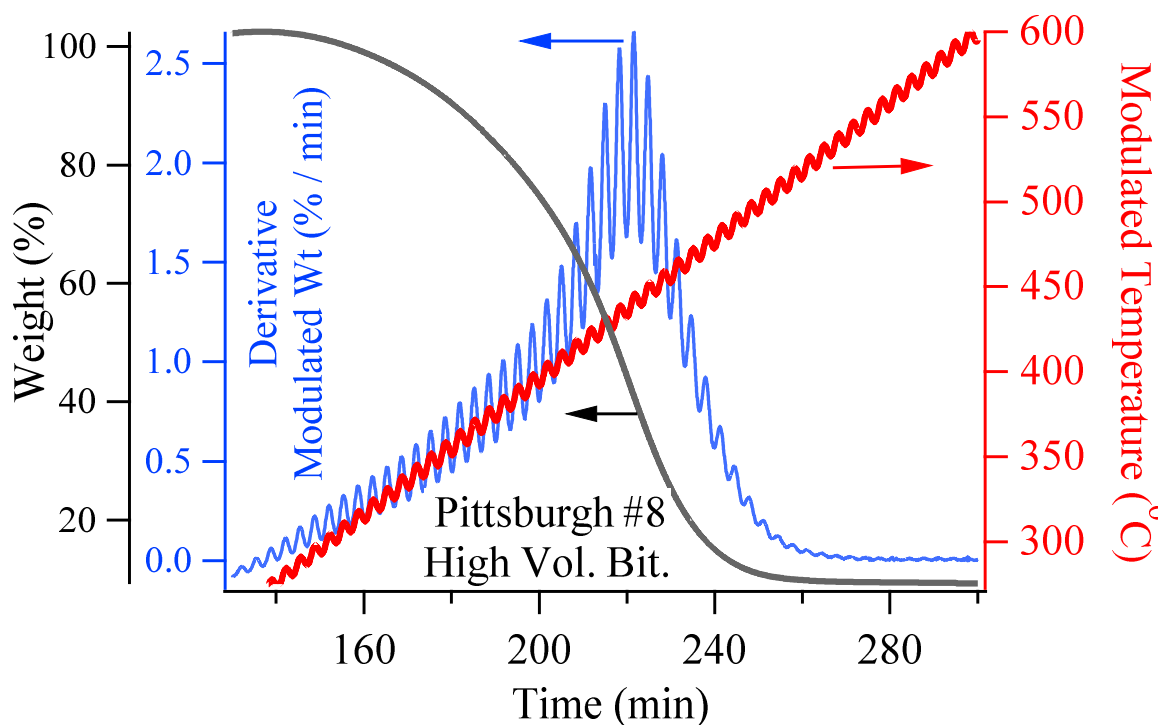


Figure 3.18: Modulated temperature, weight loss, and a derivative of modulated weight as a function of time.

The modulated TGA tests are run for all 8 samples, and the trends for activation energies were examined over the 350–500°C range.

The activation energies of the eight coals are plotted and compared in Figures 3.19-21. The figures are categorized according to the coal type.

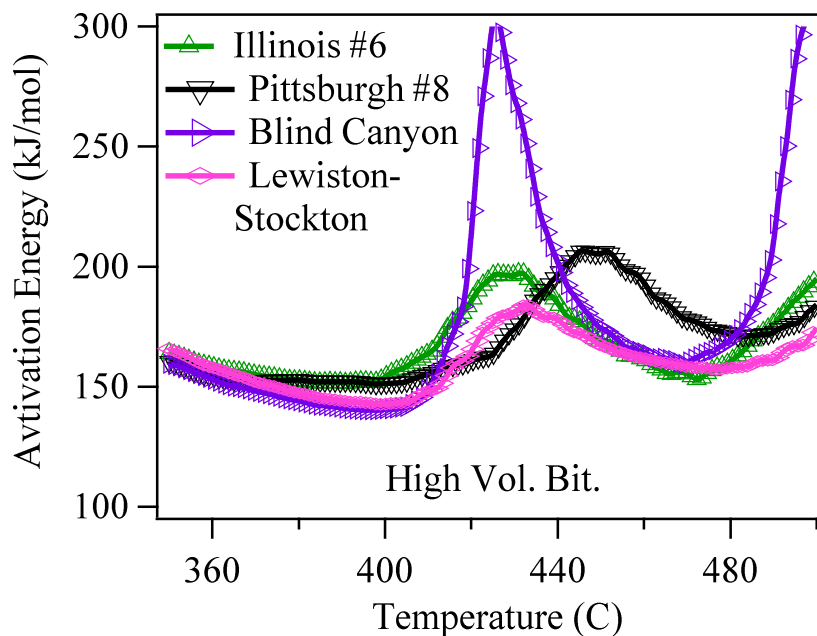


Figure 3.19: Activation energies vs. temperature for high volatile bituminous coals.

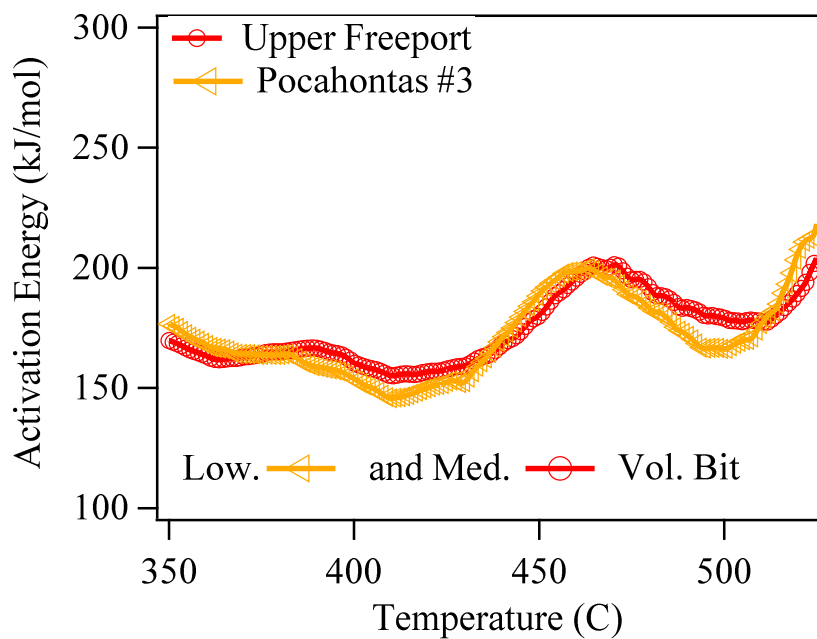


Figure 3.20: Activation energies vs. temperature for medium and low volatile bituminous coals.

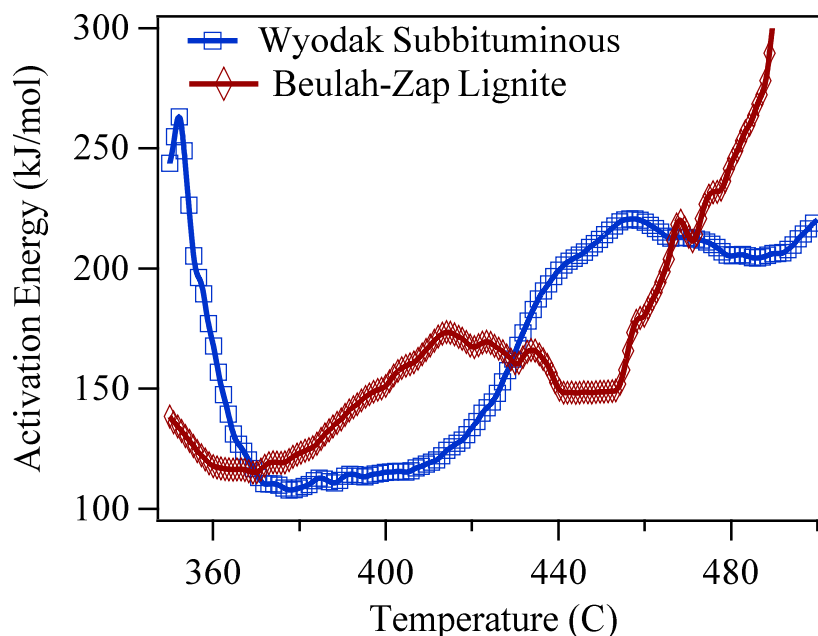


Figure 3.21: Activation energies vs. temperature for sub-bituminous and lignite coals.

The activation energies for the four high volatile bituminous coals are shown in Figure 3.19. The trends for three of the samples are very similar except for the Blind Canyon seam. All four samples exhibit a peak in the 420-440°C interval. However, the Blind Canyon seam sample has an unusually high relative peak value close to 300 kJ/mol in this region. The other three sample peaks lie approximately between 175 to 200 kJ/mol. The shape of the curves is similar for all the four samples shown in Figure 3.19. However, the Pittsburgh #8 coal shows a peak value around 450°C, which is 20°C higher than the other three samples. A comparison of the two low and medium volatile coal samples in Figure 3.20 shows that the activation energy variation with temperature is nearly identical. These two samples exhibit a local peak at a slightly higher temperature (460°C) compared to the high volatile bituminous coals (420-440°C). The activation energy trend for the sub-bituminous coal in Figure 3.21 differs from the other coals in that the processes occurring between 350-380°C are associated with a higher activation energy. The local peak for the sub-bituminous coal occurs in the similar range as the other coals

but takes place much later than the main combustion event as inferred from the weight loss characteristics (*c.f.* Figures 3.12-13). Within the temperature range of data shown in Figures 3.19-21, the sub-bituminous coal attains the lowest values of activation energy in the region associated with its main combustion event. The lignite sample shows a similar qualitative trend associated with an initial drop, followed by a local peak and trough. It differs from the other samples in that the entire combustion process occurs over a narrower temperature range.

3.4 Conclusion

Thermogravimetric analysis was used to study combustion of the Premium Argonne coal samples. They covered high, medium, and low volatile bituminous coals in addition to a sub-bituminous and lignite sample. The weight loss characteristics during combustion correlated well within the rank of coal. The weight loss profile for all samples except for the lignite and sub-bituminous coal shows that there is a slight mass gain in the temperature range of 200 to 320°C. The peak values for the rate of weight loss with temperature were closely associated with the peaks in the evolution of CO and CO₂. A qualitative comparison of the FTIR absorbance spectra shows that CO₂ evolution begins very early in the heating process for all samples. Strong absorption feature for what appear to be aromatic nitro compounds were detected for the high volatile bituminous coals. Modulated TGA experiments were used to obtain the activation energies in the temperature range of 350–500°C.

4 Discussion, Conclusion, and Future Work

The introduction of this paper describes the development of thermal analysis tools and techniques and gives credit to scientific pioneers who helped with their discovery. Even if one were to only consider improvements in these techniques and tools that have occurred over the previous century, we've gained the ability to observe chemical reactions that had only been hypothesized. Considering further into the past, Antoine Lavoisier would certainly be impressed to see that observations he made concerning the oxidation of metals has led to the ability use infrared energy to identify elemental composition of substances. The history of thermal analysis tools and techniques is followed by descriptions of working principles for equipment used in chapters 2 and 3 of this study. It is easy to be impressed by advancements in researcher's ability to obtain and analyze data especially those achieved through the rapid progress in instrumentation, but much research is still needed to fully understand combustion processes. In fact, most complete reaction mechanisms have not been discovered, and those that have are generally of the simplest cases like bimolecular homogenous combustion. The mechanism for the combustion of carbon and copper oxide studied in chapter 2 have not been found, and neither are there accepted mechanisms for the Argonne Premium coals studied in chapter 3. However, the results provided by the experimentation performed in these chapters provide qualitative and quantitative interpretations of thermogravimetry, spectrometry, and evolved gas analysis. The results of chapter 2 are discussed in greater detail in section 4.1, and those from chapter 3 are elaborated in section 4.2. It is the desire of the researchers who conducted experiments for this discussion that these results lead to a better understanding of solid combustion, and that understanding lead to solutions for clean energy production.

4.1 Thermal Analysis on Argonne Premium Coal Samples

The introduction of chapter 2 mentions the development of novel oxygen carriers for chemical-looping combustion. The benefit of chemical looping combustion is the inherent ability to produce flue gas of nearly pure carbon dioxide. The lack of multiple exhaust products allows capture and storage of gaseous products without further separation. Experimentation performed in the chapter is closely related to a unique method of CLC involving oxygen carriers, which release gas-phase oxygen at high temperatures named chemical-looping oxygen uncoupling (CLOU) [43]. Copper oxide is a desirable choice for oxygen carriers due to its high oxygen transport capacity.

The major distinction between CLOU and our study on carbon combustion with copper oxide is the lack of repeated oxidation and reduction cycles. These repeated cycles are valuable in that they replicate CLC processes, and therefore the results of those processes on oxygen carriers. One troubling result concerning CuO oxygen carriers is the tendency for the copper to agglomerate as the carrier is heated for oxygen uncoupling. Much investigation of the agglomeration of copper oxide for chemical looping has been conducted [27, 29, 31, 44]. To reduce the tendency of CuO to agglomerate, many researchers add binders such as SiO_2 , ZrO_2 , or TiO_2 ; because of this experimentation on pure CuO as an oxygen carrier is relatively rare. The work of Wang et al. [44] shows that the effect of different binders on the oxidation rates are minor, but the reaction rates increase in the following order with respect to their content of $ZrO_2 > TiO_2 > SiO_2$. Rather than focus on CLC, this study performed and examined TGA, EGA, and energy dispersive x-ray spectroscopy on well-mixed C/CuO for obtaining TG curves, activation energy, and product quantification. This conclusion relates those results to oxygen uncoupling and carbon combustion with solid oxygen carrier.

TG curves from the results section of chapter 2 show that higher heating rates lead to a reduction in time needed to begin reaction. It has also been shown that at a given temperature, the degree of decomposition is greater, the slower the heating rate proceeds [2]. This can be seen in Figure 4.1, where percent sample weight decreases at specific temperatures from the highest heating rate of $20^{\circ}\text{C}/\text{min}$ to the lowest heating rate of $5^{\circ}\text{C}/\text{min}$.

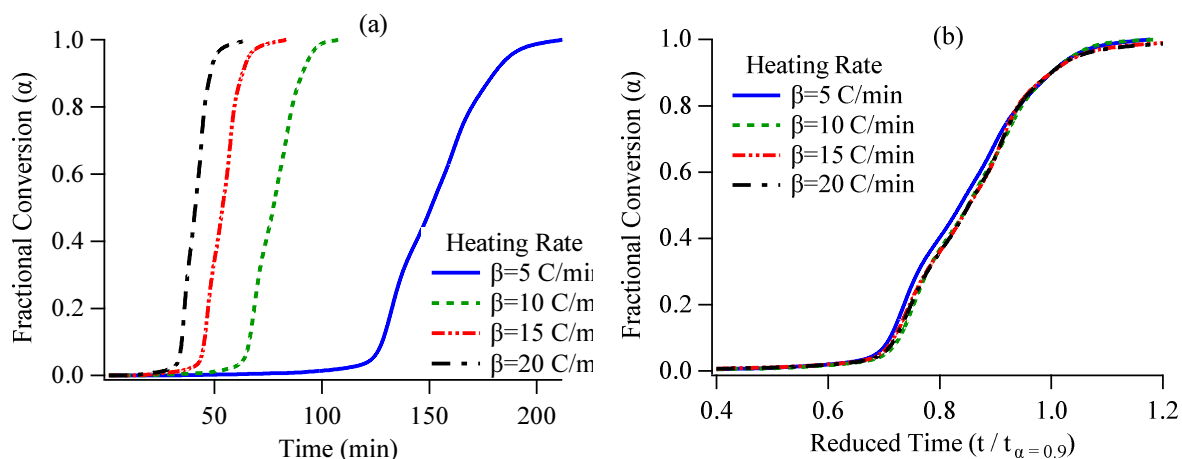


Figure 4.1: Activation energy and derivative weight as a function of temperature.

However, the section goes on to show that when these results are converted to the fractional conversion rate, described by equation 2.1, and plotted against reduced time, the degree of difference in decomposition becomes less severe. As stated in chapter 2, the existence of various sub-regions with varying slopes precludes the possibility of representing the rate of fractional conversion as a simple function of time i.e. $\frac{d\alpha}{dt} = f(\alpha, T)$. This observation is supported by heating rates having minimal effect on decomposition rates. The range of these sub-regions have been approximated as having ranges from 98-92%, 92-83%, and 83%-final percent weight of the samples, and their corresponding temperatures and activation energies are provided in the table below:

Table 4.1: Temperature and activation energies corresponding to approximated transitions in subregions of TG curves.

Heating Rate [°C/min]	Conditions at 98% Sample Weight		Conditions at 92% Sample Weight		Conditions at 83% Sample Weight	
	Temp [°C]	E_A [kJ/mol]	Temp [°C]	E_A [kJ/mol]	Temp [°C]	E_A [kJ/mol]
5	642	245	705	254	829	221
10	658	251	726	265	853	227
15	661	254	736	273	855	228
20	669	255	745	276	867	232

In the sub-region between 98 and 92 percent, there is an activation energy peak and an additional local activation energy peak in the range from 92 to 83 percent. It should be noted that techniques used to obtain the TG curves shown in Figure 4.1 (a) are different from the modulated techniques used to find activation energies, because of this each sample was of slightly different initial weight; however, all samples used to gather data for chapter 2 experiments were approximately 100 mg. The approximated weight of samples is sufficient to analyze approximate quantities. In the approximated subregions, the slopes of TG curves vary slightly, but there exist points where these slopes are most steep. The slopes, of course, represent the derivative of the curves (DTG) with respect to temperature. It is apparent in Figure 4.2 that peak activation energies occur at temperatures where the DTG curves also have peak values in the two subregions that occur earliest in combustion. It is stated in chapter 2 results that the peak values shown in the figure are $E_1 \approx 255 \frac{\text{kJ}}{\text{mol}}$ and $E_2 \approx 279 \frac{\text{kJ}}{\text{mol}}$, and the corresponding temperatures are 667 and 741°C respectively. The peaks of the DTG curve occur slightly before the activation energy peaks in the combustion process. The first peak derivative weight at 649°C and has rate 0.12 percent weight loss per °C, the second peak at 741°C and

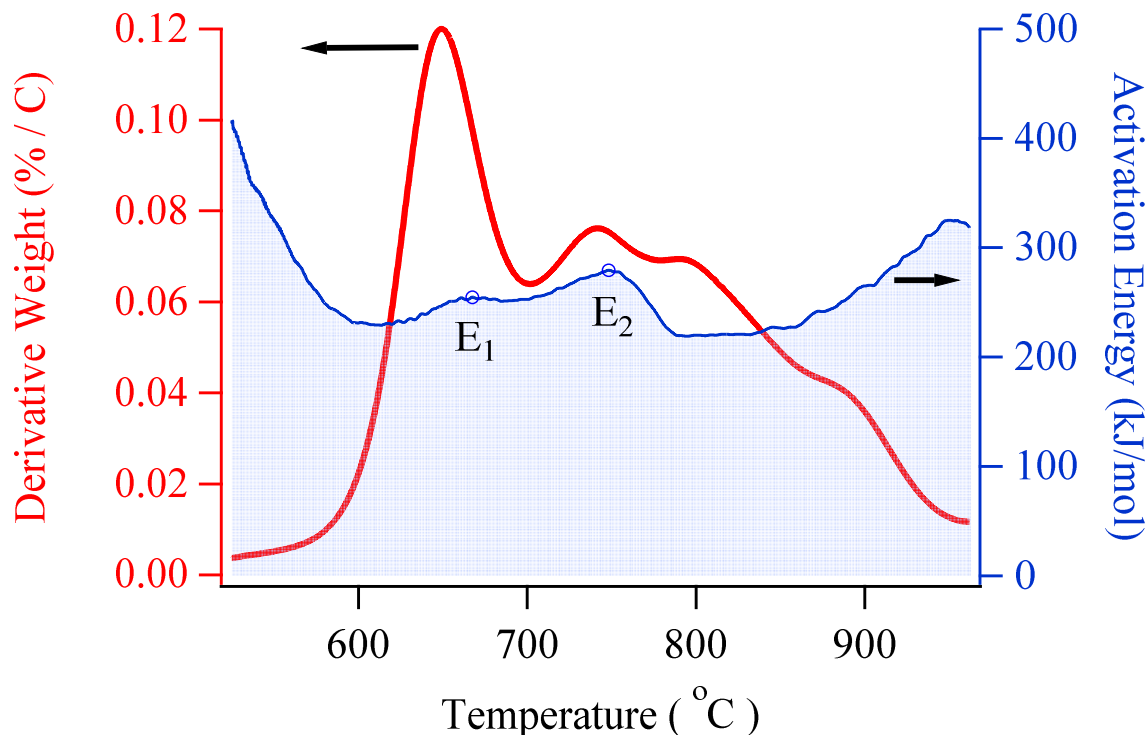


Figure 4.2: Activation energy and derivative weight as a function of temperature.

proceeds at 0.076 percent per °C. Additionally, a third derivative weight peak can be seen slightly following the second peak; however, it has no peak activation energy that can be visibly discerned. Figure 4.3 follows the progress of derivative weight with respect to temperature for all heating rates used in chapter 3 and displays temperature and activation energy at all visible peaks. Interestingly the third peak in weight derivatives for modulated experiments is less than the second peak. This behavior is only seen for the modulated test, and it is reasonable to assume that low heating rates and/or the process of heat modulation result in slower rates of decay towards the termination of combustion. Figure 4.3 also affirms the notion that slower heating rates lead to a greater degree of decomposition because the peaks of each curve occur at higher temperatures as the heating rate is increased. It also appears that the rate of decomposition, $\frac{dW}{dT}$, for initial peaks decreases with increase heat rate. The first peak of the modulated data has a

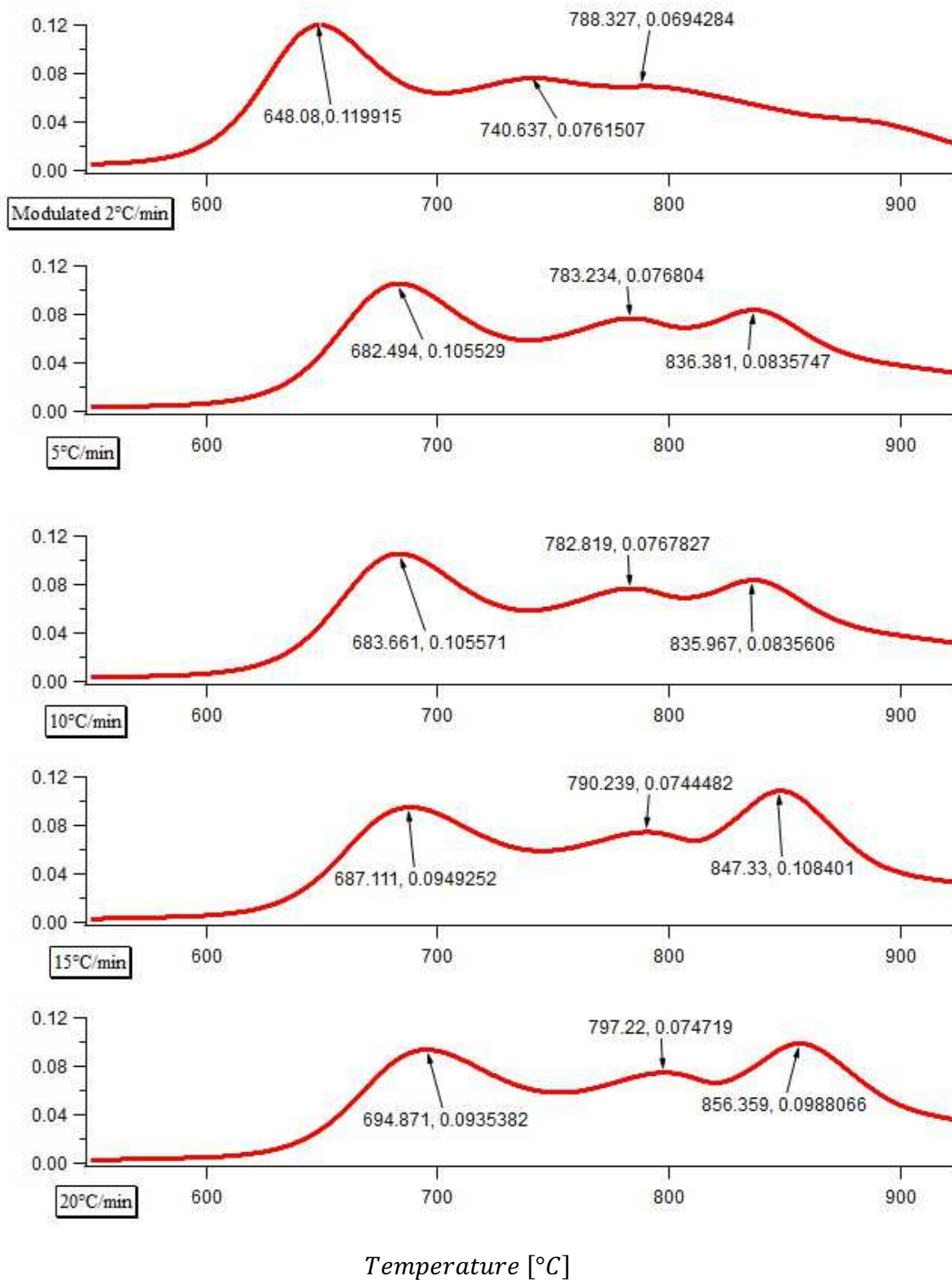


Figure 4.3: Derivative weight percent with respect to temperature at heating ramps from CuO/C experiments in chapter 2.

rate near $0.12 \frac{\%}{\text{C}}$, lowering to $0.106 \frac{\%}{\text{C}}$ for the $5^{\circ}\text{C}/\text{min}$ and $10^{\circ}\text{C}/\text{min}$ curves, then lower again for $15 \frac{\text{C}}{\text{min}}$, and the smallest first peak has a value of $0.094 \frac{\%}{\text{C}}$ for the $20^{\circ}\text{C}/\text{min}$ heating rate. The second peaks for all DTG curves have similar values around $0.076 \frac{\%}{\text{C}}$, and the final peaks tend to increase with the heating rate. These trends in decomposition for increasing heating rates give indication to the combustive behavior of the carbon/oxidizer mixture.

Figures 2.5 and 2.6 provide visuals for the evolution of gaseous products during the combustion of the nanoparticle mixture. Data for both these plots has been recorded from experiments performed with heating rate of $10^{\circ}\text{C}/\text{minute}$. While the evolution of the products shown in the plots is described in detail in section 2.3.3, the subject is worth mentioning here to emphasize the importance of those results. Figure 2.5 is shown again below.

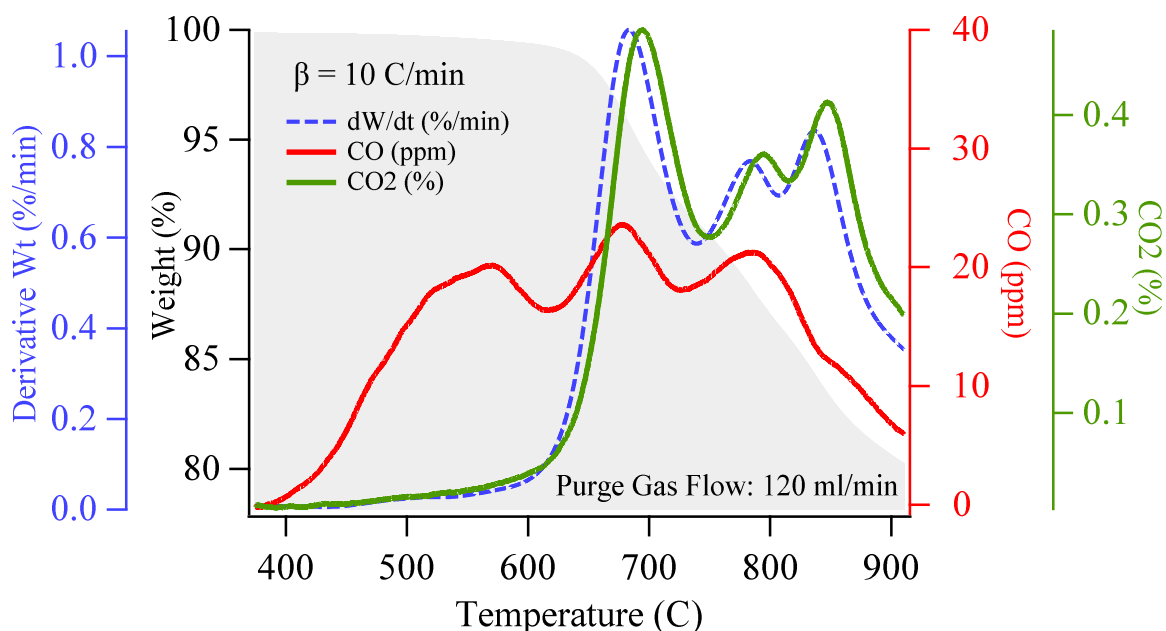


Figure 4.4: CO and CO₂ evolution with weigh and derivative weight profiles with respect to temperature.

Section 2.3.3 describes how the carbon dioxide curve is shadowed by the dotted derivative

weight curve. The nature of the oxygen carrier is responsible for the almost exact replication of the DTG by the evolution of CO_2 . As described in the introduction of this section, because the oxygen for combustion is supplied by the metal oxide rather than from air, the product gasses are of nearly pure CO_2 . It can be observed the carbon monoxide shown in Figure 4.4 is in units of parts per million; this is because the amount of CO_2 produced is significantly larger. However, recalling from section 1.4 that carbon monoxide is known to be the most common of desorbed species from the surface of carbon and often reacts with oxygen in the gas phase to form CO_2 , the evolution of CO is directly related to the evolution of CO_2 . This eludes to the importance of Figure 2.6, where the relationship between these gaseous products are compared with respect to temperature. It is assumed in the discussion following Figure 2.6: CO and CO_2 trajectory during the combustion of graphite with copper oxide.that CO evolution leads to a sharp increase in CO_2 evolution, and that this process likely represents the step shown in the reaction below:



The energy-dispersive x-ray spectroscopy (EDS) results from chapter 2 were obtained by analyzing solid products from TGA experiments which had been frozen by removing the products from the furnace at temperatures 551°C, 676°C, 975°C, and for one sample that had not been heated. SEM results shown in Figure 2.11 show the trend for pure copper oxide to agglomerate due to the low melting point of copper. This point can be further visualized without the aid of electron microscopy in Figure 4.5.

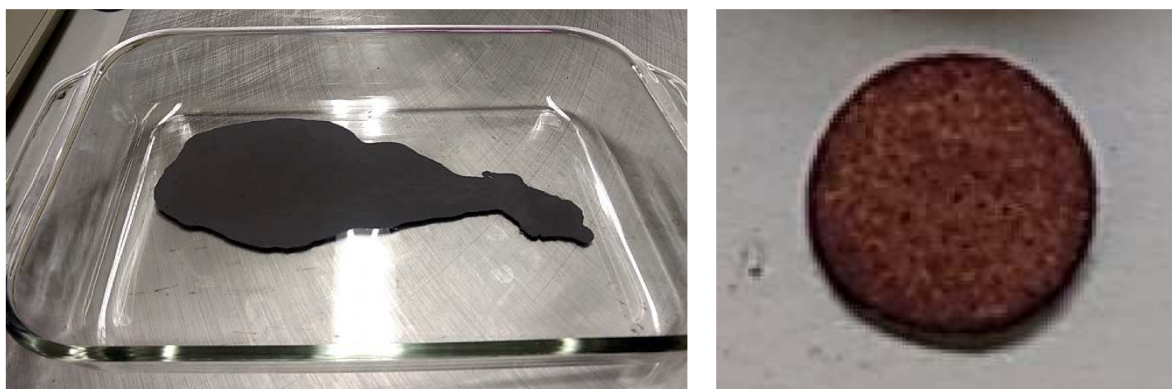


Figure 4.5: Image at left is unreacted carbon-copper oxide mixture before milling, image right is mixture post thermogravimetry.

The figure shows two images, on the left is the unreacted dried slurry of graphite, copper oxide, and methanol before it was scraped from the dish and ball milled, and shown left is a pellet of the mixture after it had been heated to 975°C. Visually one can recognize that as the mixture was heated and gaseous products evolved, the solid products were increasingly copper. This point is reinforced by Figure 2.13, which shows that as the oxygen is released the mixture becomes more purely copper and that this process follows a sigmoidal trend.

A stoichiometric mixture of graphitic carbon with copper oxide was studied using thermogravimetric analysis, derivative thermogravimetry, and energy-dispersive x-ray spectroscopy. Results obtained show CO and CO_2 emissions, TG curves, DTG curves, activation energy, and evolution of gaseous and solid products for the combustion reaction. These results relate to reaction rates and kinetic mechanisms for the process, and further progress towards a complete understanding of the elemental behavior of solid carbon combustion.

4.2 Thermal Analysis on Argonne Premium Coal Samples

The differences in experimental procedures and materials between chapters 2 and 3 are vast. Chapter 2, in some ways, is a simplified case of chapter 3. Chapter 2 describes combustion using a metal oxide oxygen carrier which ensures the gaseous products are limited to CO and CO_2 , where experimentation in chapter 3 uses bottled air for an oxygen carrier. Bottled air contains oxygen, nitrogen, and trace gasses, which add species to the combustion process. More species are added to the process through the use of coals rather than pure graphitic carbon, and it should be clear by this point in the reading that kinetics of combustion tend to increase in complexity as the number of species involved increases. There also exist differences in experimental equipment and procedures. For instance, the study involving the eight species of coal analyzes gaseous products using FTIR rather than NDIR spectrometry, and each coal is heated at the same rate. It is correct to assume that these differences between experiments lead to differences in results; however, the goal of the studies is the same; a better understanding of the combustive reaction through experimental analysis.

The TG curves from chapter 3 were gathered at a linear ramp rate of $10^{\circ}C/min$ and are grouped in Figures 3.1-3 according to their rank. The plot from Figure 3.1 is shown again below in Figure 4.6. This plot contains the TG curves for the four high volatile bituminous coals from the Premium Argonne Samples. High volatile coals have volatile matter greater than 32% on a dry mineral matter-free (dmmf) basis. These volatiles are hydrocarbons that are consumed much more rapidly than the carbon in coal during combustion. This rapid combustion adds energy to the process but also increases the complexity of the reaction. Because of the complexity added by the volatiles and because the period of combustion is dominated by carbon in coal, it is the kinetics of carbon combustion that are often the focus of analysis. Reaction

begins for the high volatile bituminous coals near 300°C and is complete for all four before the TGA furnace reaches 550°C.

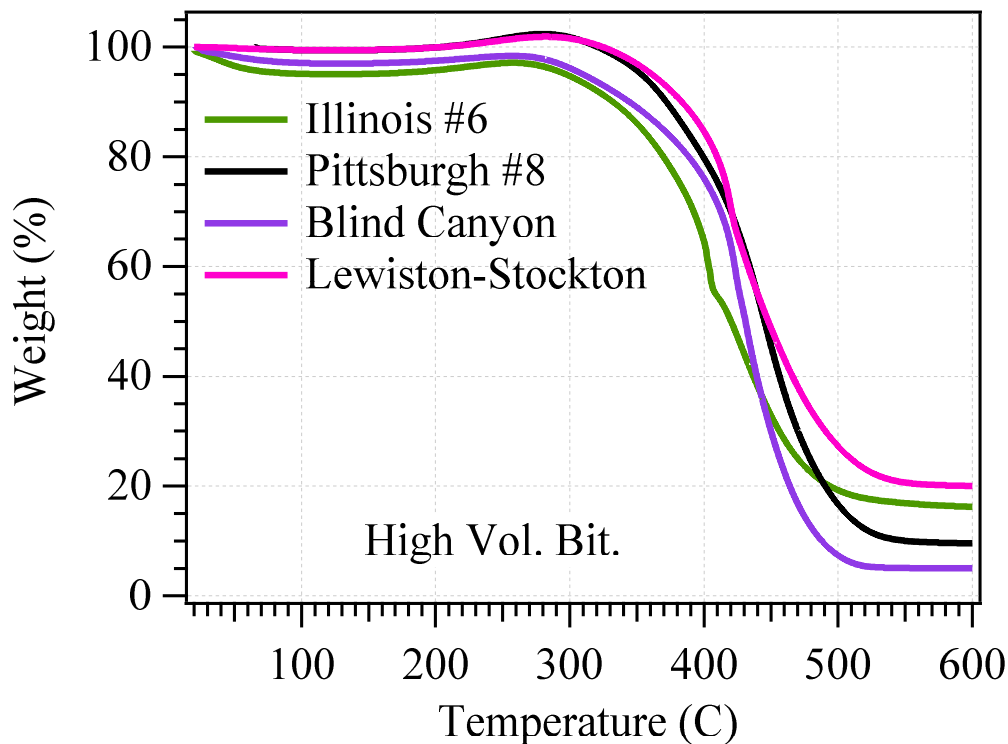


Figure 4.6: TG curves for high volatile coals from the Premium Argonne Sample Program.

After the reaction begins, there is an increased rate of decomposition for the coals until approximately 60-70% percent weight remains, at which point the slope of the TG curves increases again. The *Users Handbook for the Argonne Premium Coal Sample Program* by Vorres shows results from homogeneity analysis performed on the samples and found that the on average high volatile bituminous coals have H_2O content from most to least in the order Illinois #6 > Blind Canyon > Lewiston-Stockton > Pittsburgh #8. The water in the coal is representative of the moisture content, and the trend in decomposition before the reaction begins shows coals having the highest average values of H_2O lost the greatest percent weight in this regime. TG curves from 550-600°C represent the percent weight of the samples post-

combustion. The bulk of material post-combustion is ash, and by observing ash content from table 3.2, it is apparent that the post-combustion trends follow measured ash content.

Recalling that DTG curves shadowed the CO_2 evolutions curves from TG experiments on the carbon/copper oxide mixture from chapter 2, the shapes of these curves for coal samples reacted with air are less similar in comparison. Visual examination of Figure 4.7 reveals small differences in these curves.

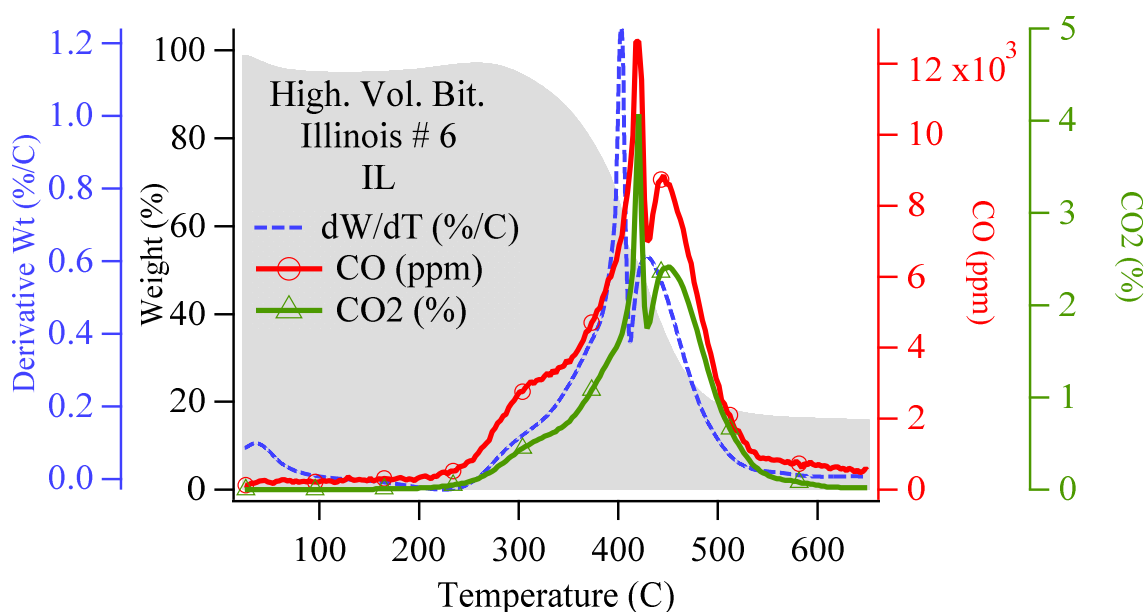


Figure 4.7: TG, DTG, and major gas evolution for high volatile bituminous coal from Illinois #6 seam.

Interestingly the slope of the CO evolution curve is similar in shape to the curve for CO_2 evolution. The similar curves contrast results from the carbon/copper oxide experiments, where early production of CO seemed to initiate the reaction for CO_2 . The DTG curve for the Illinois #6 coal has an approximate value of 1.2 percent weight per degree Celsius, which is similar for all high volatile coals and tests on carbon. This is likely because the bituminous coals have the highest amount of compositional carbon compared with lignite and brown coals. Slight

differences between the CO_2 and DTG curves imply temperatures where the evolution of other gases, like methane, may be occurring. The plot of Illinois #6 was chosen for closer inspection for discussion in this section, not because it represented the behavior of all high volatile coals from the sample program, but because it displays behavior shown in none of the other coal samples. The behavior occurs near $430^\circ C$ where exists a double peak in CO and CO_2 production, which is followed by the DTG. It is reasonable to assume that this behavior is a result of a kinetic step in the combustion process; however, without a deeper understanding of the mechanism, its origin cannot be proven. There are multiple peaks in the DTG of other coals, but they are noticeably separate compared with the curve in Figure 4.7. For instance, the medium volatile coals show a two-peak progression in Figure 3.10, and the peaks can be seen in the three axes plot shown in figure 4.8.

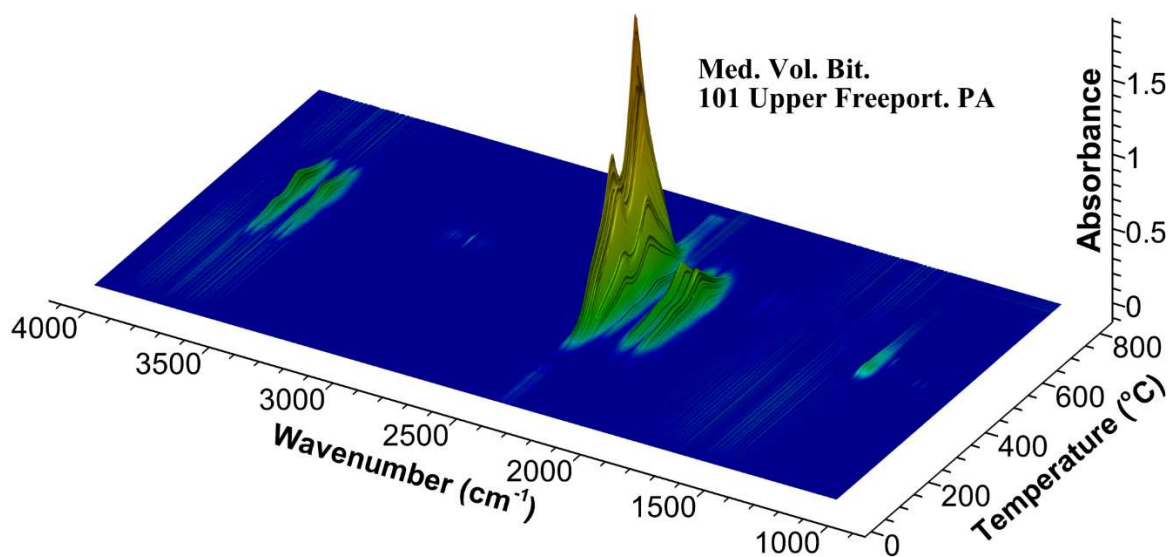


Figure 4.8: Qualitative species evolution for medium volatile bituminous coal from the Upper Freeport seam.

The plot of wavenumber, temperature, and absorbance for medium volatile bituminous coal is shown here with the color of the peaks representing the products ability to absorb IR radiation.

This manner of plotting gaseous evolution about the temperature ramp communicates more information about the process than can be seen in 2-dimensional plots like that in Figure 4.6. As explained in section 3.3.6 absorbance in the wavenumber regions $3500\text{-}4000\text{ cm}^{-1}$ and $2000\text{-}2500\text{ cm}^{-1}$ represent CO_2 and CO , where the carbon monoxide is the smaller peak near 2000 cm^{-1} . The evolution of CO_2 starts very early in the heat ramp and is present through the majority of the combustion. The remaining visible energy bands in the Figure include aromatic nitro in the $1300\text{-}1400\text{ cm}^{-1}$ range, and a barely visible methane band near 3000 cm^{-1} . The presence, although brief, of these species, offer further insight into mechanisms for combustion of these coals.

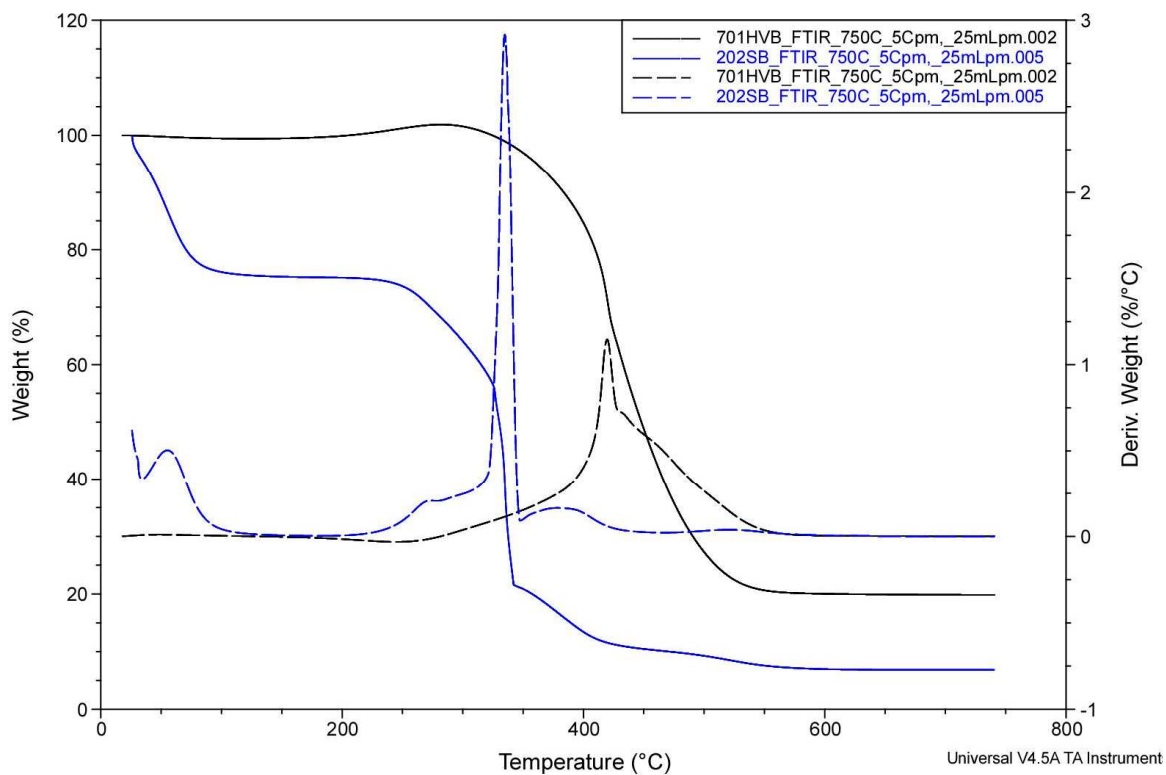


Figure 4.9: TG and DTG for 701 high volatile bituminous and 202 sub-bituminous coals.

Figures 3.14-17 shows the 3-dimensional plots like that in Figure 4.8 for four coals, where each coal indicates trends for the coals in its rank. The plot for sub-bituminous coal 202 shows an absorbance peak that far exceeds values for low, medium, and high volatile bituminous coals. This unusually steep and tall peak occurs at temperatures where the slope of TG curve is also noticeably steep. Figure 4.9 compares the TG and DTG curves for 701 high volatile bituminous coal with those from the 202 sub-bituminous coal. The derivative weight for the high volatile coal has a rate just above 1% per °C, where the rate of decomposition for the sub-bituminous coal is nearly 3% per °C. Reaction of the sub-bituminous coal also begins near 225°C, far lower than that for high volatile bituminous coals. Other noticeable features of the TG of sub-bituminous coal shown in Figure 4.9 are the rapid weight reduction at low temperatures and the low final weight post-reaction.

Section 3.3.1 mentions one other noticeable difference between the two low ranked coals and the bituminous coals. The sub-bituminous and lignite results showed no apparent gain in weight pre-combustion, the rest of the coal's TG curves did. Slovák and Taraba related this phenomenon to chemisorption and studied the process thoroughly. Experiments were conducted at low temperatures (150-300°C) on coal using TG-DSC methods. Initial sample mass, crucible material, and the flow of oxygen were analyzed, and their conclusions were:

- The effect of gas flow is negligible
- Material of the crucible does not affect parameters derived from TG
- Initial sample mass does not affect TG activation energy, frequency factor, or initial combustion temperature; however, they recommend the use of initial mass greater than 10-15 mg [45].

Masses used for experimentation for chapter 3 were 30-40 mg.

To summarize the analysis and results from chapter 3:

- The combustion of Premium Argonne coal samples was studied.
- TGA was performed to find TG and DTG curves.
 - When categorized by rank, the coal samples showed pre-combustion and post-combustion behavior that agreed with their composition with respect to moisture and ash.
 - Low ranked sub-bituminous and lignite coals had rapid reactions which began at lower temperatures than that of higher-ranked coals.
 - The pre-combustion weight gain has been attributed to chemisorption and found to have negligible effect on kinetic parameters.
 - DTG curves for all coal samples have a small plateau in the early stage of reaction.
- FTIR analysis followed gas evolution and infrared absorbance.
 - Spectra were found to have bands relative to CO , CO_2 , aromatic nitro compounds, and CH_4 .
 - The trace of CO_2 , and CO is similar to DTG curves for all coals, but there exist variations due to other gaseous species.
 - High volatile bituminous coal from the Illinois #6 seam has gas evolution profiles with an unusual double peak.
 - Low ranked coals have CO_2 absorbance peaks nearly triple the height of other coal samples.

- Modulated TGA found activation energy over the span of reaction.
 - Using the Hahn method of modulated TGA activation energy, approximations were found across the range of the experiment.
 - The high volatile bituminous coals sample from the blind canyon seam had unusually high activation energy peaks in the temperature range 350-500°C range compared with other coal samples.
 - Other than the Blind Canyon sample, coals showed similarities in activation energy trends within their rank.

4.3 Future Work

Because the field of combustion is so diverse, the possibilities for advancement on the studies in chapters 2 and 3 are numerous. The suggestions in this section exclude finding mechanisms with all kinetic reactions and the rates associated with those steps due the extensive amount of thermodynamic theory required to complete such a task. However, the experimental procedures discussed in this section will provide further insight into those kinetics.

It is mentioned in section 1.6.1 that experiments pertaining to solid oxygen carriers commonly involve repeated oxidation and reduction cycles, and experiments performed for the chapter 2 study on graphite and copper oxide lacked these cycles. However, it is likely that the agglomeration of copper would reduce its effectiveness to reoxidize, and additives like TiO_2 would be beneficial. There have been many combustive studies on CuO with additives with coal as a fuel source, but few to none with graphitic carbon. The composition of the oxidizer is one possible variation on experiments, and another beneficial study would be one with gaseous rather than solid fuels. The C/CuO mixture was mixed stoichiometrically for all chapter 2 experiments, and it is likely that the addition of lean or non-stoichiometric conditions added to

experiments with different heating rates would complexify results.

Proposed future work concerning the Argonne Premium Coals discussed in chapter 3 include comparing combustive behavior at different heating rates. All experiments (except for modulated TGA) were conducted at a furnace ramp of 10°C/min. TGA experiments should be analyzed at very high and low rates. The comparison of trends as rates increase may show how these rates would affect the evolution of pollutants. Furthermore, detection of the evolved gasses should be performed by mass spectrometry (MS). The benefit of using MS is that because it uses the mass-to-charge ratio of ions, rather than vibrational energy of molecules, to identify species, the mass spectrometer can detect symmetrically shaped molecules like diatomic molecules. These molecules are likely present during the combustion of coal and are overlooked by FTIR spectrometry.

The experimental supplements suggested in this section should be conducted first by isolating each variation, and after the effect of each is observed be combined with other experimental variations. This concludes the discussion on oxidation kinetics of graphite and coal using thermogravimetric analysis.

5 References Cited

- [1] S. S. J. Warne, in: Thermal Analysis - Techniques and Applications, a. W. S. B. Charsley E.L., (Ed.) The Royal Society of Chemistry: Thomas Graham House, Science Park, Cambridge, 1992; pp 1-16.
- [2] C. J. Keattch, An introduction to thermogravimetry / [by] C. J. Keattch and D. Dollimore, Heyden, London ; New York, 1975
- [3] G. Nagendrappa, Antoine-Laurent Lavoisier, Resonance 17 (1) (2012) 11-22.
- [4] S. A. A. Jayaweera, S. Kiefer, E. Robens, Balances : instruments, manufacturers, history, Heidelberg
New York : Springer, Heidelberg
New York, 2014
- [5] A. v. Oettingen, T. J. Seebeck, Magnetische polarisation der metalle und erze durch temperatur-differenz, Leipzig, W. Engelmann, Leipzig, 1895
- [6] L. B. Hunt, The Early History of the Thermocouple, Johnson Matthey Technology Review 8 (1) (1964) 23-28.
- [7] Y. Saito, J. Morikawa, Honda's thermobalance, Journal of Thermal Analysis and Calorimetry 113 (3) (2013) 1157-1168.
- [8] T. Instruments, TGA Thermogravimetric Analyzer; Q Series Getting Started Guide, 2006
- [9] R. L. Blaine, B. K. Hahn, Obtaining Kinetic Parameters by Modulated Thermogravimetry, Journal of Thermal Analysis 54 (1998) 695-704.
- [10] R. L. Blaine, Kinetic parameters of overlapping coal decomposition reactions by MTGA, TA instruments Report Number TA-253.
- [11] S. R. Turns, An introduction to combustion : concepts and applications, New York : McGraw-Hill, New York, 2012
- [12] 6 Things You May Not Know About Coal.
https://www.energy.gov/sites/prod/files/2017/05/f34/6%20Things%20About%20Coal%20Infographic_6.pdf
- [13] I. Glassman, Combustion, New York : Academic Press, New York, 1977

- [14] W. C. Gardiner, Rates and mechanisms of chemical reactions, New York, W.A. Benjamin, New York, 1969
- [15] H. S. Caram, N. R. Amundson, Diffusion and Reaction in a Stagnant Boundary Layer about a Carbon Particle, *Industrial & Engineering Chemistry Fundamentals* 16 (2) (1977) 171-181.
- [16] S. B. Warrington, in: *Thermal Analysis - Techniques & Applications*, The Royal Society of Chemistry: 1992; pp 90-92.
- [17] L. Fuji Electric Systems Co., *Instruction Manual*, 2007
- [18] T. N. Corporation, *Introduction to Fourier Transform Infrared Spectroscopy*, 2001.
- [19] B.-C. Chen, J. Sung, S.-H. Lim, Chemical imaging with frequency modulation coherent anti-Stokes Raman scattering microscopy at the vibrational fingerprint region, *The journal of physical chemistry. B* 114 (50) (2010) 16871.
- [20] J. R. Ferraro, L. J. Basile, J. R. Ferraro, L. J. Basile, *Fourier transform infrared spectroscopy*, New York : Academic Press, New York, 1978
- [21] J. Appel, in: 2014; pp 2792-2794.
- [22] J. Partanen, J. Kauppinen, *Fourier transforms in spectroscopy*, Berlin
New York : Wiley-VCH, Berlin
New York, 2002
- [23] R. M. Flores, in: 2014; pp 167-233.
- [24] S. P. Alan W. Scaroni, Ronald J. Morley, in: *Encyclopedia Britannica*, Encyclopedia Britannica, inc.: 2017.
- [25] K. S. Vorres, The Argonne Premium Coal Sample Program, *Energy & Fuels* 4 (5) (1990) 420-426.
- [26] EIA, *Annual Energy Outlook 2017*, DOE/EIA-0383(2017) (Washington, DC: January 2017);.
- [27] R. Siriwardane, H. J. Tian, G. Richards, T. Simonyi, J. Poston, Chemical-Looping Combustion of Coal with Metal Oxide Oxygen Carriers, *Energy & Fuels* 23 (8) (2009) 3885-3892.

- [28] X. Y. Sun, W. G. Xiang, S. Wang, W. D. Tian, X. Xu, Y. J. Xu, Y. H. Xiao, Investigation of Coal Fueled Chemical Looping Combustion Using Fe₃O₄ as Oxygen Carrier: Influence of Variables, *Journal of Thermal Science* 19 (3) (2010) 266-275.
- [29] C. Saha, S. Bhattacharya, Comparison of CuO and NiO as oxygen carrier in chemical looping combustion of a Victorian brown coal, *International Journal of Hydrogen Energy* 36 (18) (2011) 12048-12057.
- [30] M. Ishida, M. Yamamoto, T. Ohba, Experimental results of chemical-looping combustion with NiO/NiAl₂O₄ particle circulation at 1200 degrees C, *Energy Conversion and Management* 43 (9-12) (2002) 1469-1478.
- [31] S. Noorman, F. Gallucci, M. V. Annaland, H. Kuipers, Experimental Investigation of a CuO/Al₂O₃ Oxygen Carrier for Chemical-Looping Combustion, *Industrial & Engineering Chemistry Research* 49 (20) (2010) 9720-9728.
- [32] A. Fossdal, E. Bakken, B. A. Oye, C. Schoning, I. Kaus, T. Mokkelbost, Y. Larring, Study of inexpensive oxygen carriers for chemical looping combustion, *International Journal of Greenhouse Gas Control* 5 (3) (2011) 483-488.
- [33] T. Mendiara, A. Abad, L. F. de Diego, F. Garcia-Labiano, P. Gayan, J. Adanez, Use of an Fe-Based Residue from Alumina Production as an Oxygen Carrier in Chemical-Looping Combustion, *Energy & Fuels* 26 (2) (2012) 1420-1431.
- [34] Y. L. Kuo, W. M. Hsu, P. C. Chiu, Y. H. Tseng, Y. Ku, Assessment of redox behavior of nickel ferrite as oxygen carriers for chemical looping process, *Ceramics International* 39 (5) (2013) 5459-5465.
- [35] in: *Comprehensive Chemical Kinetics*, C. H. Bamford; C. F. H. Tipper, (Eds.) Elsevier: 1980; Vol. 22, p 277.
- [36] H. Y. Sohn, J. Szekely, Reactions between solids through gaseous intermediates—I reactions controlled by chemical kinetics, *Chemical Engineering Science* 28 (10) (1973) 1789-1801.
- [37] A. K. Burnham, M. S. Oh, R. W. Crawford, A. M. Samoun, Pyrolysis of Argonne Premium Coals - Activation-Energy Distributions and Related Chemistry, *Energy & Fuels* 3 (1) (1989) 42-55.
- [38] B. Li, G. Chen, H. Zhang, C. Sheng, Development of non-isothermal TGA–DSC for kinetics analysis of low temperature coal oxidation prior to ignition, *Fuel* 118 (2014) 385-391.
- [39] H. Wang, B. Z. Dlugogorski, E. M. Kennedy, Coal oxidation at low temperatures: oxygen

consumption, oxidation products, reaction mechanism and kinetic modelling, *Progress in Energy and Combustion Science* 29 (6) (2003) 487-513.

[40] S. Sarkar, *Fuels and combustion*, Hyderabad, India : Universities Press

Boca Raton, FL : Distributed in the rest of the world by CRC Press, Hyderabad, India : Boca Raton, FL, 2009

[41] V. Slovák, B. Taraba, Effect of experimental conditions on parameters derived from TG-DSC measurements of low-temperature oxidation of coal, *Journal of Thermal Analysis and Calorimetry* 101 (2010) 641+.

[42] J. C. Jones, P. S. Chiz, R. Koh, J. Matthew, Kinetic parameters of oxidation of bituminous coals from heat-release rate measurements, *Fuel* 75 (15) (1996) 1755-1757.

[43] W. T. Hu, F. Donat, S. A. Scott, J. S. Dennis, Kinetics of oxygen uncoupling of a copper based oxygen carrier, *Applied Energy* 161 (2016) 92-100.

[44] K. Wang, Q. B. Yu, Q. Qin, Reduction Kinetics of Cu-Based Oxygen Carriers for Chemical Looping Air Separation, *Energy & Fuels* 27 (9) (2013) 5466-5474.

[45] V. Slovák, B. Taraba, Effect of experimental conditions on parameters derived from TG-DSC measurements of low-temperature oxidation of coal, *Journal of Thermal Analysis and Calorimetry* 101 (2) (2010) 641-646.